SURFACE POLARITON WITH ARBITRARY DIELECTRIC AND MAGNETIC MATERIALS

LOW KA CHUN

FACULTY OF SCIENCE
UNIVERSITY OF MALAYA
KUALA LUMPUR

2013

SURFACE POLARITON WITH ARBITRARY DIELECTRIC AND MAGNETIC MATERIALS

LOW KA CHUN

DISSERTATION SUBMITTED IN FULFILMENT OF THE REQUIREMENTS FOR THE DEGREE OF MASTER OF SCIENCE

DEPARTMENT OF PHYSICS
FACULTY OF SCIENCE
UNIVERSITY OF MALAYA
KUALA LUMPUR

2013

UNIVERSITI MALAYA

ORIGINAL LITERARY WORK DECLARATION

Name of Candidate: Low Ka Chun (I.C. No.:870823105487)

Registration/Matrix No.:SGR110105

Name of Degree:Master of Science

Title of Dissertation:Surface Polariton With Aibitrary Dielectric And Magnetic Materials

Field of Study:Theoretical Physics

I do solemnly and sincerely declare that:

(1) I am the sole author/writer of this dissertation;
(2) This dissertation is original;
(3) Any use of any work in which copyright exists was done by way of fair dealing and for permitted purposes and any excerpt or extract from, or reference to or reproduction of any copyright work has been disclosed expressly and sufficiently and the title of the Work and its authorship have been acknowledged in Dissertation;
(4) I do not have any actual knowledge nor do I ought reasonably to know that the making of this dissertation constitutes an infringement of any copyright work;
(5) I hereby assign all and every rights in the copyright to this dissertation to the University of Malaya ("UM"), who henceforth shall be owner of the copyright in Dissertation and that any reproduction or use in any form or by any means whatsoever is prohibited without the written consent of UM having been first had and obtained;
(6) I am fully aware that if in the course of making Dissertation I have infringed any copyright whether intentionally or otherwise, I may be subject to legal action or any other action as may be determined by UM.

Candidate's Signature Date

Subscribed and solemnly declared before,

Witness's Signature Date

Name:
Designation:

ABSTRACT

Surface Polariton dispersion is demonstrated in the interface of two mediums and thin slab. Starting from 4 Maxwell equations, dispersion equations for s-polarization and p-polarisation are derived. Solutions of the tangential dispersion relation and normal dispersion relation for s-polarization is completely symmetrical to that of the p-polarization, due to the symmetry between the electric and magnetic responses in the Maxwell equations. If the materials are both dielectric and magnetic, μ_i , $\varepsilon_i \neq 1$, the s-polarized light can also excite the propagating surface modes, not just the p-polarized light. Analysis reveals additional new regimes of surface polariton resonances with magnetic materials for both polarizations. Coexistence of the dielectric dispersion in $\varepsilon_2(\omega)$ and the magnetic dispersion in $\mu_2(\omega)$ give rise to the second peaks in the spectra of k_x for s and p polarizations. By considering damping, large wavevector in large frequency range can be achieved if SP is excited at the interface where medium 1 is a dispersive medium and medium 2 is also a dispersive medium which contains a slightly different permittivity or permeability. SP modes in thin metamaterial slab are analysed. In such a system, each single interface can sustain bound SP. When the separation between adjacent interfaces is smaller than the decay length, interactions between SP at both interface give rise to coupled modes, odd mode and even mode. Dispersions of SP in thin slab are solved numerically. Similar to one dimensional solution, s-polarized wave can also excite propagating surface modes. Considering damping and without damping, dispersion curves are drawn for both modes with reducing slab thickness. Noticed that resonant happens at resonance frequency when $\mu_1 = -\mu_2$, $\varepsilon_1 = -\varepsilon_2$ and at resonance frequency of split ring resonator, ω_0. Odd modes for both polarisations show increasing propagation length with decreasing film thickness. Futhermore, spatial distributions of the fields at resonant enhancement are studied also for different dielectric permittivities and magnetic permeabilities for the interface of two mediums and thin slab.

ABSTRAK

Penyebaran SP ditunjukkan dalam antara muka dua medium dan filem nipis. Bermula daripada 4 persamaan Maxwell, persamaan penyebaran untuk s-polarisasi dan p-polarisasi diperolehi. Penyelesaian vektor gelombang tangen dan vektor gelombang normal untuk s-polarisasi adalah simetri sepenuhnya kepada yang p-polarisasi. Ini disebabkan oleh simetri antara respon elektrik dan magnet dalam persamaan Maxwell. Jika bahan-bahan adalah kedua-dua dielektrik dan magnet, μ_i, $\varepsilon_i \neq 1$, cahaya s-polarisasi juga boleh merangsang mod penyebaran muka, bukan cahaya p-polarisasi sahaja. Untuk kedua-dua polarisasi, analisis mendedahkan rejim baru tambahan bagi permukaan resonans polariton jika bahan magnet digunakan. Jika salah satu media mempunyai serakan fungsi dielektrik dan serakan fungsi kebolehtelapan, puncak permukaan resonans polariton tambahan muncul untuk kedua-dua polarisasi. Dengan mempertimbangkan redaman, wave vektor besar dalam julat frekuensi yang besar boleh dicapai jika SP teruja pada antara muka di mana medium 1 adalah medium serakan dan medium 2 juga merupakan medium serakan yang mengandungi fungsi dielektrik atau fungsi kebolehtelapan yang sedikit berbeza. Mod SP dalam filem metamaterial yang nipis juga dianalisis. Dalam sistem seperti ini, setiap antara muka tunggal boleh mengekalkan SP terikat. Apabila pemisahan antara muka bersebelahan adalah lebih kecil daripada panjang pereputan, interaksi antara SP di kedua-dua muka menimbulkan mod bersama, mod ganjil dan juga mod genap. Serakan SP diselesaikan secara numerik. Sama kepada satu dimensi penyelesaian, s-polarisasi gelombang juga boleh merangsang permukaan resonans polariton dalam filem nipis. Mempertimbangkan redaman dan tanpa redaman, lengkung serakan dilukis bagi kedua-dua mod dengan ketebalan filem yang semakin berkurangan. Menyedari bahawa wave vektor adalah tertinggi pada frekuensi resonans apabila $\mu_1 = -\mu_2$, $\varepsilon_1 = -\varepsilon_2$ dan pada frekuensi resonans split ring resonator, ω_0. Mod ganjil bagi kedua-dua polarisasi menunjukkan pertambahan panjang propagasi apabila ketebalan filem yang semakin berkurangan. Tambahan pula, taburan ruang medan elektrik dan magnet dalam antara muka tunggal dan filem nipis semasa resonans polariton juga dikaji bagi permittivities dielektrik dan kebolehtelapan magnet yang berbeza-beza.

ACKNOWLEDGEMENTS

First, a very thank you to my family for supporting me of all kind of help through out my master study. Then, I would like to express my special thanks of gratitude to my supervisor, Assoc. Prof. Dr Raymond Ooi, who gave me lots of guidance and helped me a lot in doing this research and I came to know about so many new things. Besides that, we appreciate the support by the Ministry of Higher Education (MOHE)/University of Malaya High Impact Research (HIR) Grant A-000004-50001, and the MOHE Exploratory Research Grant Scheme (ERGS) ER014-2011A.

TABLE OF CONTENTS

ORIGINAL LITERARY WORK DECLARATION ii

ABSTRACT iii

ABSTRAK iv

ACKNOWLEDGEMENTS v

TABLE OF CONTENTS vi

LIST OF FIGURES viii

List of Tables xi

LIST OF APPENDICES xii

CHAPTER 1: INTRODUCTION 1

CHAPTER 2: ELECTROMAGNETICS OF SURFACE POLARITON 6

2.1 Maxwell's Equations and Wave equations 6

2.2 Surface Polariton In Single Interface 10

2.2.1 s-polarised SP 10

2.2.2 p-polarised SP 13

2.3 Surface Polariton In Double Interface 16

2.3.1 s-polarized SP 16

2.3.2 p-polarised SP 19

2.3.3 Surface plasmon polariton in non-magnetic thin metal slab 24

CHAPTER 3: SINGLE INTERFACE SURFACE POLARITONS WITH ARBITRARY MAGNETIC AND DIELECTRIC MATERIALS 27

3.1 New Regimes Of Surface Polariton Resonances 27

3.1.1 μ and ε Are Mostly Real 29

3.1.2 μ and ε Are Mostly Imaginary 33

3.2 Field Distribution 34

3.2.1 Surface mode in s-polarization 35

3.2.2 Surface mode in p-polarization 39

3.3 Dispersions Of Surface Polaritons 43

3.3.1 Dispersive Dielectric And Magnetic Materials 43

3.3.2 Superconductor 51

CHAPTER 4: SP RESONANCE IN LARGE FREQUENCY RANGE 54

4.1 Metamaterial 54

4.2 Influence of Difference Values Of μ and ε Towards SP Resonance Frequency 55

4.3 Large Wavevector at Large Frequency Range 58

CHAPTER 5: SP MODES IN IDEAL AND LOSSY METAMATERIAL SLAB 63
5.1 SP Modes In Thin Slab 63
5.2 Dispersions Of Surface Polaritons In Ideal Thin slab 64
5.2.1 s-polarised SP 65
5.2.2 p-polarised SP 69
5.3 Dispersions Of Surface Polaritons In Lossy Thin slab 72
5.3.1 s-polarised SP 72
5.3.2 p-polarised SP 77
5.4 Field Distribution 81

CHAPTER 6: CONCLUSIONS 87

APPENDICES 89
REFERENCES 102

LIST OF FIGURES

Figure 2.1 SP propagation in single interface 10

Figure 2.2 SP propagation in thin slab 16

Figure 3.1 Quadrants showing regimes of enhanced tangential wave vectors k_x of surface polaritons propagating between medium 1 and medium 2 with permittivities ε_i and permeabilities μ_i for s-polarized light and p-polarized light. (a) Conventional scenario of plasmonic enhancement and its magnetic analog (indicated by open/filled dots). (b) New resonant regimes due to both electric and magnetic properties. The enhancement regions are indicated by two solid (red) lines and two dashed (green) lines slightly less and more than 1 and -1. 29

Figure 3.2 Surface mode in s-polarization: E_z field(real) with rapid oscillations (corresponding to an enhanced tangential wave vector) 37

Figure 3.3 Surface mode in s-polarization: E_z field(imaginary) with rapid oscillations (corresponding to an enhanced tangential wave vector) 37

Figure 3.4 Surface mode in s-polarization: E_x field(real) with normal oscillations with discontinuity at $y = 0$(the scale is 10 times larger). 38

Figure 3.5 Surface mode in s-polarization: E_x field(imaginary) with normal oscillations with discontinuity at $y = 0$(the scale is 10 times larger). 38

Figure 3.6 Surface mode in p-polarization: E_z field(real) with normal oscillations. 41

Figure 3.7 Surface mode in p-polarization: E_z field(imaginary) with normal oscillations. 41

Figure 3.8 Surface mode in p-polarization: E_x field(real) with rapid oscillations.(corresponding to an enhanced tangential wave vector) 42

Figure 3.9 Surface mode in p-polarization: E_x field(imaginary) with rapid oscillations. (corresponding to an enhanced tangential wave vector) 42

Figure 3.10 Real part of $\varepsilon_2(\omega)$, $\mu_2 = 5$. 45

Figure 3.11 Real part of $\varepsilon_2(\omega)$, $\mu_2(\omega)$. 45

Figure 3.12 Refractive index, $n_2(\omega) = \sqrt{\varepsilon_2(\omega)\mu_2}$ 46

Figure 3.13 Refractive index, $n_2(\omega) = \sqrt{\varepsilon_2(\omega)\mu_2(\omega)}$ 46

Figure 3.14 Wave vector dispersions for s-polarized when ε_2 and μ_2 in the same sign, $\mu_1 = \pm 1, \varepsilon_1 = \pm 1$ 47

Figure 3.15 Wave vector dispersions for s-polarized when ε_2 and μ_2 in the same sign, $\mu_1 = \pm 1, \varepsilon_1 = \pm 1$, double resonance spectra are observed. 47

Figure 3.16 Wave vector dispersions for p-polarized when ε_2 and μ_2 in the same sign, $\mu_1 = \pm 1, \varepsilon_1 = \pm 1$ 48

Figure 3.17 Wave vector dispersions for p-polarized when ε_2 and μ_2 in the same sign, $\mu_1 = \pm 1, \varepsilon_1 = \pm 1$, double resonance spectra are observed. 48

Figure 3.18 Wave vector dispersions for s-polarized when ε_2 and μ_2 in the opposite sign, $\mu_1 = \pm 1, \varepsilon_1 = \mp 1$ 49

Figure 3.19 Wave vector dispersions for s-polarized when ε_2 and μ_2 in the opposite sign, $\mu_1 = \pm 1, \varepsilon_1 = \mp 1$, double resonance spectra are observed. 49
Figure 3.20 Wave vector dispersions for p-polarized when ε_2 and μ_2 in the opposite sign, $\mu_1 = \pm 1, \varepsilon_1 = \mp 1$ 50
Figure 3.21 Wave vector dispersions for p-polarized when ε_2 and μ_2 in the opposite sign, $\mu_1 = \pm 1, \varepsilon_1 = \mp 1$, double resonance spectra are observed. 50
Figure 3.22 Dispersive superconductor with $\varepsilon_2(\omega)$ and dispersive magnetic material with $\mu_2(\omega)$ 52
Figure 3.23 $n_2(\omega) = \sqrt{\varepsilon_2(\omega)\mu_2(\omega)}$ with negative refractive index region 52
Figure 3.24 The enhancement λ/λ^s_{eff} of surface polaritons for s-polarized light. 53
Figure 3.25 The enhancement λ/λ^p_{eff} of surface polaritons for p-polarized light. 53

Figure 4.1 Left: SP dispersion for s-polarised light with $\mu_2 = 1$ (green); 3 (red); 5 (blue) $\varepsilon_2 = 1$. Right: SP dispersion with $\mu_2 = -1$ (green); -3 (red); -5 (blue) $\varepsilon_2 = -1$. 57
Figure 4.2 Left: SP dispersion for p-polarised light with $\varepsilon_2 = 1$ (green); 3 (red); 5 (blue) $\varepsilon_2 = 1$. Right: SP dispersion with $\varepsilon_2 = -1$ (green); -3 (red); -5 (blue) $\mu_2 = -1$. 57
Figure 4.3 ε_1 is dispersive Eq. (4.3); μ_1 is dispersive Eq. (4.4) with 0 loss. a) p-polarised dispersion curves for dispersive ε_2; $\mu_2 = 1$ (green), $\varepsilon_2 = 1$; $\mu_2 = 1$ (red). b) s-polarised dispersion curves for dispersive ε_2; $\mu_2 = 1$ (green), $\varepsilon_2 = 1$; $\mu_2 = 1$ (red). c) s-polarised dispersion curves for $\varepsilon_2 = 1$; dispersive μ_2 (green),$\varepsilon_2 = 1$; $\mu_2 = 1$ (red). d) s-polarised dispersion curves for $\varepsilon_2 = 1$; dispersive μ_2 (green), ,$\varepsilon_2 = 1$; $\mu_2 = 1$ (red). 60
Figure 4.4 ε_1 is dispersive Eq. (4.3); μ_1 is dispersive Eq. (4.4) with $\gamma = 1 \times 10^{14}, \Gamma = 1 \times 10^{13}$. a) p-polarised dispersion curves for dispersive ε_2; $\mu_2 = 1$ (green), $\varepsilon_2 = 1$; $\mu_2 = 1$ (red). b) s-polarised dispersion curves for dispersive ε_2; $\mu_2 = 1$ (green), $\varepsilon_2 = 1$; $\mu_2 = 1$ (red). c) s-polarised dispersion curves for $\varepsilon_2 = 1$; dispersive μ_2 (green),$\varepsilon_2 = 1$; $\mu_2 = 1$ (red). d) s-polarised dispersion curves for $\varepsilon_2 = 1$; dispersive μ_2 (green), ,$\varepsilon_2 = 1$; $\mu_2 = 1$ (red). 61
Figure 4.5 ε_1 is dispersive Eq. (4.3); μ_1 is dispersive Eq. c4) with $\gamma = 1 \times 10^{14}, \Gamma = 1 \times 10^{13}$. Left: p-polarised dispersion curves for dispersive ε_2, $\mu_2 = 1$, $\omega_p = 10.1$ (green), 10.06 (red), 10.02 (blue) Right: s-polarised dispersion curves for $\varepsilon_2 = 1$; dispersive μ_2, $\omega_0 = 2.1$ (green), 2.06 (red), 2.02 (blue). 62
Figure 4.6 ε_1 is dispersive Eq. (4.3); μ_1 is dispersive Eq. (4.4) with $\gamma = 1 \times 10^{14}, \Gamma = 1 \times 10^{13}$. Left: s-polarised dispersion curves for dispersive μ_2, $\varepsilon_2 = 1$ (green), 3 (red),5 (blue). Right: p-polarised dispersion curves for dispersive ε_2; $\mu_2 = 1$ (green), 3(red), 5(blue). 62

Figure 5.1 Dispersion of ideal s-polarized even mode 67
Figure 5.2 Dispersion of ideal s-polarized odd mode 67
Figure 5.3 Dispersion of ideal s-polarized odd mode(enlarged) 68
Figure 5.4 Dispersion of ideal p-polarized even mode 71

Figure 5.5 Dispersion of ideal p-polarized odd mode 71
Figure 5.6 Dispersion of s-polarized even mode with damping (real wavevector) 74
Figure 5.7 Dispersion of s-polarized even mode with damping (imaginary wavevector) 74
Figure 5.8 Dispersion of s-polarized odd mode (negative $d\omega/d\beta$) with damping (real wavevector) 75
Figure 5.9 Dispersion of s-polarized odd mode (negative $d\omega/d\beta$) with damping (imaginary wavevector) 75
Figure 5.10 Dispersion of s-polarized odd mode (positive $d\omega/d\beta$), propagation length increase with decreasing thickness 76
Figure 5.11 Dispersion of s-polarized odd mode (positive $d\omega/d\beta$), propagation length increase with decreasing thickness further. (no cutoff thickness) 76
Figure 5.12 Dispersion of p-polarized even mode with damping (real wavevector) 78
Figure 5.13 Dispersion of p-polarized even mode with damping (imaginary wavevector) 78
Figure 5.14 Dispersion of p-polarized odd mode with damping (real wavevector) 79
Figure 5.15 Dispersion of p-polarized odd mode with damping (imaginary wavevector) 79
Figure 5.16 Dispersion of p-polarized odd mode (positive $d\omega/d\beta$), propagation length increase with decreasing thickness 80
Figure 5.17 Dispersion of p-polarized odd mode (positive $d\omega/d\beta$), propagation length increase with decreasing thickness further. (no cutoff thickness) 80
Figure 5.18 Electric field of odd mode (anti-symmetry) 84
Figure 5.19 Electric field of even mode (symmetry) 84
Figure 5.20 Electric field of even mode(front view) 85
Figure 5.21 Electric field of odd mode with damping 85
Figure 5.22 Electric field of even mode with damping 86

LIST OF TABLES

Table 5.1 p-polarized fields symmetry property 83
Table 5.2 s-polarized fields symmetry property 83

LIST OF APPENDICES

Appendix A	Program listing to solve thin slab dispersion of s-polarised odd mode	90
Appendix B	Program listing to solve thin slab dispersion of s-polarised even mode	91
Appendix C	Program listing to solve thin slab dispersion of p-polarised odd mode	92
Appendix D	Program listing to solve thin slab dispersion of p-polarised even mode	93
Appendix E	Published Paper	94

CHAPTER 1

INTRODUCTION

The objective of this research is to explore the dispersive characteristics of surface polariton with considering arbitrary dielectric and magnetic materials. We analyze this dispersion property for both single interface and double interface.

In general, polaritons are quasiparticles resulting from strong coupling of electromagnetic waves with an electric or magnetic dipole-carrying excitation. Surface plasmon polariton and surface magnon polariton are electromagnetic (EM) surface waves that propagate at the planar interface between two dissimilar media. Surface plasmons are coherent electron oscillations that exist at the interface while surface magnon is a collective excitation of the electrons' spin. They can propagate along the surface until energy is lost either via absorption in the materials or radiation into free-space.

In optics, polarization is a property of waves that can oscillate with more than one orientation. p-polarized wave has an electric field direction parallel to the plane of incidence on a surface, and s-polarized wave has the electric field oriented perpendicular to that plane. Normally, surface polariton in metal can be excited by p-polarized light only. If the materials are both dielectric and magnetic, μ_i , $\varepsilon_i \neq 1$, the s-polarized light can also excite the propagating surface modes, not just the p-polarized light. Surface polaritons (SP) have their intensity maximum at the surface and exponentially decaying field perpendicular to it (Raether, 1988).

SPs are shorter in wavelength than the incident light. Hence, SPs can provide a significant reduction in effective wavelength and a corresponding significant increase in spatial confinement and local field intensity. These collective charge oscillations at the boundary between two mediums are able to sustain the propagation of electromagnetic waves in large range of frequency from microwave to visible. The major applications of SP are waveguides, light sources, near-field optics, surface-enhanced Raman spectroscopy, data storage, solar cells, chemical sensors and biosensors.

The existence of self-sustained collective excitations at metal surfaces has discov-

ered by Ritchie in 1957(Ritchie, 1957). Since then, there has been a significant advance in both theoretical and experimental investigations of surface plasmons. Surface plasmon-polaritons (SPPs) have promising potential for realizing compact optical circuits in next-generation compact optoelectronic systems integrated with nanoplasmonic components (Ozbay, 2006), semiconductor lasers with plasmonic polarizers (Yu et al., 2009) and plasmonic collimation that produces light beams with small divergence (Yu et al., 2008), and sensitive photodetectors using plasmonic lenses (Shackleford, Grote, Currie, Spanier, & Nabet, 2009). Low-threshold, low-current operation of semiconductor lasers and optical devices is needed. Nanosystems, e.g., quantum dots, are promising for these purposes, while nanoplasmonics and/or metamaterials provide large optical nonlinearity through the field enhancement effect.

An SPP can be excited through sculptured thin film (Polo, Jr., & Lakhtakia, 2009), a corrugated surface, triangular grooves, or wedges (Martin-Moreno, García-Vidal, Lezec, Degiron, & Ebbesen, 2003). Recently, SPPs have been incorporated into metamaterials (Zhang, Genov, Wang, Liu, & Zhang, 2008) that mimic the permeability of magnetic materials. Surface polaritons supported by left-handed medium or negative index metamaterial have been studied extensively. Such as guided modes in negative-refractive-index waveguides (Shadrivov, Sukhorukov, & Kivshar, 2003), amplification of evanescent waves in a lossy left-handed material slab(Rao & Ong, 2003), and study of the surface and bulk polaritons with a negative index metamaterial (Park, Lee, Fu, & Zhang, 2005). Some remarkable effects of SPPs are field enhancement, the subwavelength effect (Barnes, Dereux, & Ebbesen, 2003), superresolution (Smolyaninov, Hung, & Davis, 2006), efficient guiding (Moreno, Rodrigo, Bozhenyi, Martin-Moreno, & Garcia-Vidal, 2008), and tight focusing (Radko, Bozhenyi, Evlyukhin, & Boltasseva, 2007). SPPs also affect light–matter interactions, such as photoelectron generation (Farkas & Toth, 1990). They enhance the photoelectric effect (Raynaud & Kupersztych, 2007), multiphoton ionization (Varro & Ehlotzky, 1998), and acceleration of electrons (Zawadzka, Jaroszynski, Carey, & Wynne, 2001). The strong coupling (Chang, Sørensen, Hemmer, & Lukin, 2007) between SPPs and atoms enhances light emissions (Okamoto et al., 2004), nonlinear optical interactions (Sipe, So, Fukui, & Stegeman, 1980), and pulse propagation (Rokitski, Tetz, & Fainman, 2005), and alters the dynamics of interactions with fem-

tosecond lasers (Lehmann et al., 2000).

Besides, SPPs also modify the Casimir energy (Intravaia & Lambrecht, 2005) and the radiation force (Quidant, Badenes, & Petrov, 2006), causing dispersion anomalies in electron diffraction on metallic gratings (Heitmann, Kroo, Schulz, & Szentirmay, 1987). Nanoparticles of various structures use SPPs for chemical sensing. Modulation of exciton–plasmon interactions can serve as a wavelength-based biodetection tool, which can resolve difficulties in the quantification of luminescence intensity for complex media and optical pathways (Jin et al., 2001). Nanoprisms is useful in developing multicolor diagnostic labels (Lee, Hernandez, Lee, Govorov, & Kotovi, 2007). Recent works have shown that SPPs can help photons squeeze through subwavelength holes (B-Abad et al., 2006) and transmit entangled photons (Moreno, Garcia-Vidal, Erni, Cirac, & Martin-Moreno, 2004). Their subwavelength diffraction and extraordinary transmission through small apertures led to high resolution near-field microscopy (Drezet, Woehl, & Huant, 2002). Suitable designs of structures with SPPs are useful for optical trapping (Novotny, Bian, & Xie, 1997)(Rosenblit, Japha, Horak, & Folman, 2006) and laser cooling (Khurgin, 2007). Collective excitations of plasmons (Camley & Mills, 1984), stimulated emission (Seidel, Grafström, & Eng, 2005), and plasmonic lasing (Cubukcu, Kort, Crozier, & Capasso, 2006) are also enhanced by SPPs.

Surface phonon-polaritons (SFPs) and surface excitonpolaritons (SEPs) (the counterparts of dielectric and semiconductor SPPs in metals) have been widely explored in the context of thin films and multilayers (Agranovich & Mills, 1982). A number of works have shown that magnetic materials can excite surface magnon- polaritons (SMPs), i.e., strong coupling of photons to quantized magnetization waves due to collective spins (Cottam, Tilley, & Physics (Great Britain), 2005). Ruppin showed that surface polariton can exist for both s- and p-polarized light in left-handed metamaterials (Ruppin, 2000), but damping (imaginary parts) was neglected. Excitation of SMPs in gyromagnetic materials and anisotropic antiferromagnetic crystals have been discussed by Hartstein et al. (Hartstein, Burstein, Brewer, & Wallis, 1973) and Arakelian et al. (Arakelian, Bagdassarian, & Simonian, 1997), respectively. The presence of magnonpolaritons was demonstrated in a YIG slab using the attenuated total reflectance technique (Matsuura, Fukui, & Tada, 1983). The dispersion relations for magnetic polaritons have been obtained for

anisotropic systems, such as ordered ferromagnetic slabs (Marchand & Caill, 1980)[41] and uniaxial antiferromagnets (Shu & Caille, 1980)(Thibaudeau & Caille, 1993). It has been shown that s-polarized (TE) optical waves can propagate at the interface of media with negative refractive index and negative dielectric constant of low-dimensional nanowaveguides (Takahara & Kobayashi, 2004). However, the underlying theory (with magnetic materials) was not given. Despite these works, the recent boom in the field of plasmonics has been predominantly based on the p-polarized light fields to excite surface plasmon resonance (SPR) at the interface of dielectric and metallic media, while the use of s-polarized light with magnetic materials is not so popular. In this research, we will discuss surface polariton for both polarization. The use of magnetic materials extends the field of plasmonics to magnonics.

In this dissertation, we analyze the new regimes in the dispersion property and the modes (s and p polarizations) of surface waves propagating between two media with at least one with magnetic permeability that differs from unity. Complete derivations starting from Maxwell's equations of SP dispersions are found at chapter 2. The theory covers single interface and thin slab. In chapter 3, we present the underlying theoretical expressions for the wave vectors and field distributions across two media with arbitrary materials. The theory is generally valid in the entire electromagnetic spectrum, but we focus on the optical regime due to potential attractive applications in optical technologies. The theory provides insights for studying the spectrum of the surface polaritons formed by various combinations of metallic, dielectric, and magnetic materials where SMPs exist, in addition to SFPs, SEPs, and SPPs. Although dielectric and/or metallic materials can coexist, the magnetic material or metamaterial with effective permeability is the main component needed to show the new regimes/possibilities provided by SMPs.

Next, we are showing how influences of the values of permittivity constant and permeability constant of medium 2 to the surface polariton resonance frequency in metamaterials in chapter 4. Besides that, we are discussing how to have large tangential wave vectors in metamaterial for most of the frequency range, in other words, resonance at large frequency range. This large frequency range of resonance is believed will lead to further novel effects and applications such as near field optic, enhancement of fluorescence and photoelectric devices. In chapter 5, we analyze different SP modes in thin

slab. The dispersion graphs are draw for both p-polarized and s-polarized waves with decreasing thickness. In odd mode of medium with damping, at lower wavevector region, imaginary wavevector(related to propagation length) is reducing with decreasing thickness. Hence propagation length is increasing when thickness is reduced. No cutoff thickness is observed.This holds for s-polarized and p-polarized odd modes surface polariton. Furthermore, the electric/magnetic field symmetry property of different modes are solved and draw.

CHAPTER 2

ELECTROMAGNETICS OF SURFACE POLARITON

Surface polaritons are electromagnetic excitations propagating at the interface between two mediums, evanescently confined in the perpendicular direction. These electromagnetic surface waves arise via the coupling of the electromagnetic fields to oscillations of the electron and the electron spin. Taking the Maxwell's equations as a starting point, this chapter describes the fundamentals of surface polaritons both at single, flat interface and double interfaces structure.

2.1 Maxwell's Equations and Wave equations

Maxwell's equations represent one of the most elegant and concise ways to state the fundamentals of electricity and magnetism. Interaction of materials with electromagnetic fields can be firmly understood in a classical framework based on Maxwell's equations. Even metallic nanostructures down to sizes on the order of a few nanometres can be described without a need to resort to quantum mechanics. Hence, our work fully falls within classical theory.

We begin with writing the four Maxwell's equations:

i) Gauss' law for electricity

$$\bigtriangledown \cdot \vec{D} = \rho \tag{2.1}$$

ii) Gauss' law for magnetism

$$\bigtriangledown \cdot \vec{B} = 0 \tag{2.2}$$

iii) Faraday's law of induction

$$\bigtriangledown \times \vec{E} = -\frac{\partial \vec{B}}{\partial t} \tag{2.3}$$

iv) Ampere's law

$$\bigtriangledown \times \vec{H} = \frac{\partial \vec{D}}{\partial t} + J \tag{2.4}$$

In the absence of external charge and current densities, the curl equations (Eqs. (2.3) and (2.4)) can be combined to yield:

$$\begin{aligned} \bigtriangledown \times \bigtriangledown \times \vec{E} &= \bigtriangledown \times -\frac{\partial(\mu \vec{H})}{\partial t} \\ &= -\mu \frac{\partial(\mu \times \vec{H})}{\partial t} \\ &= -\mu \frac{\partial^2 \vec{D}}{\partial t^2} \end{aligned} \tag{2.5}$$

Using the identities $\bigtriangledown \times \bigtriangledown \times \vec{E} = \bigtriangledown(\bigtriangledown \cdot \vec{E}) - \bigtriangledown^2 \vec{E}$ as well as $\bigtriangledown \cdot (\varepsilon \vec{E}) = \vec{E} \cdot \bigtriangledown \varepsilon + \varepsilon \bigtriangledown \cdot \vec{E}$ and in the absence of external charge source $\bigtriangledown \cdot \vec{D} = 0$, Eq. (2.5) can be rewritten as

$$\begin{aligned} \bigtriangledown(\bigtriangledown \cdot \vec{E}) - \bigtriangledown^2 \vec{E} &= -\mu \varepsilon \frac{\partial^2 \vec{E}}{\partial t^2} \\ \bigtriangledown(\frac{1}{\varepsilon} \bigtriangledown \cdot (\varepsilon \vec{E}) - \frac{1}{\varepsilon} \vec{E} \cdot \bigtriangledown \varepsilon) - \bigtriangledown^2 \vec{E} &= -\mu \varepsilon \frac{\partial^2 \vec{E}}{\partial t^2} \\ \bigtriangledown(-\frac{1}{\varepsilon} \vec{E} \cdot \bigtriangledown \varepsilon) - \bigtriangledown^2 \vec{E} &= -\mu \varepsilon \frac{\partial^2 \vec{E}}{\partial t^2} \end{aligned} \tag{2.6}$$

For negligible variation of the dielectric profile $\varepsilon = \varepsilon(r)$, Eq. (2.6) simplifies to the central equation of electromagnetic wave theory,

$$\bigtriangledown^2 \vec{E} - \mu \varepsilon \frac{\partial^2 \vec{E}}{\partial t^2} = 0 \tag{2.7}$$

We assume in all generality a harmonic time dependence $\vec{E}(\vec{r},t) = \vec{E}(\vec{r}) e^{i\omega t}$ of the electric field. Inserted this equation into Eq. (2.7),

$$\begin{aligned} \bigtriangledown^2 \vec{E} - \mu \varepsilon \frac{\partial^2 (\vec{E}(r) e^{i\omega t})}{\partial t^2} &= 0 \\ \bigtriangledown^2 \vec{E} - \mu \varepsilon (-i\omega)^2 \vec{E}(r) e^{i\omega t} &= 0 \\ \bigtriangledown^2 \vec{E} + \frac{\omega^2 \vec{E}}{(v)^2} &= 0 \\ \bigtriangledown^2 \vec{E} + k^2 \vec{E} &= 0 \end{aligned} \tag{2.8}$$

where v and k are the velocity and wave vector of the propagating wave. Eq. (2.8) is

known as Helmholtz equation. SPW propagates along the x-direction, y direction perpendicular to the interface, $\vec{E} = \vec{E}(y)e^{i\beta x}$. The complex parameter $\beta = k_x$ is called the propagation constant of the traveling wave. Inserting this equation into Eq. (2.8),

$$\begin{aligned} \bigtriangledown^2(\vec{E}(y)e^{i\beta x}) + k^2\vec{E} &= 0 \\ (i\beta)^2\vec{E}(y)e^{i\beta x} + \frac{\partial^2\vec{E}}{\partial y^2} + k^2\vec{E} &= 0 \\ \frac{\partial^2\vec{E}}{\partial y^2} + (k^2 - \beta^2)\vec{E} &= 0 \end{aligned} \tag{2.9}$$

Eq. (2.9) is the starting point for the general analysis of guided electromagnetic modes in waveguides. We now need to find explicit expressions for the different field components of E and H:

from Eq. (2.3)

$$\bigtriangledown \times \vec{E} = -\frac{\partial\vec{B}}{\partial t}$$

$$\bigtriangledown \times \vec{E} = \begin{vmatrix} \hat{x} & \hat{y} & \hat{z} \\ \frac{\partial}{\partial x} & \frac{\partial}{\partial y} & \frac{\partial}{\partial z} \\ \vec{E}_x & E_y & E_z \end{vmatrix}$$

Equalize both sides and get:

$$\frac{\partial E_z}{\partial y} - \frac{\partial E_y}{\partial z} = i\omega\mu H_x \tag{2.10}$$

$$\frac{\partial \vec{E}_x}{\partial z} - \frac{\partial E_z}{\partial x} = i\omega\mu H_y \tag{2.11}$$

$$\frac{\partial E_z}{\partial x} - \frac{\partial E_x}{\partial y} = i\omega\mu H_z \tag{2.12}$$

Then, from Eq. (2.4)

$$\bigtriangledown \times \vec{H} = \frac{\partial\vec{D}}{\partial t}$$

$$\bigtriangledown \times \vec{H} = \begin{vmatrix} \hat{x} & \hat{y} & \hat{z} \\ \frac{\partial}{\partial x} & \frac{\partial}{\partial y} & \frac{\partial}{\partial z} \\ H_x & H_y & H_z \end{vmatrix}$$

Equalize both sides and get:

$$\frac{\partial H_z}{\partial y} - \frac{\partial H_y}{\partial z} = i\omega\varepsilon E_x \tag{2.13}$$

$$\frac{\partial H_x}{\partial z} - \frac{\partial H_z}{\partial x} = i\omega\varepsilon E_y \tag{2.14}$$

$$\frac{\partial H_z}{\partial x} - \frac{\partial H_x}{\partial y} = i\omega\varepsilon E_z \tag{2.15}$$

For propagation along the x-direction ($\frac{\partial}{\partial x} = i\beta$) and homogeneity in the z-direction $\frac{\partial}{\partial z} = 0$, this system of equations, Eq. (2.10) to Eq. (2.15) simplifiy to

$$\frac{\partial E_z}{\partial y} = i\omega\mu H_x \tag{2.16}$$

$$-i\beta E_z = i\omega\mu H_y \tag{2.17}$$

$$\frac{\partial E_x}{\partial y} - i\beta E_z = -i\omega\mu H_z \tag{2.18}$$

$$\frac{\partial H_z}{\partial y} = -i\omega\varepsilon E_x \tag{2.19}$$

$$i\beta H_z = i\omega\varepsilon E_y \tag{2.20}$$

$$\frac{\partial H_x}{\partial y} - i\beta H_z = i\omega\varepsilon E_z \tag{2.21}$$

For p-polarized mode, the system of governing equations, Eq. (2.19) and Eq. (2.20) simplify to

$$E_x = i\frac{1}{\omega\varepsilon}\frac{\partial H_z}{\partial y} \tag{2.22}$$

$$E_y = \frac{\beta}{\omega\varepsilon}H_z \tag{2.23}$$

refer to Eq. (2.9), the wave equation for p-polarized mode is

$$\frac{\partial^2 H_z}{\partial y^2} + (k^2 - \beta^2)H_z = 0 \tag{2.24}$$

For s-polarized modes, Eq. (2.16) and Eq. (2.17) simplify to

$$H_x = -i\frac{1}{\omega\mu}\frac{\partial E_z}{\partial y} \tag{2.25}$$

$$H_y = -\frac{\beta}{\omega\mu}E_z \tag{2.26}$$

and the wave equation for s-polarized mode is

$$\frac{\partial^2 E_z}{\partial y^2} + (k^2 - \beta^2)E_z = 0 \tag{2.27}$$

2.2 Surface Polariton In Single Interface

Let consider a geometry sustaining SP in a flat single interface between two mediums. The geometry of the interface is shown in Fig. (2.1). We will look into the solutions of the propagating wave confined to the interface,which with evanescent decay in the perpendicular y-direction.

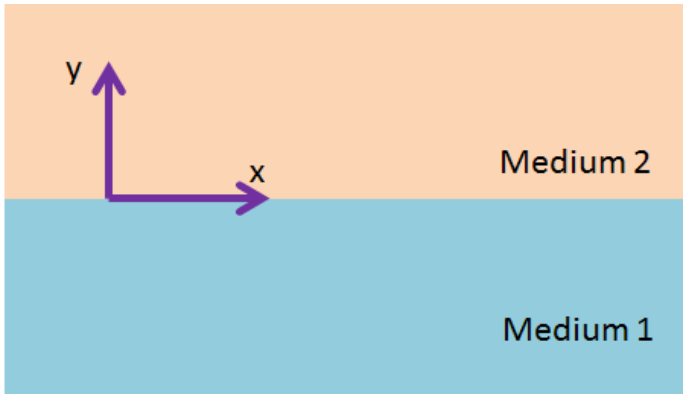

Figure 2.1: SP propagation in single interface

2.2.1 s-polarised SP

First, we will look into s-polarized solutions, with considering two different mediums where $y < 0$ is medium 1 and $y > 0$ is medium 2.

For $y > 0$ (medium 2):

$$E_z = A_2 e^{i(k_x^s x - k_{2y}^s y)}$$

from Eq. (2.25),

$$\begin{aligned} H_x &= -i\frac{1}{\omega\mu_2}\frac{\partial E_z}{\partial y} \\ &= -A_2\frac{1}{\omega\mu_2}(k_{2y}^s)e^{i(k_x^s x - k_{2y}^s y)} \end{aligned} \tag{2.28}$$

from Eq. (2.26),

$$\begin{aligned} H_y &= -\frac{k_x^s}{\omega\mu_2}E_z \\ &= -A_2\frac{k_x^s}{\omega\mu_2}e^{i(k_x^s x - k_{2y}^s y)} \end{aligned} \tag{2.29}$$

For $y < 0$ (medium 1):

$$E_z = A_1 e^{i(k_x^s x + k_{1y}^s y)}$$

from Eq. (2.25),

$$\begin{aligned} H_x &= -i\frac{1}{\omega\mu_1}\frac{\partial E_z}{\partial y} \\ &= A_1\frac{1}{\omega\mu_1}(k_{1y}^s)e^{i(k_x^s x + k_{1y}^s y)} \end{aligned} \tag{2.30}$$

from Eq. (2.26),

$$\begin{aligned} H_y &= -\frac{k_x^s}{\omega\mu_1}E_z \\ &= -A_1\frac{k_x^s}{\omega\mu_1}e^{i(k_x^s x + k_{1y}^s y)} \end{aligned} \tag{2.31}$$

The continuity of E_z and H_x at the interface gives:

$$A_2 e^{i(k_x^s x - k_{2y}^s y)} = A_1 e^{i(k_x^s x + k_{1y}^s y)} \tag{2.32}$$

$$-A_2\frac{1}{\omega\mu_2}(k_{2y}^s)e^{i(k_x^s x - k_{2y}^s y)} = A_1\frac{1}{\omega\mu_1}(k_{1y}^s)e^{i(k_x^s x + k_{1y}^s y)} \tag{2.33}$$

At interface, $y = 0$, from Eq. (2.32):

$$A_2 e^{i(k_x^s x - k_{2y}^s(0))} = A_1 e^{i(k_x^s x + k_{1y}^s(0))}$$

$$A_2 = A_1 \tag{2.34}$$

from Eq. (2.33):

$$-A_2 \frac{1}{\omega\mu_2}(k_{2y}^s) e^{i(k_x^s x - k_{2y}^s(0))} = A_1 \frac{1}{\omega\mu_1}(k_{1y}^s) e^{i(k_x^s x + k_{1y}^s(0))}$$

$$-\frac{k_{2y}^s}{\mu_2} = \frac{k_{1y}^s}{\mu_1} \tag{2.35}$$

The expression for E_z further has to fulfill the wave equation (2.27):

$$\frac{\partial^2 (A_j e^{i(k_x^s x - k_{jy}^s y))}}{\partial y^2} + (k^2 - k_x^{s2}) A_j e^{i(k_x^s x - k_{jy}^s y)} = 0$$

$$k_{jy}^{s\ 2} = (\frac{\omega}{\frac{1}{\sqrt{\varepsilon_i \mu_i \varepsilon_0 \mu_0}}})^2 - k_x^{s2}$$

$$k_{jy}^{s\ 2} = \varepsilon_i \mu_i (\frac{\omega}{c})^2 - k_x^{s2} \tag{2.36}$$

where $j = 1, 2$. Tangential wavevector for s-polarized light is found accordingly, substitute Eq. (2.36) into Eq. (2.35):

$$-\frac{\sqrt{\varepsilon_2 \mu_2 (\frac{\omega}{c})^2 - k_x^{s2}}}{\mu_2} = \frac{\sqrt{\varepsilon_1 \mu_1 (\frac{\omega}{c})^2 - k_x^{s2}}}{\mu_1}$$

$$k_x^s = \frac{\omega}{c} \sqrt{(\frac{\varepsilon_1 \mu_2 - \mu_1 \varepsilon_2}{\mu_2 - \mu_1}) \frac{\mu_1 \mu_2}{\mu_1 + \mu_2}} \tag{2.37}$$

when $\varepsilon_1 = \varepsilon_2$, Eq. (2.37) reduce to

$$k_x^s = \frac{\omega}{c} \sqrt{\varepsilon_1 \frac{\mu_1 \mu_2}{\mu_1 + \mu_2}} \tag{2.38}$$

in close analogy to the usual expression for p-polarized case (next part). Next, we will derive the equations of normal wavevector. Substitute Eq. (2.37) into Eq. (2.36),

$$k_{jy}^{s\ 2} = \varepsilon_i \mu_i (\frac{\omega}{c})^2 - (\frac{\omega}{c})^2 (\frac{\varepsilon_1 \mu_2 - \mu_1 \varepsilon_2}{\mu_2 - \mu_1}) \frac{\mu_1 \mu_2}{\mu_1 + \mu_2}$$

$$k_{jy}^{s\ 2} = (\frac{\omega}{c})^2 \frac{\mu_1^2 (\mu_2 \varepsilon_2 - \varepsilon_i \mu_i) + \mu_2^2 (\varepsilon_i \mu_i - \varepsilon_1 \mu_1)}{(\mu_2 - \mu_1)(\mu_1 + \mu_2)}$$

put $i = 1$,

$$k_{1y}^{s\ 2} = (\frac{\omega}{c})^2 \frac{\mu_1^2(\mu_2\varepsilon_2 - \varepsilon_1\mu_1) + \mu_2^2(\varepsilon_1\mu_1 - \varepsilon_1\mu_1)}{(\mu_2 - \mu_1)(\mu_1 + \mu_2)}$$
$$k_{1y}^{s} = \frac{\omega}{c}\mu_1 \sqrt{\frac{\mu_2\varepsilon_2 - \varepsilon_1\mu_1}{(\mu_2 - \mu_1)(\mu_1 + \mu_2)}} \tag{2.39}$$

put $i = 2$,

$$k_{2y}^{s\ 2} = (\frac{\omega}{c})^2 \frac{\mu_1^2(\mu_2\varepsilon_2 - \varepsilon_2\mu_2) + \mu_2^2(\varepsilon_2\mu_2 - \varepsilon_1\mu_1)}{(\mu_2 - \mu_1)(\mu_1 + \mu_2)}$$
$$k_{2y}^{s} = \frac{\omega}{c}\mu_2 \sqrt{\frac{\varepsilon_2\mu_2 - \varepsilon_1\mu_1}{(\mu_2 - \mu_1)(\mu_1 + \mu_2)}} \tag{2.40}$$

Combining Eq. (2.39) and Eq. (2.40), we have normal wavevectors for s-polarised wave as

$$k_{jy}^{s} = \frac{\omega}{c}\mu_j \sqrt{\frac{\varepsilon_2\mu_2 - \varepsilon_1\mu_1}{(\mu_2 - \mu_1)(\mu_1 + \mu_2)}} \tag{2.41}$$

where $j = 1\, or\, 2$.

2.2.2 p-polarised SP

Now, we move to p-polarised modes and derive the dispersion relation. For $y > 0$ (medium 2),

$$H_z = A_2 e^{i(k_x^p x - k_{2y}^p y)}$$

from Eq. (2.22),

$$\begin{aligned} E_x &= i\frac{1}{\omega\varepsilon_2}\frac{\partial H_z}{\partial y} \\ &= A_2 \frac{1}{\omega\varepsilon_2}(k_{2y}^p) e^{i(k_x^p x - k_{2y}^p y)} \end{aligned} \tag{2.42}$$

from Eq. (2.23),

$$\begin{aligned} E_y &= \frac{k_x^p}{\omega\varepsilon_2} H_z \\ &= A_2 \frac{k_x^p}{\omega\varepsilon_2} e^{i(k_x^p x - k_{2y}^p y)} \end{aligned} \tag{2.43}$$

For $y < 0$ (medium 1):

$$H_z = A_1 e^{i(k_x^p x + k_{1y}^p y)}$$

from Eq. (2.22),

$$\begin{aligned} E_x &= i\frac{1}{\omega\varepsilon_1}\frac{\partial H_z}{\partial y} \\ &= -A_1\frac{1}{\omega\varepsilon_1}(k_{1y}^p)e^{i(k_x^p x + k_{1y}^p y)} \end{aligned} \tag{2.44}$$

from Eq. (2.23),

$$\begin{aligned} E_y &= \frac{k_x^p}{\omega\varepsilon_1}H_z \\ &= A_1\frac{k_x^p}{\omega\varepsilon_1}e^{i(k_x^p x + k_{1y}^p y)} \end{aligned} \tag{2.45}$$

The continuity of H_z and E_x at the interface gives:

$$A_2 e^{i(k_x^p x - k_{2y}^p y)} = A_1 e^{i(k_x^p x + k_{1y}^p y)} \tag{2.46}$$

$$A_2\frac{1}{\omega\varepsilon_2}(k_{2y}^p)e^{i(k_x^p x - k_{2y}^p y)} = -A_1\frac{1}{\omega\varepsilon_1}(k_{1y}^p)e^{i(k_x^p x + k_{1y}^p y)} \tag{2.47}$$

At interface, $y = 0$, from Eq. (2.46):

$$\begin{aligned} A_2 e^{i(k_x^p x - k_{2y}^p(0))} &= A_1 e^{i(k_x^p x + k_{1y}^p(0))} \\ A_2 &= A_1 \end{aligned} \tag{2.48}$$

from Eq. (2.47):

$$\begin{aligned} A_2\frac{1}{\omega\varepsilon_2}(k_{2y}^p)e^{i(k_x^p x - k_{2y}^p(0))} &= -A_1\frac{1}{\omega\varepsilon_1}(k_{1y}^p)e^{i(k_x^p x + k_{1y}^p(0))} \\ \frac{k_{2y}^p}{\varepsilon_2} &= -\frac{k_{1y}^p}{\varepsilon_1} \end{aligned} \tag{2.49}$$

The expression for H_z further has to fulfill the wave equation (2.24):

$$\frac{\partial^2(A_j e^{i(k_x^p x - k_{jy}^p y))}}{\partial y^2} + (k^2 - k_x^{p2})A_j e^{i(k_x^p x - k_{jy}^p y)} = 0$$

$$k_{jy}^{p\ 2} = (\frac{\omega}{\frac{1}{\sqrt{\varepsilon_i \mu_i \varepsilon_0 \mu_0}}})^2 - k_x^{p2}$$

$$k_{jy}^{p\ 2} = \varepsilon_i \mu_i (\frac{\omega}{c})^2 - k_x^{p2} \tag{2.50}$$

where $j = 1,2$. This is exactly the same as the s-polarized solution. The tangential wavevector for s-polarized light is found accordingly, substitute Eq. (2.50) into Eq. (2.49):

$$-\frac{\sqrt{\varepsilon_2 \mu_2 (\frac{\omega}{c})^2 - k_x^{p2}}}{\varepsilon_2} = \frac{\sqrt{\varepsilon_1 \mu_1 (\frac{\omega}{c})^2 - k_x^{p2}}}{\varepsilon_1}$$

$$k_x^p = \frac{\omega}{c}\sqrt{\frac{(\mu_1 \varepsilon_2 - \varepsilon_1 \mu_2)\varepsilon_1 \varepsilon_2}{(\varepsilon_2 - \varepsilon_1)(\varepsilon_1 + \varepsilon_2)}} \tag{2.51}$$

For nonmagnetic materials when $\mu_1 = \mu_2 = 1$, Eq. (2.51) reduces to

$$k_x^p = \frac{\omega}{c}\sqrt{\frac{\varepsilon_1 \varepsilon_2}{\varepsilon_1 + \varepsilon_2}} \tag{2.52}$$

Eq. (2.51) generalizes the usual plasmonic enhancement of p-polarization to magnetic materials while Eq. (2.37) is obtained by interchanging μ and ε. Next, we will derive the equations of normal wavevector. Substituting Eq. (2.51) into Eq. (2.50),

$$k_{jy}^{p\ 2} = \varepsilon_i \mu_i (\frac{\omega}{c})^2 - (\frac{\omega}{c})^2 \frac{(\mu_1 \varepsilon_2 - \varepsilon_1 \mu_2)\varepsilon_1 \varepsilon_2}{(\varepsilon_1 - \varepsilon_2)(\varepsilon_1 + \varepsilon_2)}$$

$$= (\frac{\omega}{c})^2 (\frac{\varepsilon_1^2(\mu_2 \varepsilon_2 - \varepsilon_i \mu_i) + \varepsilon_2^2(\varepsilon_i \mu_i - \varepsilon_1 \mu_1)}{(\varepsilon_2 - \varepsilon_1)(\varepsilon_1 + \varepsilon_2)})$$

for $i = 1$,

$$k_{1y}^{p\ 2} = (\frac{\omega}{c})^2 (\frac{\varepsilon_1^2(\mu_2 \varepsilon_2 - \varepsilon_1 \mu_1) + \varepsilon_2^2(\varepsilon_1 \mu_1 - \varepsilon_1 \mu_1)}{(\varepsilon_2 - \varepsilon_1)(\varepsilon_1 + \varepsilon_2)})$$

$$k_{1y}^p = \frac{\omega}{c}\varepsilon_1 \sqrt{\frac{(\mu_2 \varepsilon_2 - \varepsilon_1 \mu_1)}{(\varepsilon_2 - \varepsilon_1)(\varepsilon_1 + \varepsilon_2)}} \tag{2.53}$$

for $i = 2$,

$$k_{2y}^{p\ 2} = (\frac{\omega}{c})^2(\frac{\varepsilon_1^2(\mu_2\varepsilon_2 - \varepsilon_2\mu_2) + \varepsilon_2^2(\varepsilon_2\mu_2 - \varepsilon_1\mu_1)}{(\varepsilon_2 - \varepsilon_1)(\varepsilon_1 + \varepsilon_2)})$$
$$k_{2y}^{p} = \frac{\omega}{c}\varepsilon_2\sqrt{\frac{(\mu_2\varepsilon_2 - \varepsilon_1\mu_1)}{(\varepsilon_2 - \varepsilon_1)(\varepsilon_1 + \varepsilon_2)}} \tag{2.54}$$

Combining Eq. (2.53) and Eq. (2.54) , we have normal wavevectors for p-polarised wave as

$$k_{jy}^{p} = \frac{\omega}{c}\varepsilon_j\sqrt{\frac{(\mu_2\varepsilon_2 - \varepsilon_1\mu_1)}{(\varepsilon_2 - \varepsilon_1)(\varepsilon_1 + \varepsilon_2)}} \tag{2.55}$$

where $j = 1$ or 2.

2.3 Surface Polariton In Double Interface

In this section, we turn our focus to thin slab. Consider a thin slab of thinkness $2a$ located between $y = a$ and $y = -a$ with media 1 sandwiched between two infinite half medium 2 and 3. The geometry is shown in Fig. (2.2).

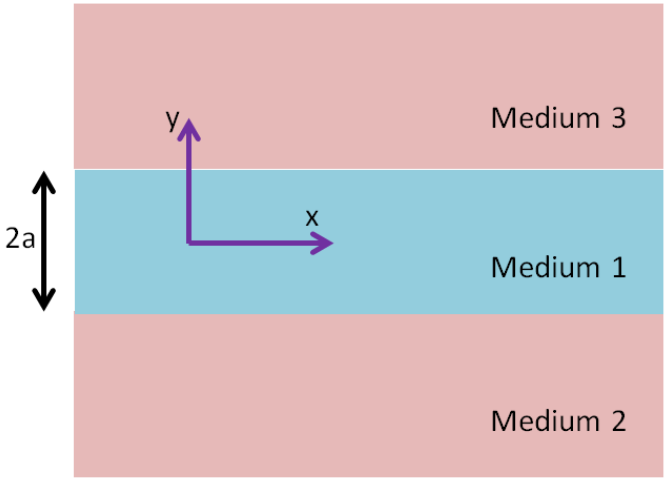

Figure 2.2: SP propagation in thin slab

2.3.1 s-polarized SP

In the case of a thin film, the electromagnetic fields of both surfaces interact and the frequency splits into a high-frequency mode and a low-frequency mode. Look into

s-polarized SP, for $y > a$ (medium3), the field components are:

$$E_z = A\exp(i\beta x)\exp(-k_3 y) \tag{2.56}$$

from Eq. (2.25),

$$\begin{aligned} H_x &= -i\frac{1}{\omega\mu_0\mu_3}\frac{\partial(A\exp(i\beta x)\exp(-k_3 y))}{\partial y} \\ &= iA\frac{1}{\omega\mu_0\mu_3}k_3\exp(i\beta x)\exp(-k_3 y) \end{aligned} \tag{2.57}$$

from Eq. (2.26),

$$\begin{aligned} H_y &= -\frac{\beta}{\omega\mu_0\mu_3}(A\exp(i\beta x)\exp(-k_3 y)) \\ &= -A\frac{\beta}{\omega\mu_0\mu_3}\exp(i\beta x)\exp(-k_3 y) \end{aligned} \tag{2.58}$$

while for$y < -a$ (medium2),

$$E_z = B\exp(i\beta x)\exp(k_2 y) \tag{2.59}$$

$$\begin{aligned} H_x &= -i\frac{1}{\omega\mu_0\mu_2}\frac{\partial(B\exp(i\beta x)\exp(k_2 y))}{\partial y} \\ &= -iB\frac{1}{\omega\mu_0\mu_2}k_2\exp(i\beta x)\exp(k_2 y) \end{aligned} \tag{2.60}$$

$$\begin{aligned} H_y &= -\frac{\beta}{\omega\mu_0\mu_2}(B\exp(i\beta x)\exp(k_2 y)) \\ &= -B\frac{\beta}{\omega\mu_0\mu_2}\exp(i\beta x)\exp(k_2 y) \end{aligned} \tag{2.61}$$

For simplicity, we denote the component of the wave vector perpendicular to the interfaces simply as $k_i = k_{y,i}$. The fields decay exponentially in the medium 2 and medium 3. In the core region $-a < y < a$ (medium1), the modes localized at the bottom and top interface couple, yielding

$$E_z = C\exp(i\beta x)\exp(k_1 y) + D\exp(i\beta x)\exp(-k_1 y) \tag{2.62}$$

$$H_x = -i\frac{1}{\omega\mu_0\mu_1}\frac{\partial(C\exp(i\beta x)\exp(k_1 y)+D\exp(i\beta x)\exp(-k_1 y))}{\partial y}$$
$$= -iC\frac{1}{\omega\mu_0\mu_r}k_1\exp(i\beta x)\exp(k_1 y)+iD\frac{1}{\omega\mu_0\mu_1}k_1\exp(i\beta x)\exp(-k_1 y) \quad (2.63)$$

$$H_y = -\frac{\beta}{\omega\mu_0\mu_1}(C\exp(i\beta x)\exp(k_1 y)+D\exp(i\beta x)\exp(-k_1 y))$$
$$= -C\frac{\beta}{\omega\mu_0\mu_1}\exp(i\beta x)\exp(k_1 y)-D\frac{\beta}{\omega\mu_0\mu_1}\exp(i\beta x)\exp(-k_1) \quad (2.64)$$

The continuity of E_z at $y = a$ givess:

$$A\exp(i\beta x)\exp(-k_3 y) = C\exp(i\beta x)\exp(k_1 y)+D\exp(i\beta x)\exp(-k_1 y)$$
$$A\exp(-k_3 a) = C\exp(k_1 a)+D\exp(-k_1 a) \quad (2.65)$$

The continuity of H_x at $y = a$ gives:

$$\frac{iA}{\omega\mu_0\mu_1}k_3\exp(i\beta x)\exp(-k_3 y) = -\frac{iC}{\omega\mu_0\mu_1}k_1\exp(i\beta x)\exp(k_1 y)+\frac{iD}{\omega\mu_0\mu_1}k_1\exp(i\beta x)\exp(-k_1 y)$$
$$\frac{A}{\mu_3}k_3\exp(-k_3 a) = -\frac{C}{\mu_1}k_1\exp(k_1 a)+\frac{D}{\mu_1}k_1\exp(-k_1 a) \quad (2.66)$$

The continuity of E_z at $y = -a$ gives:

$$B\exp(i\beta x)\exp(k_2 y) = C\exp(i\beta x)\exp(k_1 y)+D\exp(i\beta x)\exp(-k_1 y)$$
$$B\exp(-k_2 a) = C\exp(-k_1 a)+D\exp(k_1 a) \quad (2.67)$$

The continuity of H_x at $y = -a$ gives:

$$-\frac{iB}{\omega\mu_0\mu_2}k_2\exp(i\beta x)\exp(k_2 y) = -\frac{iC}{\omega\mu_0\mu_r}k_1\exp(i\beta x)\exp(k_1 y)+\frac{iD}{\omega\mu_0\mu_1}k_1\exp(i\beta x)\exp(-k_1 y)$$
$$-\frac{B}{\mu_2}k_2\exp(-k_2 a) = -\frac{C}{\mu_1}k_1\exp(-k_1 a)+\frac{D}{\mu_1}k_1\exp(k_1 a) \quad (2.68)$$

E_z further has to fulfill the wave equation (2.27) in the three distinct regions for s-polarized wave, working is same as the p-polarized wave(look at p-polarized solution).

$$k_i^2 = \beta^2 - k_0^2\varepsilon_i\mu_i \quad (2.69)$$

where i=1,2,3. For the continuity solutions, Eq. (2.65), Eq. (2.66), Eq. (2.67), Eq. (2.68), they are similiar with the continuity solutions for the p-polarized wave.(look at next section with changing ε_i to μ_i.) Hence, we get

$$\exp(-4k_1a) = \left(\frac{\frac{k_1}{\mu_1}+\frac{k_2}{\mu_2}}{\frac{k_1}{\mu_1}-\frac{k_2}{\mu_2}}\right)\left(\frac{\frac{k_1}{\mu_1}+\frac{k_3}{\mu_3}}{\frac{k_1}{\mu_1}-\frac{k_3}{\mu_3}}\right) \tag{2.70}$$

For infinite thickness $a \to \infty$, Eq. (2.70) reduces to Eq. (2.35), the equations of two uncoupled SPP at the respective interfaces for s-polarized wave are:

$$\begin{aligned}
\exp(-4k_1\infty) &= \left(\frac{\frac{k_1}{\mu_1}+\frac{k_2}{\mu_2}}{\frac{k_1}{\mu_1}-\frac{k_2}{\mu_2}}\right)\left(\frac{\frac{k_1}{\mu_1}+\frac{k_3}{\mu_3}}{\frac{k_1}{\mu_1}-\frac{k_3}{\mu_3}}\right) \\
0 &= \left(\frac{k_1}{\mu_1}+\frac{k_2}{\mu_2}\right)\left(\frac{k_1}{\mu_1}+\frac{k_3}{\mu_3}\right) \\
\frac{k_1}{\mu_1} &= -\frac{k_2}{\mu_2} \quad ; \quad \frac{k_1}{\mu_1} = -\frac{k_3}{\mu_3}
\end{aligned} \tag{2.71}$$

Let medium 2 is identical with medium 3, hence $\mu_2 = \mu_3$ and thus $k_2 = k_3$. The dispersion relation Eq. (2.70) can be split into a pair of equations: (look at p-polarized solution)

$$\tanh(k_1a) = -\frac{\mu_1 k_2}{\mu_2 k_1} \tag{2.72}$$

$$\coth(k_1a) = -\frac{\mu_1 k_2}{\mu_2 k_1} \tag{2.73}$$

Eq. (2.72) is s-polarised odd mode(anti-symmetry) while Eq. (2.73) is s-polarised even modes(symmetry). There is no analytic solution method to solve the equations above, hence we will solve these dispersion formula numerically in chapter 5.

2.3.2 p-polarised SP

We now turn into p-polarized SP. The solutions of electric and magnetic field are found. For $y > a$(medium 3),

$$H_z = A\exp(i\beta x)\exp(-k_3 y) \tag{2.74}$$

$$E_x = iA\frac{1}{\omega\varepsilon_0\varepsilon_3}k_3\exp(i\beta x)\exp(-k_3 y) \tag{2.75}$$

$$E_y = -A\frac{\beta}{\omega\varepsilon_0\varepsilon_3}\exp(i\beta x)\exp(-k_3 y) \tag{2.76}$$

while for $y < -a$(medium 2)

$$H_z = B\exp(i\beta x)\exp(k_2 y) \tag{2.77}$$

$$E_x = -iB\frac{1}{\omega\varepsilon_0\varepsilon_2}k_2\exp(i\beta x)\exp(k_2 y) \tag{2.78}$$

$$E_y = -B\frac{\beta}{\omega\varepsilon_0\varepsilon_2}\exp(i\beta x)\exp(k_2 y) \tag{2.79}$$

The fields decay exponentially in the medium 2 and medium 3. Also for simplicity, we denote the component of the wave vector perpendicular to the interfaces simply as $k_i = k_{y,i}$. In the core region $-a < y < a$, the modes localized at the bottom and top interface couple, yielding

$$H_z = C\exp(i\beta x)\exp(k_1 y) + D\exp(i\beta x)\exp(-k_1 y) \tag{2.80}$$

$$E_x = -iC\frac{1}{\omega\varepsilon_0\varepsilon_1}k_1\exp(i\beta x)\exp(k_1 y) + iD\frac{1}{\omega\varepsilon_0\varepsilon_1}k_1\exp(i\beta x)\exp(-k_1 y) \tag{2.81}$$

$$E_y = C\frac{\beta}{\omega\varepsilon_0\varepsilon_1}\exp(i\beta x)\exp(k_1 y) + D\frac{\beta}{\omega\varepsilon_0\varepsilon_1}\exp(i\beta x)\exp(-k_1 y) \tag{2.82}$$

The continuity of H_z at y=a gives:

$$\begin{aligned} A\exp(i\beta x)\exp(-k_3 y) &= C\exp(i\beta x)\exp(k_1 y) + D\exp(i\beta x)\exp(-k_1 y) \\ A\exp(-k_3 a) &= C\exp(k_1 a) + D\exp(-k_1 a) \end{aligned} \tag{2.83}$$

The continuity of E_x at y=a gives:

$$\begin{aligned} \frac{iA}{\omega\varepsilon_0\varepsilon_3}k_3\exp(i\beta x)\exp(-k_3 y) &= -\frac{iC}{\omega\varepsilon_0\varepsilon_1}k_1\exp(i\beta x)\exp(k_1 y) + \frac{iD}{\omega\varepsilon_0\varepsilon_1}k_1\exp(i\beta x)\exp(-k_1 y) \\ \frac{A}{\varepsilon_3}k_3\exp(-k_3 a) &= -\frac{C}{\varepsilon_1}k_1\exp(k_1 a) + \frac{D}{\varepsilon_1}k_1\exp(-k_1 a) \end{aligned} \tag{2.84}$$

The continuity of H_z at y=-a gives:

$$\begin{aligned} B\exp(i\beta x)\exp(k_2 y) &= C\exp(i\beta x)\exp(k_1 y) + D\exp(i\beta x)\exp(-k_1 y) \\ B\exp(-k_2 a) &= C\exp(-k_1 a) + D\exp(k_1 a) \end{aligned} \tag{2.85}$$

The continuity of E_x at y=-a gives:

$$-\frac{iB}{\omega\varepsilon_0\varepsilon_2}k_2\exp(i\beta x)\exp(k_2 y) = -\frac{iC}{\omega\varepsilon_0\varepsilon_1}k_1\exp(i\beta x)\exp(k_1 y) + \frac{iD}{\omega\varepsilon_0\varepsilon_1}k_1\exp(i\beta x)\exp(-k_1 y)$$

$$-\frac{B}{\varepsilon_2}k_2\exp(-k_2 a) = -\frac{C}{\varepsilon_1}k_1\exp(-k_1 a) + \frac{D}{\varepsilon_1}k_1\exp(k_1 a) \quad (2.86)$$

H_z further has to fulfill the wave equation (2.24) in the three distinct regions for p-polarized wave:

in medium 3, $y > a$

$$\frac{\partial^2(A\exp(i\beta x)\exp(-k_3 y))}{\partial y^2} + (k^2-\beta^2)(A\exp(i\beta x)\exp(-k_3 y)) = 0$$

$$k_3^2 = \beta^2 - (\frac{\omega}{\frac{1}{\sqrt{\varepsilon_3\mu_3\varepsilon_0\mu_0}}})^2$$

$$k_3^2 = \beta^2 - k_0^2\varepsilon_3\mu_3 \quad (2.87)$$

in medium 2, $y < -a$

$$\frac{\partial^2(B\exp(i\beta x)\exp(k_2 y))}{\partial y^2} + (k^2-\beta^2)(B\exp(i\beta x)\exp(k_2 y)) = 0$$

$$k_2^2 = \beta^2 - (\frac{\omega}{\frac{1}{\sqrt{\varepsilon_2\mu_2\varepsilon_0\mu_0}}})^2$$

$$k_2^2 = \beta^2 - k_0^2\varepsilon_2\mu_2 \quad (2.88)$$

in thin film(medium 1), $-a < y < a$

$$\frac{\partial^2(C\exp(i\beta x)\exp(k_1 y) + D\exp(i\beta x)\exp(-k_1 y)}{\partial y^2}$$

$$+(k^2-\beta^2)(C\exp(i\beta x)\exp(k_1 y) + D\exp(i\beta x)\exp(-k_1 y) = 0$$

$$k_1^2 = \beta^2 - (\frac{\omega}{\frac{1}{\sqrt{\varepsilon_1\mu_1\varepsilon_0\mu_0}}})^2$$

$$k_1^2 = \beta^2 - k_0^2\varepsilon_1\mu_1 \quad (2.89)$$

hence, comparing Eq. (2.87), Eq. (2.88) and Eq. (2.89) , we get

$$k_i^2 = \beta^2 - k_0^2\varepsilon_i\mu_i \quad (2.90)$$

for i=1,2,3.

From Eq. (2.83), Eq. (2.84), Eq. (2.85) and Eq. (2.86), we have 4 equations as below:

$$A\exp(-k_3a) = C\exp(k_1a) + D\exp(-k_1a) \qquad (i)$$

$$\frac{A}{\varepsilon_3}k_3\exp(-k_3a) = -\frac{C}{\varepsilon_1}k_1\exp(k_1a) + \frac{D}{\varepsilon_1}k_1\exp(-k_1a) \qquad (ii)$$

$$B\exp(-k_2a) = C\exp(-k_1a) + D\exp(k_1a) \qquad (iii)$$

$$-\frac{B}{\varepsilon_2}k_2\exp(-k_2a) = -\frac{C}{\varepsilon_1}k_1\exp(-k_1a) + \frac{D}{\varepsilon_1}k_1\exp(k_1a) \qquad (iv)$$

Next, we will solve this 4 equations simultaneously, put (i) into (ii), (iii) into (iv) and add them together:

$$\frac{k_3}{\varepsilon_3}C\exp(k_1a) + \frac{k_3}{\varepsilon_3}D\exp(-k_1a) - \frac{k_2}{\varepsilon_2}C\exp(-k_1a) - \frac{k_2}{\varepsilon_2}D\exp(k_1a)$$
$$+\frac{k_1}{\varepsilon_1}C\exp(k_1a) - \frac{k_1}{\varepsilon_1}D\exp(-k_1a) + \frac{k_1}{\varepsilon_1}C\exp(-k_1a) - \frac{k_1}{\varepsilon_1}D\exp(k_1a) = 0$$

$$\downarrow$$

$$\exp(2k_1a)(C(\frac{k_3}{\varepsilon_3}+\frac{k_1}{\varepsilon_1}) - D(\frac{k_2}{\varepsilon_2}+\frac{k_1}{\varepsilon_1})) = D(\frac{k_1}{\varepsilon_1}-\frac{k_3}{\varepsilon_3}) - C(\frac{k_1}{\varepsilon_1}-\frac{k_2}{\varepsilon_2})$$

$$\exp(-2k_1a) = \frac{C(\frac{k_3}{\varepsilon_3}+\frac{k_1}{\varepsilon_1}) - D(\frac{k_2}{\varepsilon_2}+\frac{k_1}{\varepsilon_1})}{D(\frac{k_1}{\varepsilon_1}-\frac{k_3}{\varepsilon_3}) - C(\frac{k_1}{\varepsilon_1}-\frac{k_2}{\varepsilon_2})} \qquad (2.91)$$

put (i) into (ii) and rearrange for C.

$$C = \left(D(\frac{\frac{k_1}{\varepsilon_1}\exp(-k_1a) - \frac{k_3}{\varepsilon_3}\exp(-k_1a)}{\frac{k_3}{\varepsilon_3}\exp(k_1a) + \frac{k_1}{\varepsilon_1}\exp(k_1a)}) \right) \qquad (2.92)$$

Then, substitute Eq. (2.92) into Eq. (2.91).

$$\exp(-2k_1a) = \frac{\left(D(\frac{\frac{k_1}{\varepsilon_1}\exp(-k_1a)-\frac{k_3}{\varepsilon_3}\exp(-k_1a)}{\frac{k_3}{\varepsilon_3}\exp(k_1a)+\frac{k_1}{\varepsilon_1}\exp(k_1a)})\right)(\frac{k_3}{\varepsilon_3}+\frac{k_1}{\varepsilon_1}) - D(\frac{k_2}{\varepsilon_2}+\frac{k_1}{\varepsilon_1})}{D(\frac{k_1}{\varepsilon_1}-\frac{k_3}{\varepsilon_3}) - \left(D(\frac{\frac{k_1}{\varepsilon_1}\exp(-k_1a)-\frac{k_3}{\varepsilon_3}\exp(-k_1a)}{\frac{k_3}{\varepsilon_3}\exp(k_1a)+\frac{k_1}{\varepsilon_1}\exp(k_1a)})\right)(\frac{k_1}{\varepsilon_1}-\frac{k_2}{\varepsilon_2})}$$

$$= \left[\frac{\exp(-k_1a) - \exp(k_1a)(\frac{\frac{k_2}{\varepsilon_2}+\frac{k_1}{\varepsilon_1}}{\frac{k_1}{\varepsilon_1}-\frac{k_3}{\varepsilon_3}})}{\exp(k_1a) - \exp(-k_1a)(\frac{\frac{k_1}{\varepsilon_1}-\frac{k_2}{\varepsilon_2}}{\frac{k_3}{\varepsilon_3}+\frac{k_1}{\varepsilon_1}})}\right]$$

$$\downarrow$$

$$\exp(-k_1a) - \exp(-3k_1a)(\frac{\frac{k_1}{\varepsilon_1}-\frac{k_2}{\varepsilon_2}}{\frac{k_3}{\varepsilon_3}+\frac{k_1}{\varepsilon_1}}) = \exp(-k_1a) - \exp(k_1a)(\frac{\frac{k_2}{\varepsilon_2}+\frac{k_1}{\varepsilon_1}}{\frac{k_1}{\varepsilon_1}-\frac{k_3}{\varepsilon_3}})$$

$$\exp(-4k_1a) = \left(\frac{\frac{k_1}{\varepsilon_1}+\frac{k_2}{\varepsilon_2}}{\frac{k_1}{\varepsilon_1}-\frac{k_2}{\varepsilon_2}}\right)\left(\frac{\frac{k_1}{\varepsilon_1}+\frac{k_3}{\varepsilon_3}}{\frac{k_1}{\varepsilon_1}-\frac{k_3}{\varepsilon_3}}\right) \tag{2.93}$$

For infinite thickness $a \to \infty$, Eq. (2.93) reduces to Eq. (2.49), the equations of two uncoupled SPP at the respective interfaces.

$$\exp(-4k_1\infty) = \left(\frac{\frac{k_1}{\varepsilon_1}+\frac{k_2}{\varepsilon_2}}{\frac{k_1}{\varepsilon_1}-\frac{k_2}{\varepsilon_2}}\right)\left(\frac{\frac{k_1}{\varepsilon_1}+\frac{k_3}{\varepsilon_3}}{\frac{k_1}{\varepsilon_1}-\frac{k_3}{\varepsilon_3}}\right)$$

$$0 = \left(\frac{k_1}{\varepsilon_1}+\frac{k_2}{\varepsilon_2}\right)\left(\frac{k_1}{\varepsilon_1}+\frac{k_3}{\varepsilon_3}\right)$$

$$\frac{k_1}{\varepsilon_1} = -\frac{k_2}{\varepsilon_2} \quad ; \quad \frac{k_1}{\varepsilon_1} = -\frac{k_3}{\varepsilon_3} \tag{2.94}$$

Let medium 2 is identical to medium 3, hence $\varepsilon_2 = \varepsilon_3$ and thus $k_2 = k_3$

$$\exp(-4k_1a) = \left(\frac{\frac{k_1}{\varepsilon_1}+\frac{k_2}{\varepsilon_2}}{\frac{k_1}{\varepsilon_1}-\frac{k_2}{\varepsilon_2}}\right)\left(\frac{\frac{k_1}{\varepsilon_1}+\frac{k_2}{\varepsilon 2}}{\frac{k_1}{\varepsilon_1}-\frac{k_2}{\varepsilon_2}}\right)$$

$$= \left(\frac{\varepsilon_2 k_1 + \varepsilon_1 k_2}{\varepsilon_2 k_1 - \varepsilon_1 k_2}\right)^2 \tag{2.95}$$

Taking the positive solution,

$$\begin{aligned} \exp(-2k_1a) &= \frac{\varepsilon_2 k_1 + \varepsilon_1 k_2}{\varepsilon_2 k_1 - \varepsilon_1 k_2} \\ \frac{\exp(k_1a) - \exp(-k_1a)}{\exp(k_1a) + \exp(-k_1a)} &= -\frac{\varepsilon_1 k_2}{\varepsilon_2 k_1} \\ \tanh(k_1a) &= -\frac{\varepsilon_1 k_2}{\varepsilon_2 k_1} \end{aligned} \tag{2.96}$$

then the negative solution,

$$\begin{aligned} -\exp(-2k_1a) &= \frac{\varepsilon_2 k_1 + \varepsilon_1 k_2}{\varepsilon_2 k_1 - \varepsilon_1 k_2} \\ \frac{\exp(k_1a) + \exp(-k_1a)}{\exp(k_1a) - \exp(-k_1a)} &= -\frac{\varepsilon_1 k_2}{\varepsilon_2 k_1} \\ \coth(k_1a) &= -\frac{\varepsilon_1 k_2}{\varepsilon_2 k_1} \end{aligned} \tag{2.97}$$

Eq. (2.96) is p-polarised odd mode(anti-symmetry) while Eq. (2.97) is p-polarised even mode (symmetry). There is no analytic solution method to solve the equations above, hence we will solve these dispersion formula numerically in chapter 5.

2.3.3 Surface plasmon polariton in non-magnetic thin metal slab

Collective electronic excitations at metal surfaces are well known to play a key role in a wide spectrum of science. Thin metal slab are also known to support surface collective oscillations. For this geometry, the electromagnetic fields of both surfaces interact and split into two new conditions depending on whether electrons in the two surfaces oscillate in phase or not in phase. Next, we will solve for SP dispersions in thin metal slab.
For large β , $k_1 = k_2 = \beta$, Eq. (2.96) become

$$\begin{aligned} \tanh(k_1a) &= -\frac{\varepsilon_1 k_2}{\varepsilon_2 k_1} \\ \frac{\exp(\beta a) - \exp(-\beta a)}{\exp(\beta a) + \exp(-\beta a)} &= -\frac{\varepsilon_1 \beta}{\varepsilon_2 \beta} \\ \frac{(\varepsilon_2 + \varepsilon_1)}{(\varepsilon_2 - \varepsilon_1)} &= \exp(-2\beta a) \end{aligned} \tag{2.98}$$

while Eq. (2.97) become

$$\begin{aligned}
\coth(k_1 a) &= -\frac{\varepsilon_1 k_2}{\varepsilon_2 k_1} \\
\frac{\exp(\beta a)+\exp(-\beta a)}{\exp(\beta a)-\exp(-\beta a)} &= -\frac{\varepsilon_1 \beta}{\varepsilon_2 \beta} \\
\frac{(\varepsilon_2+\varepsilon_1)}{(\varepsilon_2-\varepsilon_1)} &= -\exp(-2\beta a)
\end{aligned} \tag{2.99}$$

Dielectric function of metal can be described by drude model (Maier, 2007), dielectric function of free electron gas. For negligible damping, $\varepsilon(\omega)$ is predominantly real, and

$$\varepsilon(\omega) = 1 - \frac{\omega_p^2}{\omega^2} \tag{2.100}$$

where ω_p is plasma frequency of metal. To find ω in terms of β for odd mode, substitute Eq. (2.100) into Eq. (2.98) to get

$$\begin{aligned}
\frac{\varepsilon_2 + (1-\frac{\omega_p^2}{\omega^2})}{\varepsilon_2 - (1-\frac{\omega_p^2}{\omega^2})} &= \exp(-2\beta a) \\
\omega^2 &= \frac{\omega_p^2(1+\exp(-2\beta a))}{\varepsilon_2(1-\exp(-2\beta a)) + (1+\exp(-2\beta a))} \\
\omega^+ &= \frac{\omega_p(1+\exp(-2\beta a))^{\frac{1}{2}}}{(1+\varepsilon_2)^{\frac{1}{2}}\,(1-\frac{\varepsilon_2-1}{\varepsilon_2+1}\exp(-2\beta a))^{\frac{1}{2}}}
\end{aligned} \tag{2.101}$$

Also, for even mode, substituting Eq. (2.100) into Eq. (2.99), we get

$$\omega^- = \frac{\omega_p(1-\exp(-2\beta a))^{\frac{1}{2}}}{(1+\varepsilon_2)^{\frac{1}{2}}\,(1+\frac{\varepsilon_2-1}{\varepsilon_2+1}\exp(-2\beta a))^{\frac{1}{2}}} \tag{2.102}$$

These equations, Eq. (2.101) and Eq. (2.102), demonstrate the splitting in the nonretarded region. In order to find the resonance frequency, let $\beta = \infty$

$$\begin{aligned}
\omega &= \frac{\omega_p(1-\exp(-2\infty a))^{\frac{1}{2}}}{(1+\varepsilon_2)^{\frac{1}{2}}\,(1+\frac{\varepsilon_2-1}{\varepsilon_2+1}\exp(-2\infty a))^{\frac{1}{2}}} \\
&= \frac{\omega_p}{(1+\varepsilon_2)^{\frac{1}{2}}}
\end{aligned} \tag{2.103}$$

Hence, we can calculate the SP resonance frequency by substituting the values of ε_2 and ω_p.

To conclude, starting from maxwell equations, SP dispersion solutions are derived for single interface and double interface. The expression of the tangential wave vector for s-polarization is completely symmetrical to that of the p-polarization, due to the symmetry between the electric and magnetic responses in the Maxwell equations. With known values of ε, μ and ω in medium 1 and medium 2, we can solve for β analytically for single interface and numerically for double interface. The electric and magetic fields can be drawn accordingly.

CHAPTER 3

SINGLE INTERFACE SURFACE POLARITONS WITH ARBITRARY MAGNETIC AND DIELECTRIC MATERIALS

In this chapter, we analyze the dispersion property of surface polariton between two media with at least one with magnetic permeability that differs from unity. We present the underlying theoretical expressions for the wave vectors and field distributions across two media with arbitrary materials. The theory is generally valid in the entire electromagnetic spectrum, but we focus on the optical regime due to potential attractive applications in optical technologies. The theory provides insights into the study of the spectrum of the surface polaritons formed by various combinations of metallic, dielectric, and magnetic materials where SMPs exist, in addition to SFPs, SEPs, and SPPs. Although dielectric and/or metallic materials can coexist, the magnetic material or metamaterial with effective permeability is the main component needed to show the new regimes/possibilities provided by SMPs.

3.1 New Regimes Of Surface Polariton Resonances

The tangential wave vector solutions are found in previous chapter. In view of Eq. (2.37) and Eq. (2.51), the tangential wave vector for s-polarization is

$$k_x^s = \frac{\omega}{c}\sqrt{(\frac{\varepsilon_1\mu_2 - \mu_1\varepsilon_2}{\mu_2 - \mu_1})\frac{\mu_1\mu_2}{\mu_1 + \mu_2}} \tag{3.1}$$

and tangential wave vector for p-polarization is

$$k_x^p = \frac{\omega}{c}\sqrt{(\frac{\mu_1\varepsilon_2 - \varepsilon_1\mu_2}{\varepsilon_2 - \varepsilon_1})\frac{\varepsilon_1\varepsilon_2}{\varepsilon_1 + \varepsilon_2}} \tag{3.2}$$

Besides, using Eq. (2.41) and Eq. (2.55)), normal wave vector for s-polarization is

$$k_{jy}^s = \frac{\omega}{c}\mu_j\sqrt{\frac{\varepsilon_2\mu_2 - \varepsilon_1\mu_1}{(\mu_2 - \mu_1)(\mu_1 + \mu_2)}} \tag{3.3}$$

and normall wave vector for p-polarization is

$$k_{jy}^{p} = \frac{\omega}{c}\varepsilon_j \sqrt{\frac{(\mu_2\varepsilon_2 - \varepsilon_1\mu_1)}{(\varepsilon_2 - \varepsilon_1)(\varepsilon_1 + \varepsilon_2)}} \tag{3.4}$$

where $j = 1$ or 2. Let us first analyze the surface polariton regimes as summarized in Fig. (3.1). In the case of using only dielectric materials with single interface $\frac{\mu_1}{\mu_2} = 1$, the ratio Re $\frac{\varepsilon_1}{\varepsilon_2}$ has to be negative to excite a p-polarized surface polariton [Fig. (3.1)(a)] with the well known tangential wave vector $k_x^p = \frac{\omega}{c}\sqrt{\frac{\varepsilon_1\varepsilon_2}{\varepsilon_1+\varepsilon_2}}$. On the other hand, using only magnetic materials $\frac{\varepsilon_1}{\varepsilon_2} = 1$, we have the opposite result, $k_x^s = \frac{\omega}{c}\sqrt{\varepsilon_1\frac{\mu_1\mu_2}{\mu_1+\mu_2}}$, for s polarization. Fig. (3.1)(b) shows the new regimes where surface waves also exist for an s-polarized field when the materials are both dielectric and magnetic. The red solid lines in the second (fourth) quadrant show that s-polarized light can excite surface waves with large wave vectors if the materials are slightly magnetic, such as paramagnetic and ferromagnetic insulators (Hartstein et al., 1973), provided that Re μ_1 and Re μ_2 are almost equal in magnitude but with the same (opposite) sign, while Re ε_1 and Re ε_2 have opposite (same) signs. Similarly, the green dashed lines in the second (fourth) quadrant show that a p-polarized surface polariton with an enhanced wave vector can also be excited if the materials are slightly dielectric, provided Re ε_1 and Re ε_2 are almost equal but with opposite (same) signs while μ_1 and Re μ_2 have the same (opposite) sign.

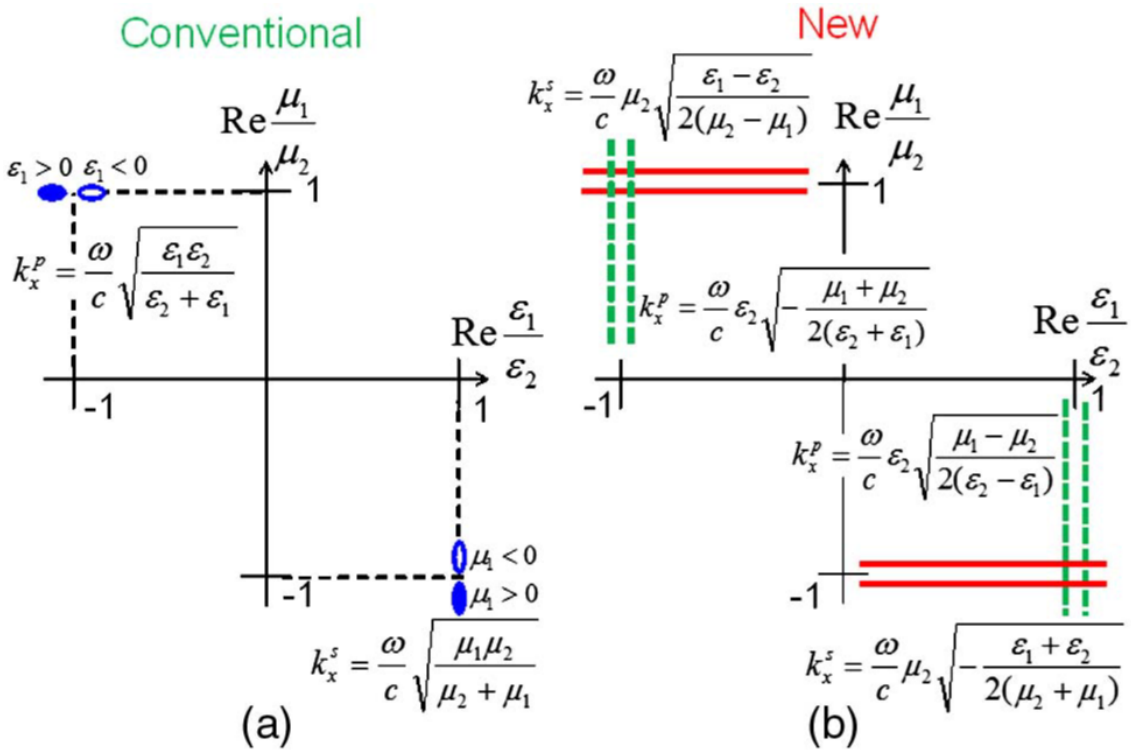

Figure 3.1: Quadrants showing regimes of enhanced tangential wave vectors k_x of surface polaritons propagating between medium 1 and medium 2 with permittivities ε_i and permeabilities μ_i for s-polarized light and p-polarized light. (a) Conventional scenario of plasmonic enhancement and its magnetic analog (indicated by open/filled dots). (b) New resonant regimes due to both electric and magnetic properties. The enhancement regions are indicated by two solid (red) lines and two dashed (green) lines slightly less and more than 1 and -1.

We consider the limiting possibilities when both $\mu = \mu^r + i\mu^i$ and $\varepsilon = \varepsilon^r + i\varepsilon^i$ are approximately (a) real and (b) imaginary, and show that the resulting tangential wave vector is real, describing a propagating surface polariton. Approximate relationships between k_x, the tangential wave vector, and k_jy the normal wave vector, can be found when k_x is enhanced by surface polariton resonance.

3.1.1 μ and ε Are Mostly Real

In the conventional case, the p-polarized surface polariton enhancement effect gives large k_x^p when ε_1 or ε_2 has a negative value, as in metals, such that $\varepsilon_1 + \varepsilon_2 \simeq 0$. It is known that there is no plasmonic enhancement for s-polarized light. However, Eq. (3.1) clearly

shows that, for s polarization, it is also possible to have surface polariton enhancement, when $\varepsilon_1 = \varepsilon_2$ are real, but the material must be magnetic with μ_1 and μ_2 having opposite signs, as illustrated in Fig. (3.1). Let us analyze the new resonance regimes, particularly due to the bracketed terms of Eq. (3.1) and Eq. (3.2).

Second Quadrant (in Fig. (3.1))

To have large wavevector, denominator of both equations need to be equal or near to zero. For s-polarization, if $\delta_m = \mu_1 - \mu_2 \simeq 0$

$$\begin{aligned} k_x^s &= \frac{\omega}{c}\sqrt{(\frac{\varepsilon_1\mu_2 - \mu_1\varepsilon_2}{\mu_2 - \mu_1})\frac{\mu_1\mu_2}{\mu_1 + \mu_2}} \\ &\simeq \frac{\omega}{c}\sqrt{(\frac{\mu_2\,(\varepsilon_1 - \varepsilon_2)}{\delta_m})\frac{\mu_1\mu_2}{2\mu_1}} \\ &\simeq \frac{\omega}{c}\mu_2\sqrt{\frac{\varepsilon_1 - \varepsilon_2}{2\delta_m}} \end{aligned} \tag{3.5}$$

In order for k_x^s to be real, the term inside square root of Eq. (3.5) need to be positive. Hence, wave vector k_s^x is large when $\delta_m = \mu_2 - \mu_1 \simeq 0^+(0^-)$, with $|Re\ \delta_m| \simeq 0$, provided $\varepsilon_1 > \varepsilon_2(\varepsilon_1 < \varepsilon_2)$. Note that, in nonmagnetic materials or materials with the same magnetic properties, Eq. (3.5) is not valid since $\delta_m = 0$, so there is no surface mode for s polarization. Note that k_x^s would be negative, if μ_2 is negative. At surface polariton resonances, normal wave vector k_{jy}^s, Eq. (3.3), has equal magnitude with k_x^s:

$$\begin{aligned} k_{jy}^s &= \frac{\omega}{c}\mu_j\sqrt{\frac{(\varepsilon_2\mu_2 - \varepsilon_1\mu_1)}{(\mu_2 - \mu_1)(\mu_1 + \mu_2)}} \\ &\simeq \frac{\omega}{c}\mu_j\sqrt{\frac{\mu_2(\varepsilon_2 - \varepsilon_1)}{(\delta_m)2\mu_2}} \\ &\simeq i\frac{\omega}{c}\mu_j\sqrt{\frac{\varepsilon_1 - \varepsilon_2}{2\delta_m}} \end{aligned}$$

Hence,

$$k_x^s \simeq \frac{\omega}{c}\mu_2\sqrt{\frac{\varepsilon_1 - \varepsilon_2}{2\delta_m}} \simeq ik_{1y}^s \simeq ik_{2y}^s \tag{3.6}$$

Fourth Quadrant (in Fig. (3.1))

Besides that, if $\delta_m^+ = \mu_1 + \mu_2 \simeq 0$

$$\begin{aligned} k_x^s &= \frac{\omega}{c}\sqrt{(\frac{\varepsilon_1\mu_2 - \mu_1\varepsilon_2}{\mu_2 - \mu_1})\frac{\mu_1\mu_2}{\mu_1 + \mu_2}} \\ &\simeq \frac{\omega}{c}\sqrt{(\frac{\mu_2(\varepsilon_1 + \varepsilon_2)}{2\mu_2})\frac{-\mu_2^2}{\delta_m^+}} \\ &\simeq \frac{\omega}{c}\mu_2\sqrt{(-\frac{\varepsilon_1 + \varepsilon_2}{2\delta_m^+})} \end{aligned} \tag{3.7}$$

In order for k_x^s to be real, the term inside square root of Eq. (3.7) need to be positive. Hence, when $\delta_m^+ = \mu_1 + \mu_2 \simeq 0^+(0^-)$ with $|Re\delta_m^+| \simeq 0$ while ε_2 and ε_1 are both negative (positive), or vice-versa, we have a large enhancement of the propagating wave vector (for $\mu_2 > 0$). At surface polariton resonances, normal wave vector k_{jy}^s, Eq. (3.3), has equal magnitude with k_x^s:

$$\begin{aligned} k_{jy}^s &= \frac{\omega}{c}\mu_j\sqrt{\frac{(\varepsilon_2\mu_2 - \varepsilon_1\mu_1)}{(\mu_2 - \mu_1)(\mu_1 + \mu_2)}} \\ &\simeq \frac{\omega}{c}\mu_j\sqrt{\frac{\mu_2(\varepsilon_2 + \varepsilon_1)}{2\mu_2(\delta_m^+)}} \\ &\simeq i\frac{\omega}{c}\mu_j\sqrt{-\frac{\varepsilon_1 + \varepsilon_2}{2\delta_m^+}} \end{aligned}$$

Hence,

$$k_x^s \simeq \frac{\omega}{c}\mu_2\sqrt{-\frac{\varepsilon_1 + \varepsilon_2}{2\delta_m^+}} \simeq ik_{1y}^s \simeq ik_{2y}^s \tag{3.8}$$

Fourth Quadrant (in Fig. (3.1))

Similarly, for p-polarization, if $\delta_e = \varepsilon_2 - \varepsilon_1 \simeq 0$

$$\begin{aligned} k_x^p &= \frac{\omega}{c}\sqrt{(\frac{\mu_1\varepsilon_2 - \varepsilon_1\mu_2}{\varepsilon_2 - \varepsilon_1})\frac{\varepsilon_1\varepsilon_2}{\varepsilon_1 + \varepsilon_2}} \\ &\simeq \frac{\omega}{c}\sqrt{(\frac{\varepsilon_2(\mu_1 - \mu_2)}{\delta_e})\frac{\varepsilon_1\varepsilon_2}{2\varepsilon_1}} \\ &\simeq \frac{\omega}{c}\varepsilon_2\sqrt{\frac{\mu_1 - \mu_2}{2\delta_e}} \end{aligned} \tag{3.9}$$

In order for k_x^p to be real, the term inside square root of Eq. (3.9) need to be positive.

Hence, wave vector k_x^p can take a large value when ε_2 and ε_1 are almost equal (with the same sign), i.e., $\delta_e = \varepsilon_2 - \varepsilon_1 \simeq 0^+(0^-)$, while $\mu_1 > \mu_2$ ($\mu_1 < \mu_2$). This equation is essentially Eq. (3.5) obtained by interchanging ε and μ. Propagating exists when $Re(\mu_2 - \mu_1)$ has opposite sign from $Re(\varepsilon_2 - \varepsilon_1)$. Here, k_x^p is negative if ε_2 is negative. When $Re\mu_1$ and $Re\mu_2$ have opposite signs and are nearly equal in magnitude, the wave vector has the largest value

$$\begin{aligned} k_x^p &\simeq \frac{\omega}{c}\varepsilon_2\sqrt{\frac{\mu_1-\mu_2}{2\delta_e}} \\ k_x^p &\simeq \frac{\omega}{c}\varepsilon_2\sqrt{\frac{2\mu_1}{2\delta_e}} \\ k_x^p &\simeq \frac{\omega}{c}\varepsilon_2\sqrt{\frac{|Re\mu_1|}{\delta_e}} \end{aligned} \tag{3.10}$$

Similiar to s-polarization solution at surface polariton resonances, normal wave vector k_{jy}^p, Eq. (3.4), has equal magnitude with k_x^p.

$$\begin{aligned} k_{jy}^p &= \frac{\omega}{c}\varepsilon_j\sqrt{\frac{(\mu_2\varepsilon_2-\varepsilon_1\mu_1)}{(\varepsilon_2-\varepsilon_1)(\varepsilon_1+\varepsilon_2)}} \\ &\simeq \frac{\omega}{c}\varepsilon_j\sqrt{\frac{\varepsilon_1(\mu_2-\mu_1)}{(\delta_e)(2\varepsilon_1)}} \\ &\simeq i\frac{\omega}{c}\varepsilon_j\sqrt{\frac{\mu_1-\mu_2}{2\delta_e}} \end{aligned}$$

Hence,

$$k_x^p \simeq \frac{\omega}{c}\varepsilon_2\sqrt{\frac{\mu_1-\mu_2}{2\delta_e}} \simeq ik_{1y}^p \simeq ik_{2y}^p \tag{3.11}$$

Second Quadrant (in Fig. (3.1))

If ε_2 and ε_1 have opposite signs, i.e, $\delta_e^+ = \varepsilon_1 + \varepsilon_2 \simeq 0^+$, while μ_2 and μ_1 have the same sign (assuming $\varepsilon_2 > 0$) we have, similar to Eq. (3.7),

$$\begin{aligned} k_x^p &= \frac{\omega}{c}\sqrt{(\frac{\mu_1\varepsilon_2-\varepsilon_1\mu_2}{\varepsilon_2-\varepsilon_1})\frac{\varepsilon_1\varepsilon_2}{\varepsilon_1+\varepsilon_2}} \\ &\simeq \frac{\omega}{c}\sqrt{\frac{\varepsilon_2(\mu_1+\mu_2)}{2\varepsilon_2}\frac{-\varepsilon_2\varepsilon_2}{\delta_e^+}} \\ &\simeq \frac{\omega}{c}\varepsilon_2\sqrt{-\frac{\mu_1+\mu_2}{2\delta_e^+}} \end{aligned} \tag{3.12}$$

Again, similiar to s-polarization solution at surface polariton resonances, normal wave vector k_{jy}^p, (3.4), has equal magnitude with k_x^p.

$$\begin{aligned} k_{jy}^p &= \frac{\omega}{c}\varepsilon_j\sqrt{\frac{(\mu_2\varepsilon_2-\varepsilon_1\mu_1)}{(\varepsilon_2-\varepsilon_1)(\varepsilon_1+\varepsilon_2)}} \\ &\simeq \frac{\omega}{c}\varepsilon_j\sqrt{\frac{\varepsilon_2(\mu_2+\mu_1)}{(2\varepsilon_2)(\delta_e^+)}} \\ &\simeq i\frac{\omega}{c}\varepsilon_j\sqrt{-\frac{\mu_1+\mu_2}{2\delta_e^+}} \end{aligned}$$

Hence,

$$k_x^p \simeq \frac{\omega}{c}\varepsilon_2\sqrt{-\frac{\mu_1+\mu_2}{2\delta_e^+}} \simeq ik_{1y}^p \simeq ik_{2y}^p \tag{3.13}$$

3.1.2 μ and ε Are Mostly Imaginary

Here, $\mu^i >> \mu^r$ and $\varepsilon^i >> \varepsilon^r$. So, the denominator of k_x^s may be approximated as

$$\begin{aligned} (\mu_2-\mu_1)(\mu_1+\mu_2) &\simeq (i\mu_2^i - i\mu_1^i)(i\mu_1^i + i\mu_2^i) \\ &\simeq i(\mu_2^i-\mu_1^i)i(\mu_1^i+\mu_2^i) \\ &\simeq -(\mu_2^i-\mu_1^i)(\mu_1^i+\mu_2^i) \end{aligned} \tag{3.14}$$

Similarly, for k_x^p.

$$\begin{aligned} (\varepsilon_2-\varepsilon_1)(\varepsilon_1+\varepsilon_2) &\simeq (i\varepsilon_2^i - i\varepsilon_1^i)(i\varepsilon_1^i + i\varepsilon_2^i) \\ &\simeq i(\varepsilon_2^i-\varepsilon_1^i)i(\varepsilon_1^i+\varepsilon_2^i) \\ &\simeq -(\varepsilon_2^i-\varepsilon_1^i)(\varepsilon_1^i+\varepsilon_2^i) \end{aligned} \tag{3.15}$$

Therefore, the tangential wave vectors have expressions similar to that of Eq. (3.1) and Eq. (3.2), except there is a negative sign:

$$k_x^s \simeq \frac{\omega}{c}\sqrt{-(\frac{\varepsilon_1^i\mu_2^i-\mu_1^i\varepsilon_2^i}{\mu_2^i-\mu_1^i})\frac{\mu_1^i\mu_2^i}{\mu_1^i+\mu_2^i}} \tag{3.16}$$

$$k_x^p \simeq \frac{\omega}{c}\sqrt{-(\frac{\mu_1^i\varepsilon_2^i-\varepsilon_1^i\mu_2^i}{\varepsilon_2^i-\varepsilon_1^i})\frac{\varepsilon_1^i\varepsilon_2^i}{\varepsilon_1^i+\varepsilon_2^i}} \tag{3.17}$$

Thus, the discussions above for real μ and ε apply, except that the numerator is $\varepsilon_1^i\mu_2^i - \mu_1^i\varepsilon_2^i$ instead of $\varepsilon_1\mu_2 - \mu_1\varepsilon_2$ for s-polarization, and $\mu_1^i\varepsilon_2^i - \varepsilon_1^i\mu_2^i$ instead of $\mu_1\varepsilon_2 - \varepsilon_1\mu_2$ for p-polarization.

To summarize, the tangential wave vector for s-polarized light is finite for magnetic materials, according to Eq. (3.6) and Eq. (3.8). The magnetic materials also give surface polariton resonant enhancement for s polarization [Eq. (3.6)] just like metallic materials give plasmonic enhancement in p polarization. In addition, the magnetic materials also give new regimes of the enhancement effect for p polarization, based on Eq. (3.11). These analyses show that metals are not the only means for achieving surface enhancement effects. Thus, plasmonics can be extended to magnonics, by using magnetic materials and also metamaterials whose magnetic response can be tailored structurally using nonmagnetic materials.

3.2 Field Distribution

Consider a plane wave traversing the interface between medium 1 and 2 on the $x-y$ plane. For s polarization,

$$\vec{E}_j^s(r,t) = E_j^s(0,0,1)e^{i(k_x^s + k_{jy}^s y)} \tag{3.18}$$

and, for p-polarization,

$$\vec{E}_j^p(r,t) = E_j^p(-\frac{k_{jy}^p}{k_j}, \frac{k_x^p}{k_j}, 0)e^{i(k_x^p + k_{jy}^p y)} \tag{3.19}$$

where $j = 1,2$ is the index for the medium. A linear combination of these fields yields the resulting field $\vec{E}_j = \vec{E}_j^s e^{i\phi} + \vec{E}_j^p$ that is generally elliptically polarized:

$$\vec{E}_j = [-E_j^p \frac{k_{jy}^p}{k_j} e^{i\vec{\Phi}_j^p}, E_j^p \frac{k_x^p}{k_j} e^{i\vec{\Phi}_j^p}, E_j^s e^{i(\vec{\Phi}_j^s + \phi)}] \tag{3.20}$$

where $\vec{\Phi}_j^\lambda(x,y) = k_x^\lambda x + k_{jy}^\lambda y$. Since the two vector fields are orthogonal, there would be no interference between the two in the total intensity $|\vec{E}_j|^2$. An interesting effect of

the surface polariton enhancement is that a circularly/elliptically polarized light becomes almost linearly y-polarized light, since $,E_j^p\frac{k_x^p}{k_j} \gg E_j^p\frac{k_{jy}^p}{k_j}, E_j^s$. Now, we show what the field distribution of the surface polariton looks like and how it can be achieved with one of the two possible polarizations.

3.2.1 Surface mode in s-polarization

Consider medium 1 is a nonmagnetic dielectric [$\mu_1 = 1$ with $\varepsilon_1 = 5$ (e.g., class)] and medium 2 is paramagnetic [$\mu_2 = 1.008$ with $\varepsilon_2 = 1$ (e.g., FeO)], corresponding to the second quadrant in Fig. (3.1)(b) and Eq. (3.6). Taking $\omega = 8\times10^{13}\,s^{-1}$, the tangential wave vector for s-polarization is

$$\begin{aligned} k_x^s &= \frac{8\times10^{13}}{3\times10^8}\sqrt{(\frac{(5)(1.008)-(1)(1)}{1.008-1})\frac{(1)(1.008)}{1+1.008}} \\ &= 4.2459\times10^6 \end{aligned} \tag{3.21}$$

normal wave vector for s-polarization in medium 1 is:

$$\begin{aligned} k_{1y}^s &= \frac{8\times10^{13}}{3\times10^8}(1)\sqrt{\frac{((1)(1.008)-(5)(1))}{(1.008-1)(1+1.008)}} \\ &= 4.2038\times10^6 i \end{aligned} \tag{3.22}$$

normal wave vector for s-polarization in medium 2 is:

$$\begin{aligned} k_{2y}^s &= \frac{8\times10^{13}}{3\times10^8}(1.008)\sqrt{\frac{((1)(1.008)-(5)(1))}{(1.008-1)(1+1.008)}} \\ &= 4.2374\times10^6 i \end{aligned} \tag{3.23}$$

tangential wave vector for p-polarization is:

$$\begin{aligned} k_x^p &= \frac{8\times10^{13}}{3\times10^8}\sqrt{(\frac{(1)(1)-(5)(1.008)}{1-5})\frac{(5)(1)}{5+1}} \\ &= 2.4465\times10^5 \end{aligned} \tag{3.24}$$

normal wave vector for p-polarization in medium 1 is:

$$k_{1y}^{p} = \frac{8\times10^{13}}{3\times10^{8}}(5)\sqrt{\frac{((1.008)(1)-(5)(1))}{(1-5)(5+1)}}$$
$$= 5.4379\times10^{5} \tag{3.25}$$

normal wave vector for p-polarization in medium 2 is:

$$k_{2y}^{p} = \frac{8\times10^{13}}{3\times10^{8}}(1)\sqrt{\frac{((1.008)(1)-(5)(1))}{(1-5)(5+1)}}$$
$$= 1.0876\times10^{5} \tag{3.26}$$

Substituting these values into Eq. (3.20), the electric fields of E_z and E_x of surface mode in s-polarization are plotted. The normalization factor is $\lambda = 2\pi c/\omega$.

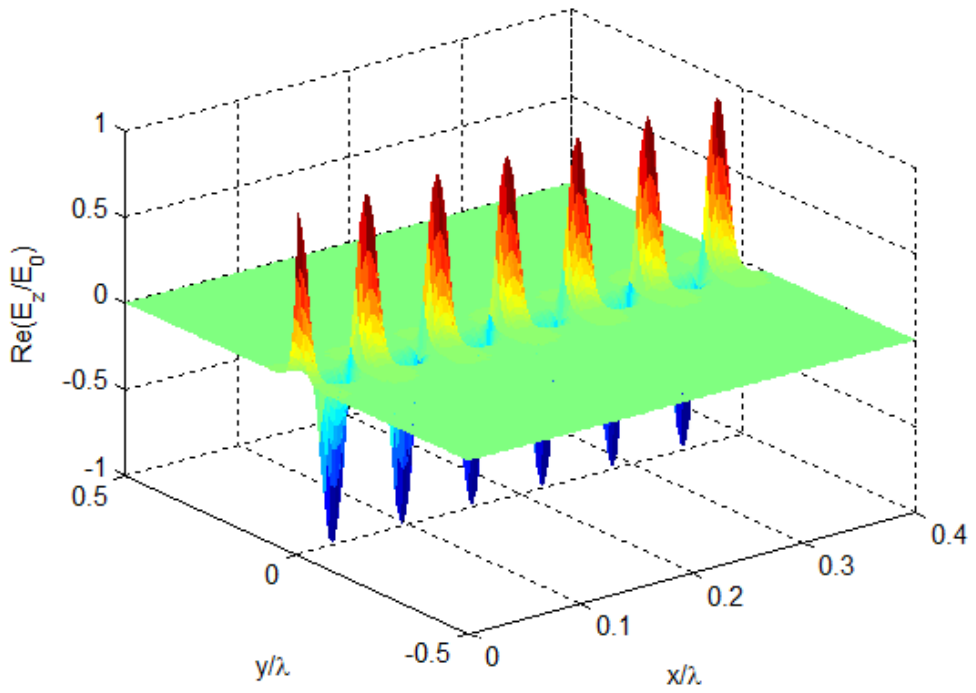

Figure 3.2: Surface mode in s-polarization: E_z field(real) with rapid oscillations (corresponding to an enhanced tangential wave vector)

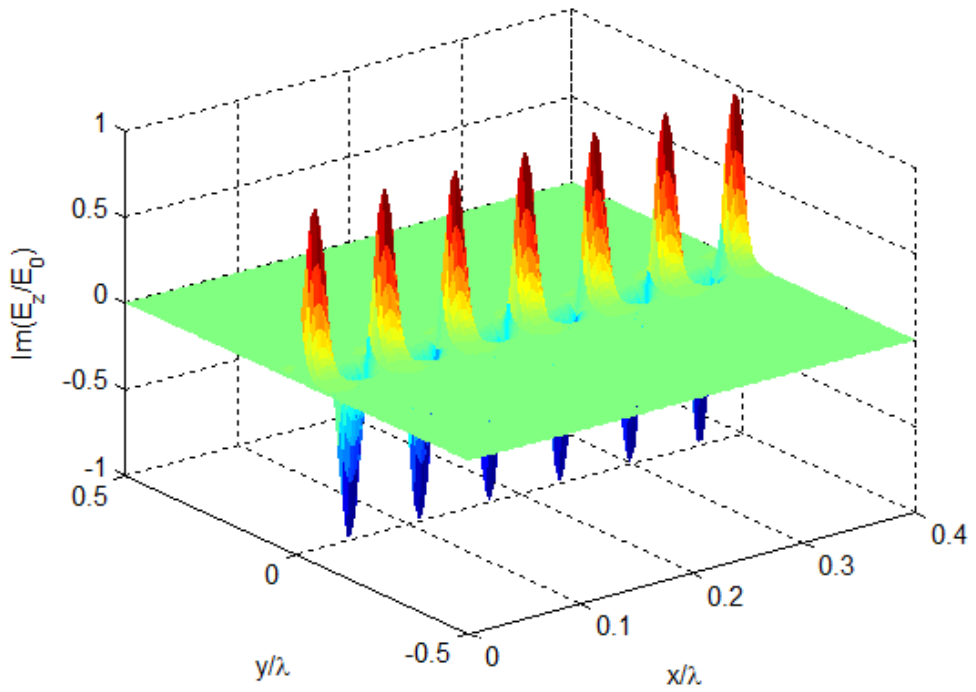

Figure 3.3: Surface mode in s-polarization: E_z field(imaginary) with rapid oscillations (corresponding to an enhanced tangential wave vector)

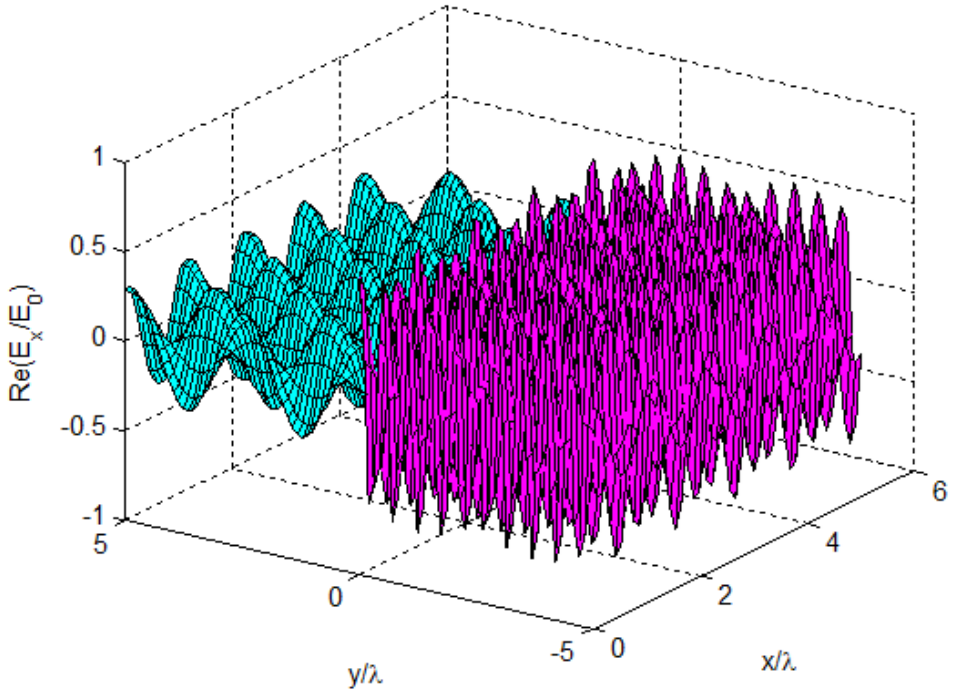

Figure 3.4: Surface mode in s-polarization: E_x field(real) with normal oscillations with discontinuity at $y = 0$(the scale is 10 times larger).

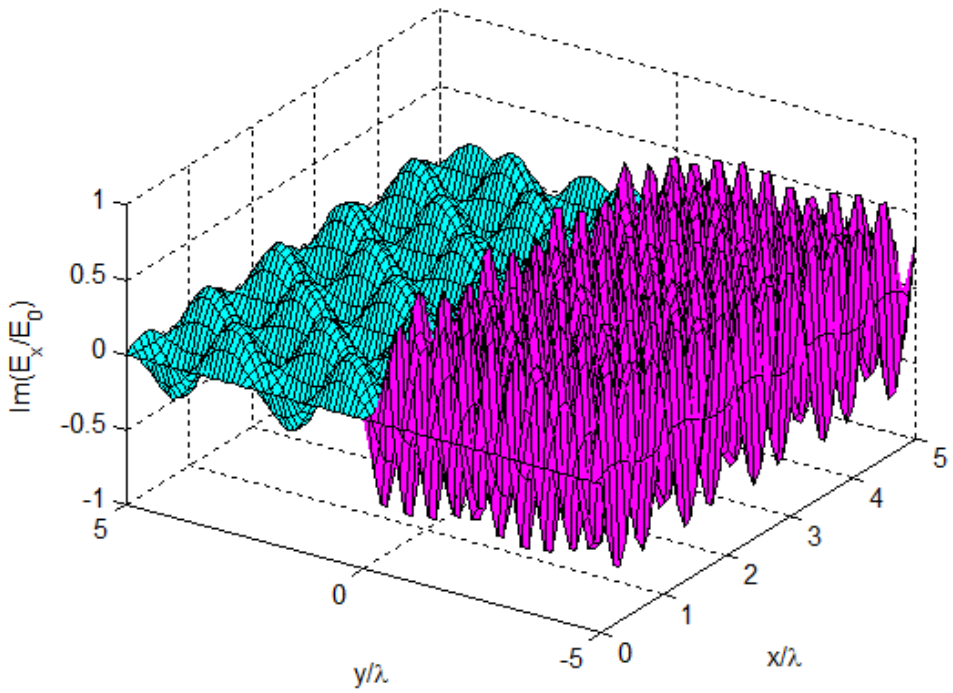

Figure 3.5: Surface mode in s-polarization: E_x field(imaginary) with normal oscillations with discontinuity at $y = 0$(the scale is 10 times larger).

The permeabilities with nearly equal magnitudes provide the propagating feature of the surface polariton for s-polarized light; i.e., the ReE_z oscillates rapidly across the x direction, corresponding to a large real tangential wave vector k_x^s, but decays along the y direction away from the interface due to imaginary k_{jy}^s. The tangential z component of the E field is continuous. However, the x component of the E field is not continuous (it is the H_x that is continuous). The field distribution around the interface shows large surface enhancement of the tangential wave vector k_x^s for s-polarization, as illustrated in Fig. (3.2). For small $|\delta_m|$, the oscillations for E_z across the x direction are more rapid (with period $2\pi/k_x^s$) than the oscillations for E_x, since k_x^s is enhanced. The tangential component of the E field, i.e., the E_z, is continuous. However, the tangential x component, E_x need not be continuous (see Fig. (3.3)). It is the H_x that must be continuous for s-polarized light.

3.2.2 Surface mode in p-polarization

Let us assume that medium 1 is a ferromagnet ($\varepsilon_1 = 1$ with $\mu_1 = 4$ (e.g., AlNiCo), while medium 2 is almost pure diamagnetic ($\varepsilon_2 = 1.009$ at 13 eV with $\mu_2 = -3$ (e.g., mercury [(Inagaki, Arakawa, & Williams, 1981)]), corresponding to the fourth quadrant in Fig. (3.1)(b) and Eq. (3.11). Taking $\omega = 8 \times 10^{13}\, s^{-1}$, the tangential wave vector for p-polarization is

$$\begin{aligned} k_x^p &= \frac{8\times 10^{13}}{3\times 10^8}\sqrt{\left(\frac{(4)(1.009)-(1)(-3)}{1.009-1}\right)\frac{(1)(1.009)}{1+1.009}} \\ &= 5.284\times 10^6 \end{aligned} \tag{3.27}$$

normal wave vector for p-polarization in medium 1 is:

$$\begin{aligned} k_{1y}^p &= \frac{8\times 10^{13}}{3\times 10^8}(1)\sqrt{\frac{((-3)(1.009)-(1)(4))}{(1.009-1)(1+1.009)}} \\ &= 5.2571\times 10^6 i \end{aligned} \tag{3.28}$$

normal wave vector for p-polarization in medium 2 is:

$$k_{2y}^{p} = \frac{8\times10^{13}}{3\times10^{8}}(1.009)\sqrt{\frac{((-3)(1.009)-(1)(4))}{(1.009-1)(1+1.009)}}$$
$$= 5.3044\times10^{6}i \tag{3.29}$$

tangential wave vector for s-polarization is:

$$k_{x}^{s} = \frac{8\times10^{13}}{3\times10^{8}}\sqrt{(\frac{(1)(-3)-(4)(1.009)}{-3-4})\frac{(4)(-3)}{4+(-3)}}$$
$$= 9.2613\times10^{5}i \tag{3.30}$$

normal wave vector for s-polarization in medium 1 is:

$$k_{1y}^{s} = \frac{8\times10^{13}}{3\times10^{8}}(4)\sqrt{\frac{((1.009)(-3)-(1)(4))}{((-3)-4)(4+(-3))}}$$
$$= 1.0687\times10^{6} \tag{3.31}$$

normal wave vector for s-polarization in medium 2 is:

$$k_{2y}^{s} = \frac{8\times10^{13}}{3\times10^{8}}(-3)\sqrt{\frac{((1.009)(-3)-(1)(4))}{((-3)-4)(4+(-3))}}$$
$$= -8.0154\times10^{5} \tag{3.32}$$

Substituting these values into Eq. (3.20), we plot (Figs. (3.6)-(3.9)) the electric fields E_z and E_x of the surface mode in the s-polarization. The normalization factor is $\lambda = 2\pi c/\omega$.

From the figures, the surface propagation feature is shown by the p-polarized field or E_x corresponding to a large k_x^p. In this combinations of ε and μ, p polarization shows enhancement in the tangential wave vector k_x^p. For small $|\delta_e|$, the oscillations for E_x across the x direction are more rapid (with period $2\pi/k_x^p$) than the oscillations of E_z, since, here, the k_x^p is enhanced, instead. Also, E_z and E_x are continuous at $y = 0$, again since k_x^p is enhanced.

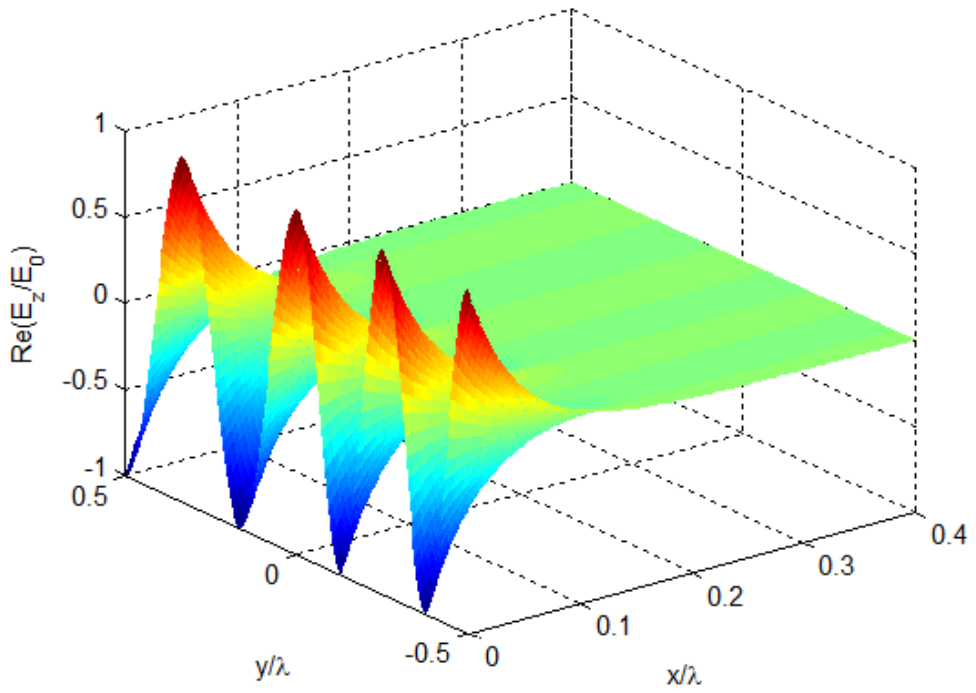

Figure 3.6: Surface mode in p-polarization: E_z field(real) with normal oscillations.

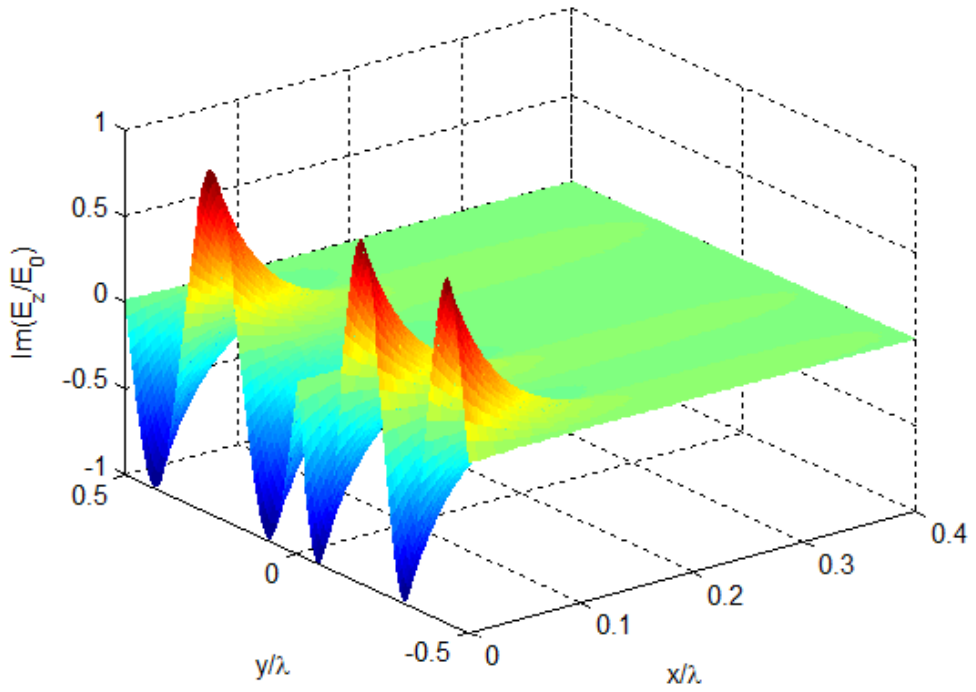

Figure 3.7: Surface mode in p-polarization: E_z field(imaginary) with normal oscillations.

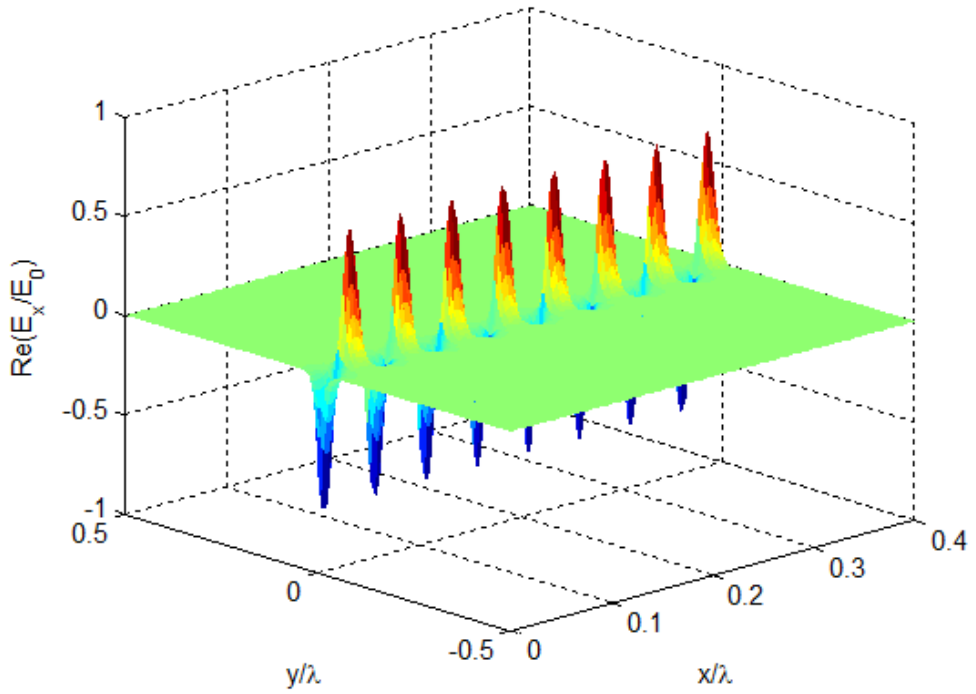

Figure 3.8: Surface mode in p-polarization: E_x field(real) with rapid oscillations.(corresponding to an enhanced tangential wave vector)

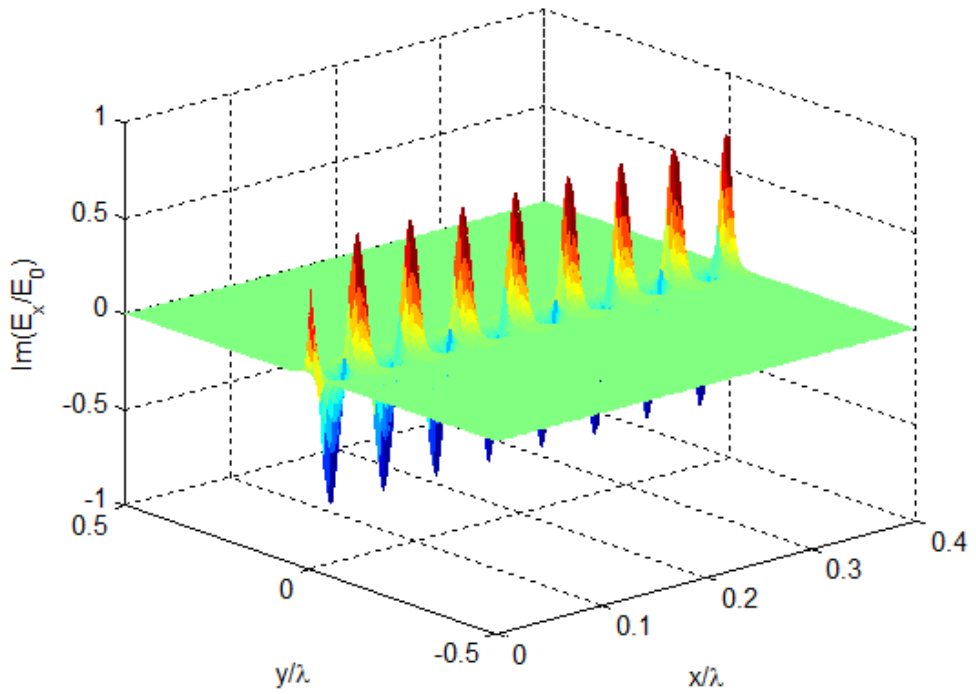

Figure 3.9: Surface mode in p-polarization: E_x field(imaginary) with rapid oscillations. (corresponding to an enhanced tangential wave vector)

3.3 Dispersions Of Surface Polaritons

Dispersion is the phenomenon in which the phase velocity(or wave vector) of a wave depends on its frequency. Dispersion is occured for any kind of wave that interacts with a medium which is dispersive. This occurs because each component frequency of light(electromagnetic wave), is refracted by a slightly different angle. In this section, we will show the dispersions of surface polariton in dispersive dielectric, dispersive magnetic materials and superconductor.

3.3.1 Dispersive Dielectric And Magnetic Materials

To study the effects of dispersions in SMR and SFR, we model the dielectric permittivity ε and magnetic permeability μ using [(Agranovich & Mills, 1982),(Pendry, Holden, Robbins, & Stewart, 1999)]

$$\alpha(\omega) = 1 + \frac{\tilde{\omega}_\alpha^2}{\omega_\alpha^2 - \omega^2 - i\gamma_\alpha\omega} \tag{3.33}$$

with single resonances ω_α of line widths γ_α and oscillator strengths $\tilde{\omega}_\alpha(\alpha = \varepsilon, \mu)$. The $\varepsilon(\omega)$ in Eq. (3.33) describes the dispersion of typical dielectric material due to phonon-polaritons and $\mu(\omega)$ gives the magnetic response of typical metamaterials with single resonance. For $\varepsilon(\omega)$, we use parameters for ionic (BeO) crystal (Ribbing, Högström, & Rung, 2006): $\omega_\varepsilon = 2\pi 2.1036 \times 10^1 3\, s^{-1}$, $\gamma_\varepsilon = 2\pi 3.6512 \times 10^{11}\, s^{-1}$, and $\tilde{\omega}_\alpha = 2.8532 \times 10^{14}\, s^{-1}$. For $\mu_2(\omega)$, the magnetic resonance is characterized by $\omega_\mu = 0.9\omega_\varepsilon, \tilde{\omega}_\mu = 1.1\tilde{\omega}_\varepsilon$, and $\gamma_\mu = \gamma_\varepsilon$. Using these parameters and substituting into Eq. (3.33), dielectric permittivity ε and magnetic permeability are calculated and plotted in Figs. (3.10) and (3.11). The refractive indices are calculated accordingly by $n_2(\omega) = \sqrt{\varepsilon_2(\omega)\mu_2(\omega)}$. As in Fig. (3.11), when both ε and μ are negative, the refractive index is negative. By using Eq. (3.1) and Eq. (3.2), dispersions curves are draw for p-polarization and s-polarization. We compare the curves between

i) dispersive dielectric $\varepsilon_2(\omega)$ and a constant positive permeability $\mu_2 = 5$(Positive refractive index case)

ii) dispersive dielectric $\varepsilon_2(\omega)$ and a dispersively permeability $\mu_2(\omega)$(Negative refractive index case)

Figs. (3.10) and (3.11) show dielectric and magnetic properties of medium 2 for both cases discussed above. For the first case, there is no negative region of refractive index as in Fig. (3.12). While Fig. (3.13) shows a negative refractive index region of medium 2 if both ε and μ are dispersive. From the result, interesting double resonance spectra are found in the tangential wave vectors when one of the media is filled with dispersive dielectric and magnetic materials. This can be seen clearly from Figs. (3.15), (3.17), (3.19), and (3.21). While there is only a single resonant peak for non-dispersive magnetic material, as shown in Figs. (3.14),(3.16),(3.18) and (3.20).

For single resonance case, resonant for s-polarization happens at $\omega_\varepsilon = 1.32 \times 10^{14}\, s^{-1}$ (the resonance of $\varepsilon_2(\omega)$), while, for p-polarization, the peak is at a higher frequency $\sqrt{\omega_\varepsilon^2 + \frac{1}{2}\tilde{\omega}_\varepsilon^2} = 2.41 \times 10^{14}\, s^{-1}$. The analytical expressions for the locations of the peaks are obtained from the root in the denominator of k_x^s for both polarizations (ignoring the damping γ_α) and valid for all possibilities of $\varepsilon_1 = \pm 1$ and $\mu_1 = \pm 1$.

For double resonance case, there is a negative refractive index region around the resonance. The two peaks corresponding to two roots in the denominator of k_x^2. The s-polarization shows the second peak at a higher frequency $\sqrt{\omega_\mu^2 + \frac{1}{2}\tilde{\omega}_\mu^2} = 2.52 \times 10^{14}\, s^{-1}$, while p polarization shows a second peak around $\omega_\mu = 1.19 \times 10^{14}\, s^{-1}$ [the magnetic resonance of $\mu_2(\omega)$].

Hence, we may deduce that the coexistence of the dielectric dispersion in $\varepsilon_2(\omega)$ and the magnetic dispersion in $\mu_2(\omega)$ giving rise to the second peaks in the spectra of k_x for s and p polarizations.

Positive refractive index case ($\varepsilon_2(\omega)$[Eq. (3.33)], $\mu_2 = 5$)

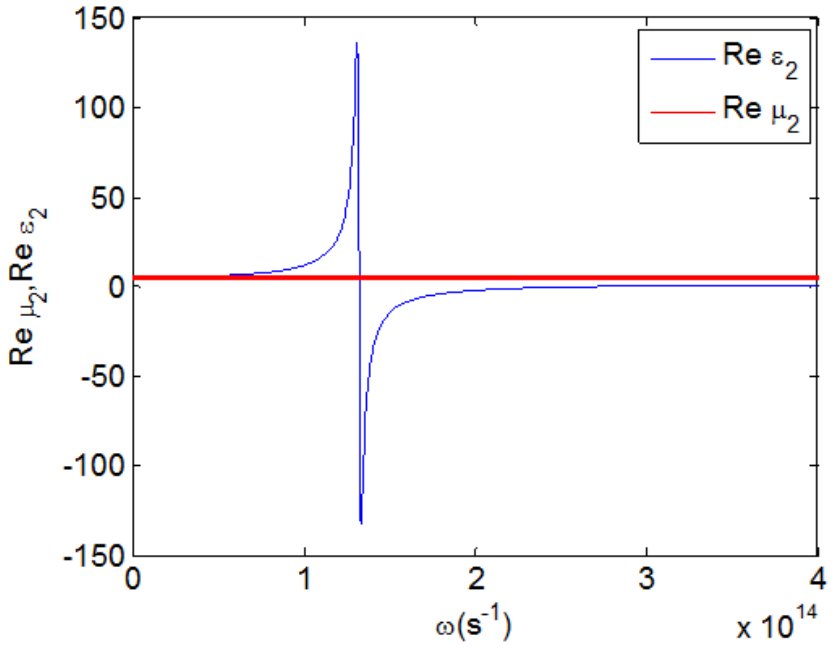

Figure 3.10: Real part of $\varepsilon_2(\omega)$, $\mu_2 = 5$.

Negative refractive index case ($\varepsilon_2(\omega)$[Eq. (3.33)], $\mu_2(\omega)$[Eq. (3.33)])

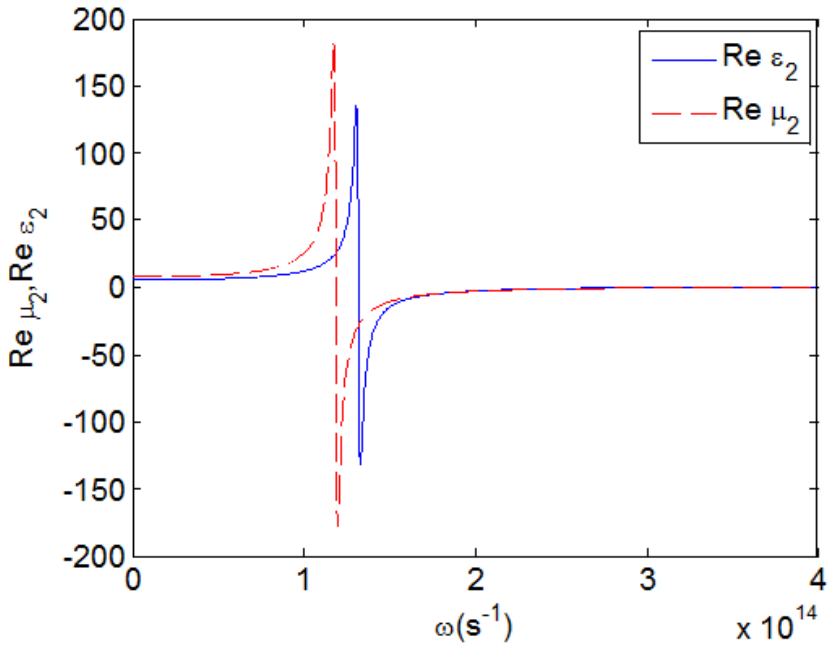

Figure 3.11: Real part of $\varepsilon_2(\omega)$, $\mu_2(\omega)$.

Positive refractive index case ($\varepsilon_2(\omega)$[Eq. (3.33)], $\mu_2 = 5$)

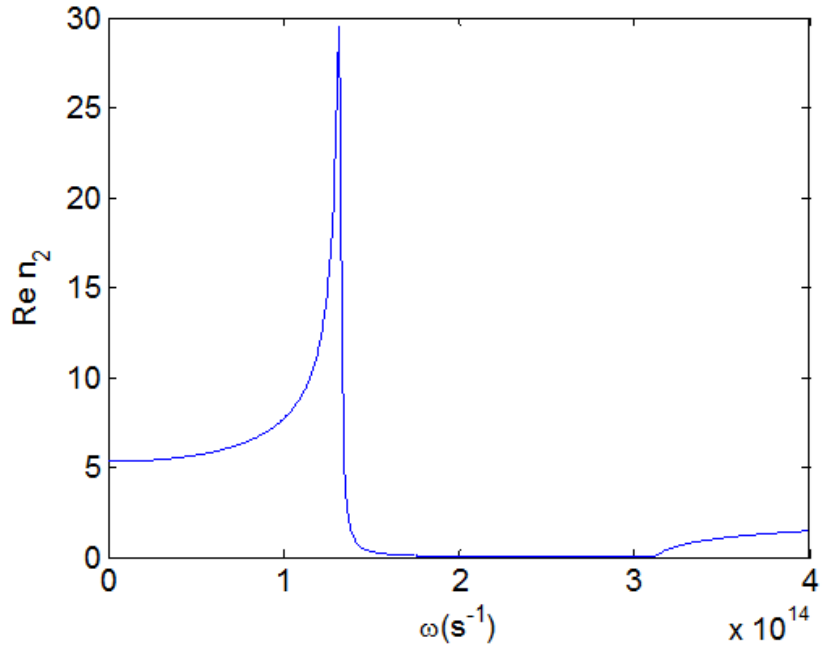

Figure 3.12: Refractive index, $n_2(\omega) = \sqrt{\varepsilon_2(\omega)\mu_2}$

Negative refractive index case ($\varepsilon_2(\omega)$[Eq. (3.33)], $\mu_2(\omega)$[Eq. (3.33)])

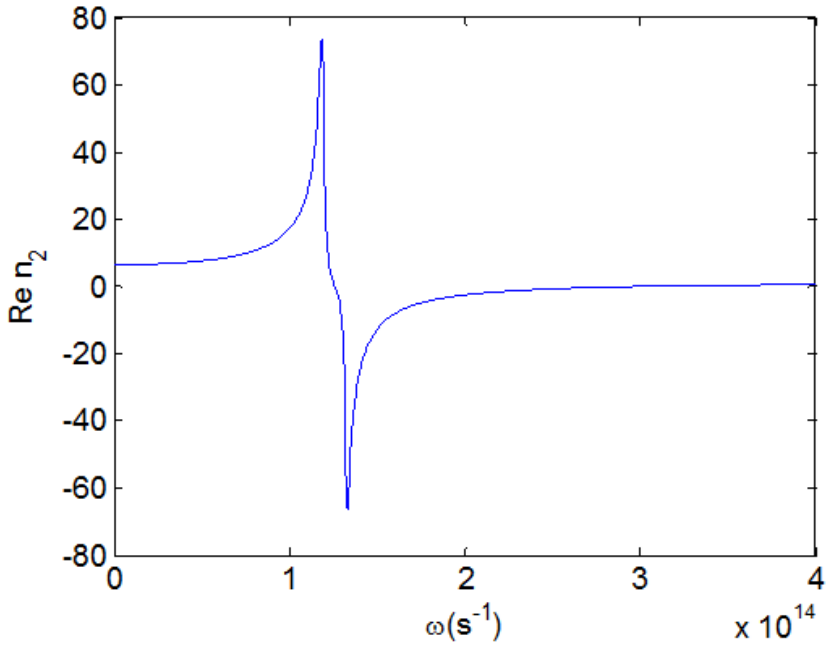

Figure 3.13: Refractive index, $n_2(\omega) = \sqrt{\varepsilon_2(\omega)\mu_2(\omega)}$

Positive refractive index case ($\varepsilon_2(\omega)$[Eq. (3.33)], $\mu_2 = 5$)

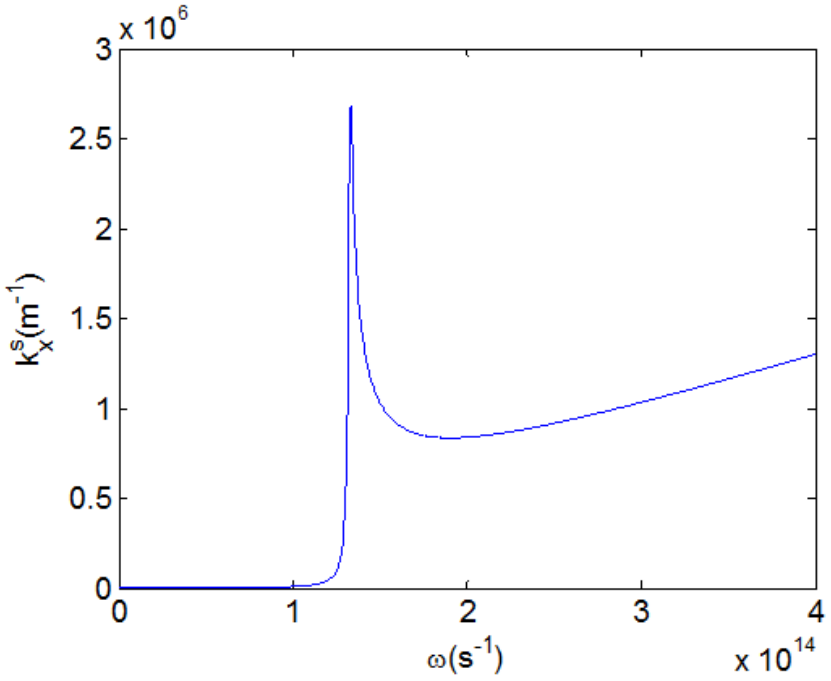

Figure 3.14: Wave vector dispersions for s-polarized when ε_2 and μ_2 in the same sign, $\mu_1 = \pm 1, \varepsilon_1 = \pm 1$

Negative refractive index case ($\varepsilon_2(\omega)$[Eq. (3.33)], $\mu_2(\omega)$[Eq. (3.33)])

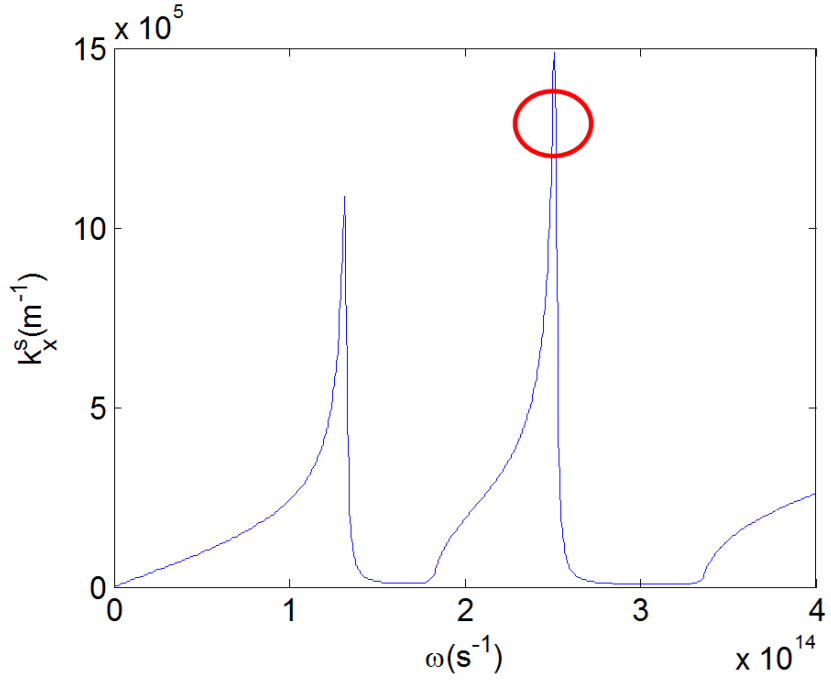

Figure 3.15: Wave vector dispersions for s-polarized when ε_2 and μ_2 in the same sign, $\mu_1 = \pm 1, \varepsilon_1 = \pm 1$, double resonance spectra are observed.

Positive refractive index case ($\varepsilon_2(\omega)$[Eq. (3.33)], $\mu_2 = 5$)

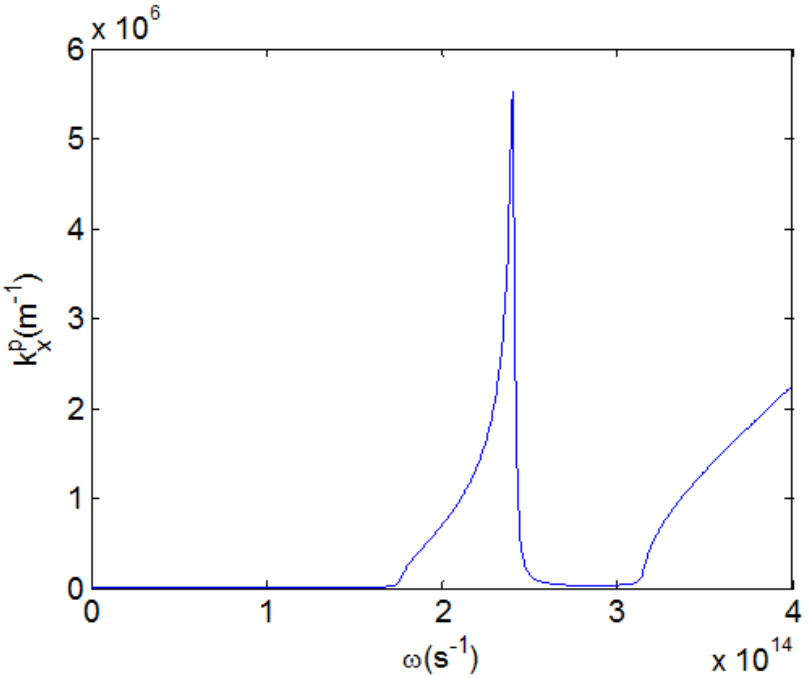

Figure 3.16: Wave vector dispersions for p-polarized when ε_2 and μ_2 in the same sign, $\mu_1 = \pm 1, \varepsilon_1 = \pm 1$

Negative refractive index case ($\varepsilon_2(\omega)$[Eq. (3.33)], $\mu_2(\omega)$[Eq. (3.33)])

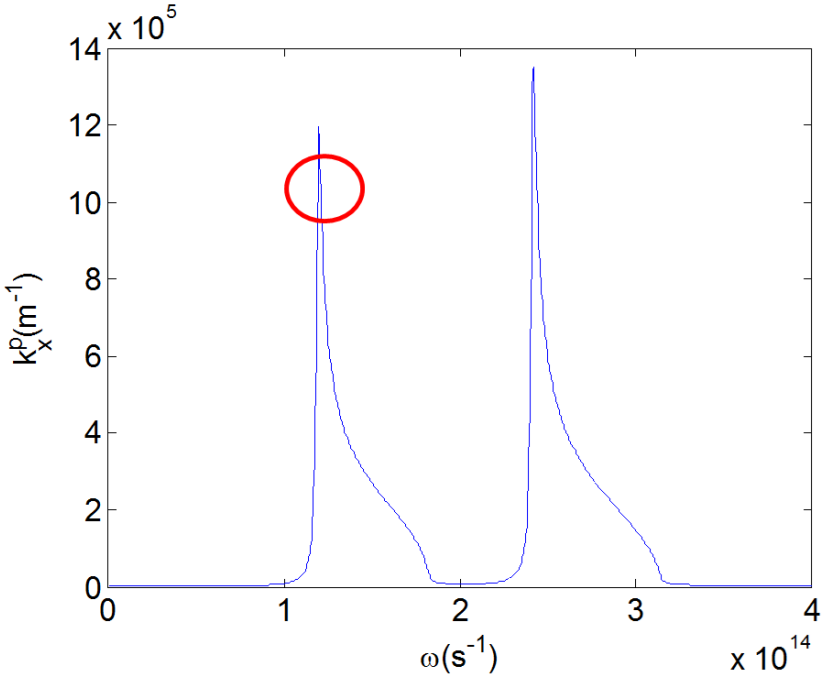

Figure 3.17: Wave vector dispersions for p-polarized when ε_2 and μ_2 in the same sign, $\mu_1 = \pm 1, \varepsilon_1 = \pm 1$, double resonance spectra are observed.

Positive refractive index case ($\varepsilon_2(\omega)$[Eq. (3.33)], $\mu_2 = 5$)

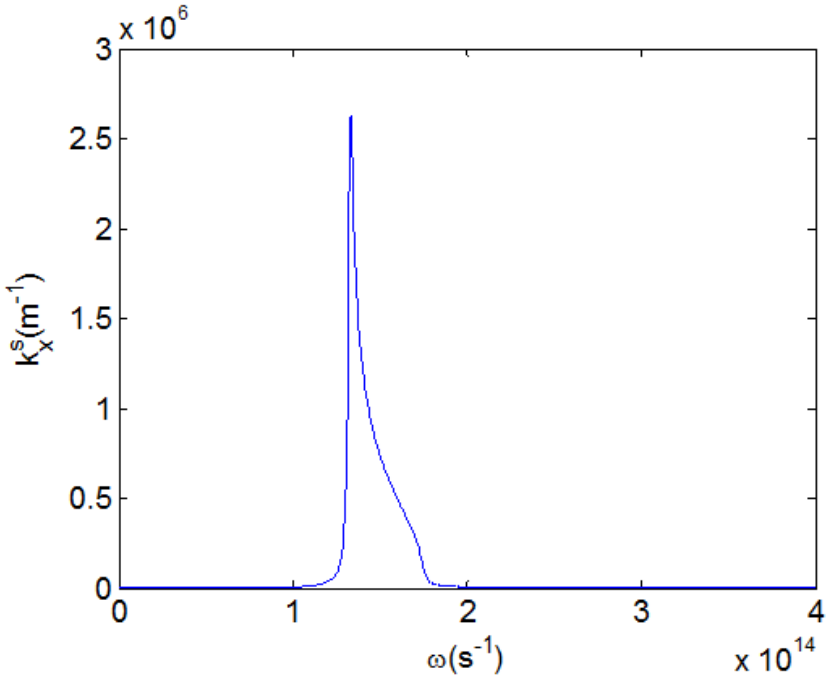

Figure 3.18: Wave vector dispersions for s-polarized when ε_2 and μ_2 in the opposite sign, $\mu_1 = \pm 1, \varepsilon_1 = \mp 1$

Negative refractive index case ($\varepsilon_2(\omega)$[Eq. (3.33)], $\mu_2(\omega)$[Eq. (3.33)])

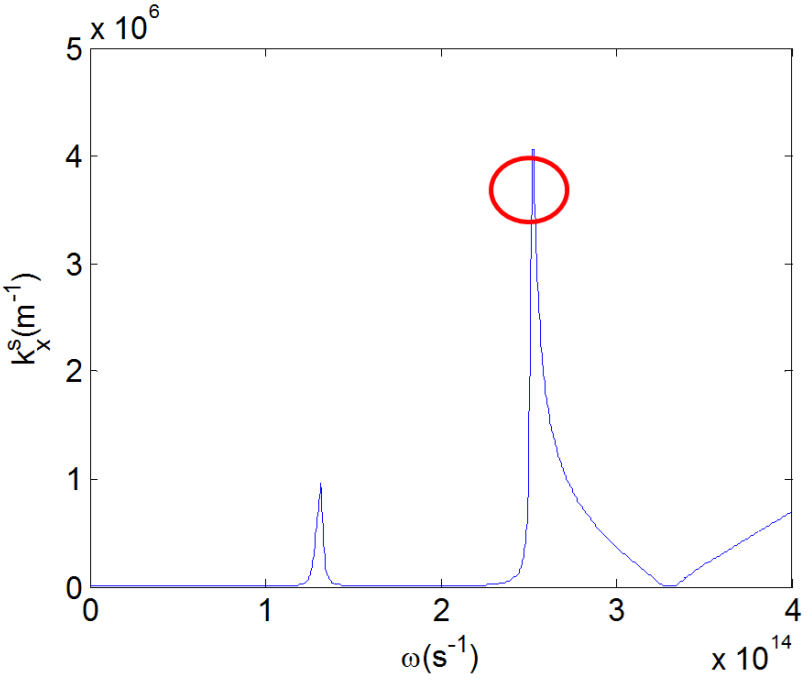

Figure 3.19: Wave vector dispersions for s-polarized when ε_2 and μ_2 in the opposite sign, $\mu_1 = \pm 1, \varepsilon_1 = \mp 1$, double resonance spectra are observed.

Positive refractive index case ($\varepsilon_2(\omega)$[Eq. (3.33)], $\mu_2 = 5$)

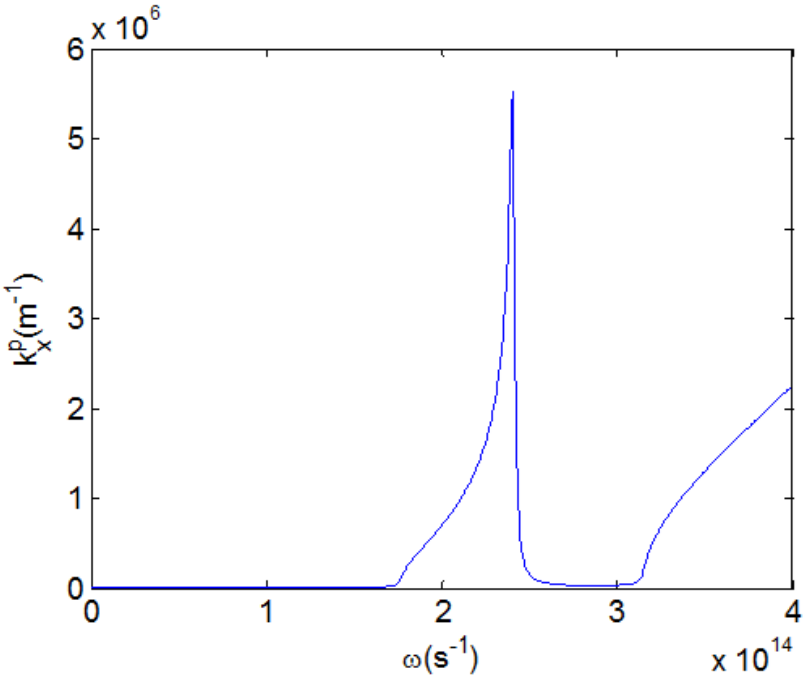

Figure 3.20: Wave vector dispersions for p-polarized when ε_2 and μ_2 in the opposite sign, $\mu_1 = \pm 1, \varepsilon_1 = \mp 1$

Negative refractive index case ($\varepsilon_2(\omega)$[Eq. (3.33)], $\mu_2(\omega)$[Eq. (3.33)])

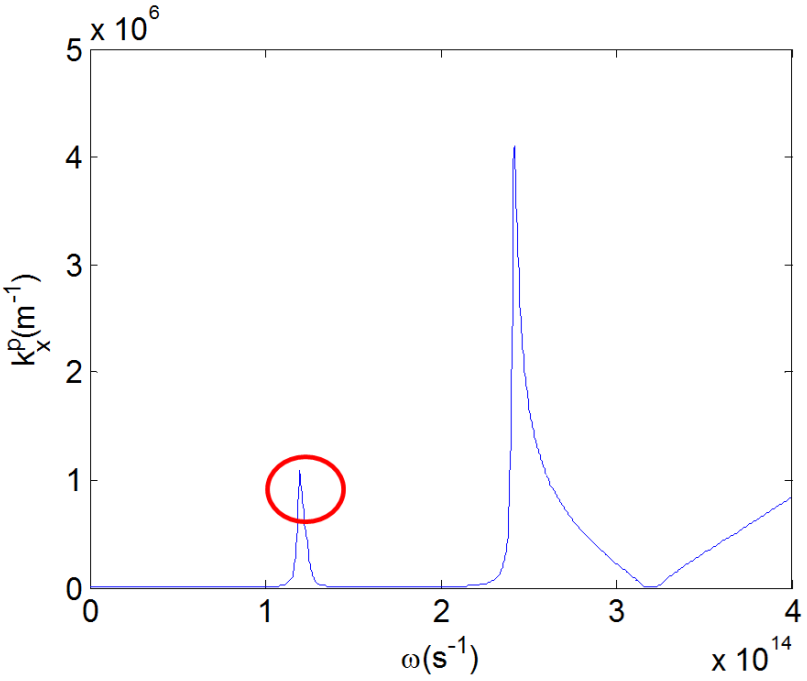

Figure 3.21: Wave vector dispersions for p-polarized when ε_2 and μ_2 in the opposite sign, $\mu_1 = \pm 1, \varepsilon_1 = \mp 1$, double resonance spectra are observed.

3.3.2 Superconductor

Here we show a remarkable effect of using superconducting material. Superconductor is an element or compound that will conduct electricity without resistant below a certain temperature. Once set in motion, electrical current will flow forever in a closed loop of superconducting materials. The effect of SPR is modelled by the dielectric function of metals, which includes both conductors and superconductors (Ooi, Yeung, Kam, & Lim, 2006):

$$\varepsilon_s(\omega) = 1 - \omega_p^2[\frac{f_n}{\omega(\omega + i\gamma)} + \frac{f_s}{\omega^2}] \tag{3.34}$$

where $f_n = n_n/n = 0.2$ is the normal (n) fluid fraction, $f_s = n_s/n = 0.8$ the superfluid fraction, with $n = n_s + n_n$ as the total electron number density, $\omega_p = \sqrt{\frac{ne^2}{me_0}} = 2.5 \times 10^{14}\, s^{-1}$ is the plasma frequency, and $\gamma = 1.3 \times 10^{13}\, s^{-1}$. Typically $\omega_p = 3 \times 10^{12}\, m^{-1}$ and $3 \times 10^{14}\, m^{-1}$ for $BiSr_2Ca_2Cu_2O_{8+x}$ and metallic superconductors, respectively (Van Duzer & Turner, 1981). Figure shows the dispersive superconductor with $\varepsilon_2(\omega)$ and dispersive magnetic material with $\mu_2(\omega)$. While a negative refractive index region is showed in Fig. (3.23). The s-polarization wave vector is large for small frequency, enabling superresolution at terahertz frequency range $\omega = 10^{12}\, s^{-1}$, with the effective wave vector reduced almost 80 times: $\lambda/\lambda^s_{eff} \simeq 80$, where $k^q_s = \frac{2\pi}{\lambda^q_{eff}}$, $\frac{\omega}{c} = \frac{2\pi}{\lambda}, q = s$, and p. The magnetic material, as in Figs. (3.23) and (3.25), creates the second peaks for the s- and p-polarization cases.

To conclude, if the materials are both dielectric and magnetic, $\mu_i, \varepsilon_i \neq 1$, the s-polarized light can also excite the propagating surface modes not just the p-polarized light. The requirement for enhancement is that either the μ or the ε has opposite signs in the two media and either the μ or the ε has almost equal value in the two media, as sumarized in Fig. (3.1) . For s-polarised enhancement, E_z field oscillates rapidly across the x direction. While for p-polarised enhancement, E_x field oscillates rapidly across the x direction. Next, we observed that the presence of dispersion with a resonance in μ gives rise to an additional peak in the spectrum of k_x for both polarizations. By introducing superconductor as in section 3.3.1, the s-polarization wave vector is large for small frequency, enabling superresolution at terahertz frequency range.

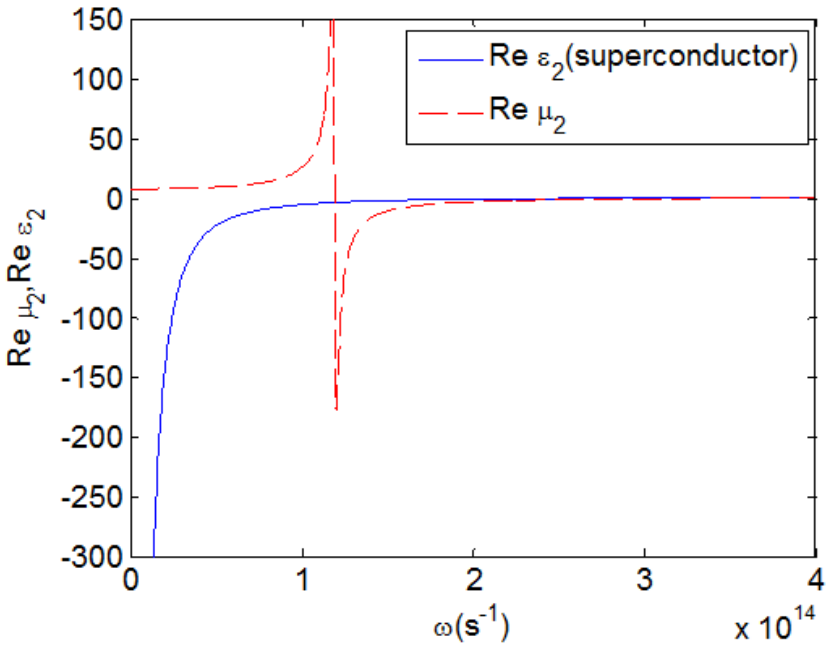

Figure 3.22: Dispersive superconductor with $\varepsilon_2(\omega)$ and dispersive magnetic material with $\mu_2(\omega)$

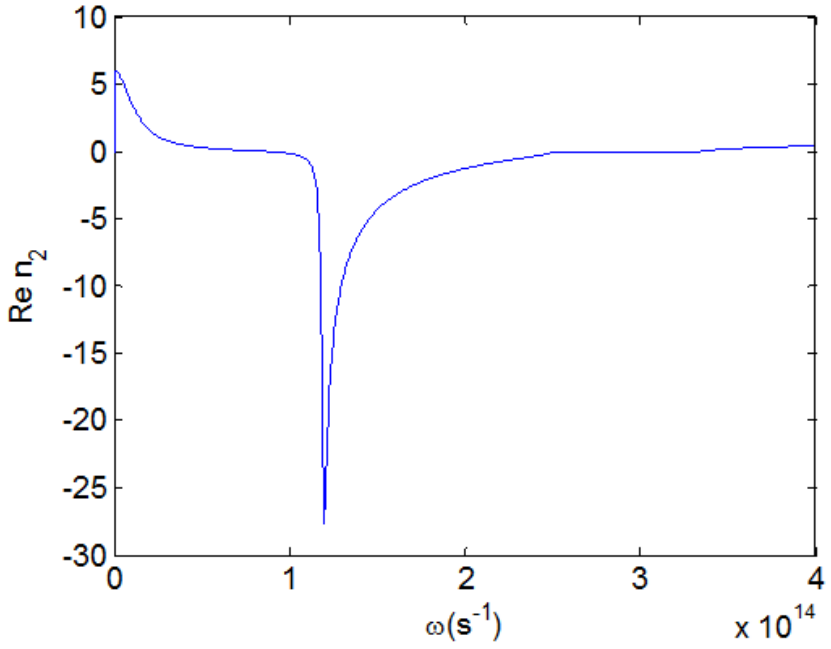

Figure 3.23: $n_2(\omega) = \sqrt{\varepsilon_2(\omega)\mu_2(\omega)}$ with negative refractive index region

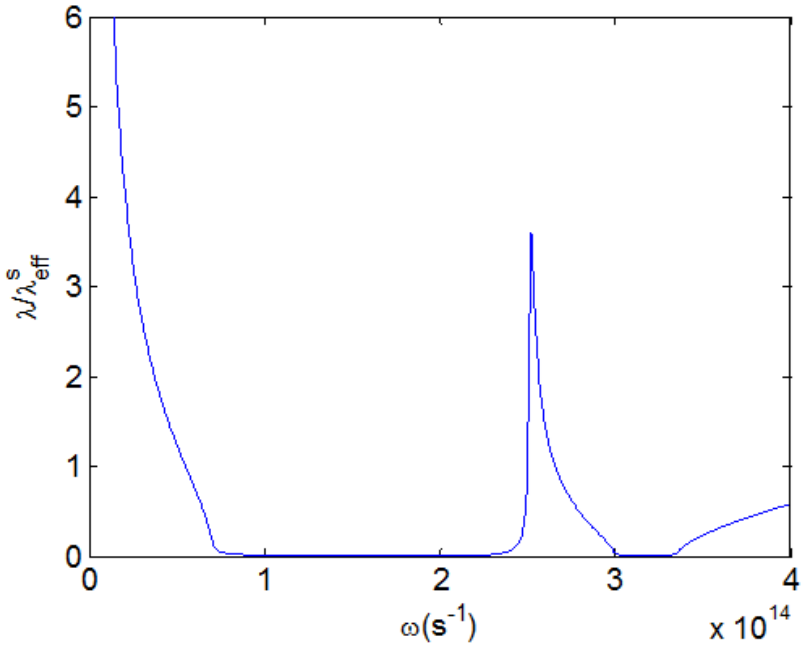

Figure 3.24: The enhancement $\lambda/\lambda_{eff}^{s}$ of surface polaritons for s-polarized light.

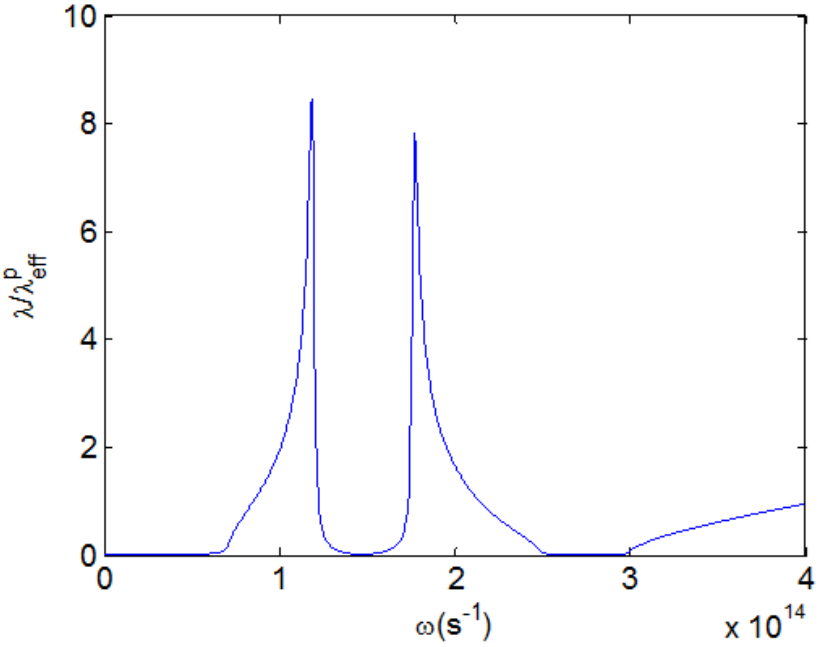

Figure 3.25: The enhancement $\lambda/\lambda_{eff}^{p}$ of surface polaritons for p-polarized light.

CHAPTER 4

SP RESONANCE IN LARGE FREQUENCY RANGE

In this chapter, we present the underlying theoretical expressions for the tangential wave vectors and discuss their property. We divide our result into two parts. The first part shows the influences of the values of permittivity constant and permeability constant of medium 2 on the surface polariton resonance frequency. In the second part, we discuss the possibility of achieving large tangential wave vectors for most of the frequency ranges.

4.1 Metamaterial

Metamaterials are artificial materials engineered to have properties that may not be found in nature. It is a material that gains its properties from its structure rather than directly from its composition. In 1999, the term "metamaterials" was coined by Rodger M. Walser of the University of Texas at Austin. He defined metamaterials as :

Macroscopic composites having a manmade, three-dimensional, periodic cellular architecture designed to produce an optimized combination, not available in nature, of two or more responses to specific excitation.

Their precise shape, size, geometry, orientation and arrangement can affect the electromagnetic waves in an unconventional manner, creating material properties which are unachievable with conventional materials. In order for its structure to affect electromagnetic waves, a metamaterial must have structural properties at least as small as the wavelength of the electromagnetic radiation it interacts with. For instance, if a metamaterial is to behave as a homogeneous material accurately described by an effective refractive index, the feature sizes must be much smaller than the wavelength.

The emergence of metamaterials has an impact on nearly all branches of modern optics and photonics from geometrical optics and diffraction theory, to nonlinear and guided waves optics. Recent years, negative refractive index material has been a hot topic for researcher since the first artificial medium for which the electric permittivity and the magnetic permeability are simultaneously negative are built at 1999 by an array of wires

interspersed with an array of split ring resonators (Smith, Padilla, Vier, Nemat-Nasser, & Schultz, 2000). This left-handed materials presents unusual properties due to various anomalous effects such as reversed Doppler shift, reversed Cerenkov radiation, negative radiation pressure and inverse Snell-Descartes law (Veselago, 1968)(Pendry & Smith, 2004)(Shelby, Smith, & Schultz, 2001). Consequently, surface polaritons supported by left-handed medium have been studied extensively.

4.2 Influence of Difference Values Of μ and ε Towards SP Resonance Frequency

In Chapter 2, we compute the tangential wavevector, β versus frequency, ω for s-polarized and p-polarized plane wave traversing the interface between medium 1 and 2. By applying the continuity of the tangential components for the E field and the H field, the tangential wave vector for s-polarized light is found:

$$k_x^s = \frac{\omega}{c}\sqrt{(\frac{\varepsilon_1\mu_2 - \mu_1\varepsilon_2}{\mu_2 - \mu_1})\frac{\mu_1\mu_2}{\mu_1 + \mu_2}} \tag{4.1}$$

Similarly, for p-polarized light,

$$k_x^p = \frac{\omega}{c}\sqrt{(\frac{\mu_1\varepsilon_2 - \varepsilon_1\mu_2}{\varepsilon_2 - \varepsilon_1})\frac{\varepsilon_1\varepsilon_2}{\varepsilon_1 + \varepsilon_2}} \tag{4.2}$$

These two formulae are only valid if either one of the mediums or both with effective permeability not equal to unity. Taking medium 1 to be metamaterial which is constructed of an array of wires interspersed with an array of split ring resonators, the dielectric function will be:

$$\varepsilon(\omega) = 1 - \frac{\omega_p^2}{\omega(\omega + i\gamma)} \tag{4.3}$$

where γ is damping term, $\omega_p^2 = 2\pi c^2/a^2\, ln(a/r)$; with wires separation distance, a and wire radius, r; ω_p is plasma frequency of the medium which depends on the dimensions of the structure (Pendry, Holden, Stewart, & Youngs, 1996). While magnetic permeability:

$$\mu(\omega) = 1 - \frac{F\omega^2}{\omega^2 - \omega_0^2 + i\omega\Gamma} \tag{4.4}$$

where F is fractional area of the unit cell occupied by the interior of the split ring, Γ is

the dissipation factor, and $\omega_0^2 = 3dc^2/\pi^2 r^3$, with separation distance of cylinder, d and radius of cylinder, r, ω_0 is resonance frequency of split ring resonator, which depends on the dimensions of the structure also (Pendry et al., 1999). In this numerical calculation, $F = 0.56$, $\omega_0 = 2 \times 10^{14} Hz$, $\omega_p = 10 \times 10^{14} Hz$, so that the dispersion curves will be in optical range.

In normal plasmonics approach, SP resonance can only happen if $\varepsilon_1 = -\varepsilon_2$ or $\mu_1 = -\mu_2$. From the denominator of Eq. (4.1) and Eq. (4.2), it is clearly indicating that SP resonance will happen if $\varepsilon_1 = \varepsilon_2$ (new regime) and $\varepsilon_1 = -\varepsilon_2$ for p-polarised case while $\mu_1 = \mu_2$ (new regime) and $\mu_1 = -\mu_2$ for s-polarised case. From Figs. (4.1) and (4.2), SP resonance frequency for s-polarised and p-polarised light can be controlled by having different permittivity or permeability constant of medium 2. The higher values of the permittivity/permeability constant of medium 2 (positive), the lower values of SP resonance frequency, for both s and p polarised light. Resonance happens due to $\varepsilon_1 = -\varepsilon_2$ and $\mu_1 = -\mu_2$ (left graphs). Besides that, the resonance can happen if ε_2 or μ_2 are both negative (right graphs). The more negative of permittivity/permeability constant of medium 2, the lower of the SP resonance frequency for both s and p polarised light. In contrast to the previous approach, this resonances are due to $\varepsilon_1 = \varepsilon_2$ and $\mu_1 = \mu_2$ (new regime). The dispersions are exactly equal with the positive permittivity/permeability curves. This result is used for computing the next part.

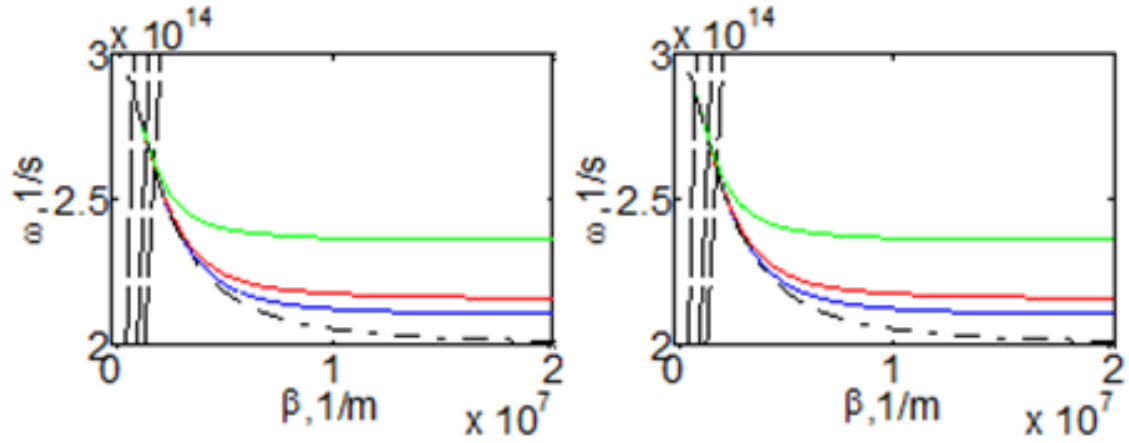

Figure 4.1: Left: SP dispersion for s-polarised light with $\mu_2 = 1$ (green); 3 (red); 5 (blue) $\varepsilon_2 = 1$. Right: SP dispersion with $\mu_2 = -1$ (green); -3 (red); -5 (blue) $\varepsilon_2 = -1$.

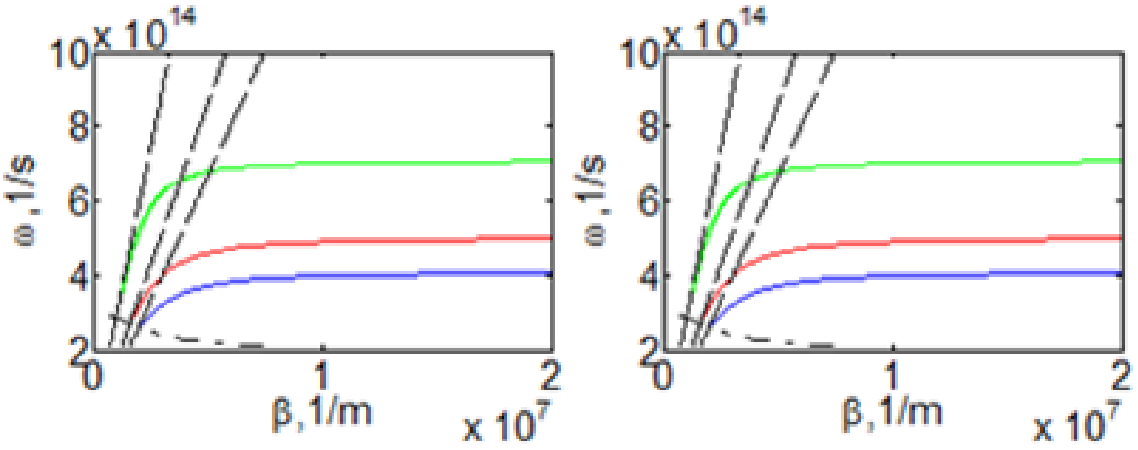

Figure 4.2: Left: SP dispersion for p-polarised light with $\varepsilon_2 = 1$ (green); 3 (red); 5 (blue) $\varepsilon_2 = 1$. Right: SP dispersion with $\varepsilon_2 = -1$ (green); -3 (red); -5 (blue) $\mu_2 = -1$.

4.3 Large Wavevector at Large Frequency Range

Usually, the resonance (large wavevector) happen in single frequency, but from above result,$\varepsilon_1 = \varepsilon_2$ and $\mu_1 = \mu_2$ can give resonance too. Hence, we can have large wavevector if ε_1 is almost equal to ε_2 and μ_1 is almost equal to μ_2 for every frequency of dispersive medium 1 and dispersive medium 2. Due to advancement of metamaterial technology, it is believed that two mediums with slightly dissimilar permittivity and permeability can be built. Let see Eq. (4.3) and Eq. (4.4), we can have slightly different ω_p and ω_0 by building with slightly different of a, r and d, r respectively. Hence, at every frequency, ε_1 is almost equal to ε_2 and μ_1 is almost equal to μ_2, large wavevector can be obtained for a large range of frequency. In view of Eq. (4.1), in order for β_s to be real and has large wavevector, conditions $\mu_2 - \mu_1 \approx 0^-$ (ε_2 positive) and $\mu_2 - \mu_1 \approx 0^+$ (ε_2 negative) have to be satisfied. Also, for Eq. (4.2), in order for β_p to be real and has large wavevector, conditions $\varepsilon_2 - \varepsilon_1 \approx 0^-$ ($\mu_1 < \mu_2$) and$\varepsilon_2 - \varepsilon_1 \approx 0^-$ ($\mu_1 > \mu_2$) have to be satisfied.

In Fig. (4.3)(a), for an ideal dispersive medium 1, both permittivity and permeability are dispersive with frequency, joint with a medium 2 which permittivity is dispersive, p-polarised SP wavevector at the interface is large for large range of frequency. While s-polarised SP does not get influenced by this combination (Fig. (4.3)(b)). In the meantime, the dispersive medium 1, joint with medium 2 which permeability is dispersive (Fig. (4.3)(c)), s-polarised SP wavevector is large for large range of frequency and cover most the frequency range which originally does not cover if medium 2 is non-dispersive. While p-polarised SP does not get affected by this combination (Fig. (4.3)(d)). Note, the black doted and broken lines are the lines of $k_0^2\varepsilon_i\mu_i$, for $i = 1, 2$. In order for SP to exist, β must be larger than $k_0^2\varepsilon_i\mu_i$.

Real materials come with losses. We introduce damping term and dissipation factor into ε and μ. The dispersion curves are again plotted in Fig. (4.4). From the result, a non-dispersive medium 2 leads to single resonance peak for both p and s polarised wave. However a dispersive medium 2 with slightly dissimilar permittivity or permeability with medium 1, clearly demonstrates that this combination leads to large wavevector for almost all the frequency. Also the values are larger than the resonance peak of a non-dispersive medium 2. It can be said that, when a white light of combination from various frequency

is illuminated to excite SP, every single frequency will cause large wavevector. In other word, every single frequency will cause resonance. This enhancement will lead to further novel effects and applications such as near field optic, enhancement of fluorescence and photoelectric devices.

Besides that, looking into the denominator of Eq. (4.1) and Eq. (4.2), the nearer the dispersive ε_2 to ε_1 or μ_2 to μ_1, the bigger the wavevector will be. As in Fig. (4.5), when plasma frequency of medium 2 is closer to medium 1, wavevector for p-polarised light is increasing. Meanwhile, as resonance frequency of medium 2 is closer to medium 1, wavevector for s-polarised light is increasing too. We can also enhance the wavevector if the non-dispersive ε and μ constants are increasing as in Fig. (4.6).

To conclude, new regime of surface resonance occurs when two mediums have almost equal permittivity constant or permeability constant. For a dispersive medium 1 with both permittivity and permeability are dispersive with frequency, surface polariton resonance in large frequency range can be achieved if permittivity or permeability of medium 2 is always close to medium 1.

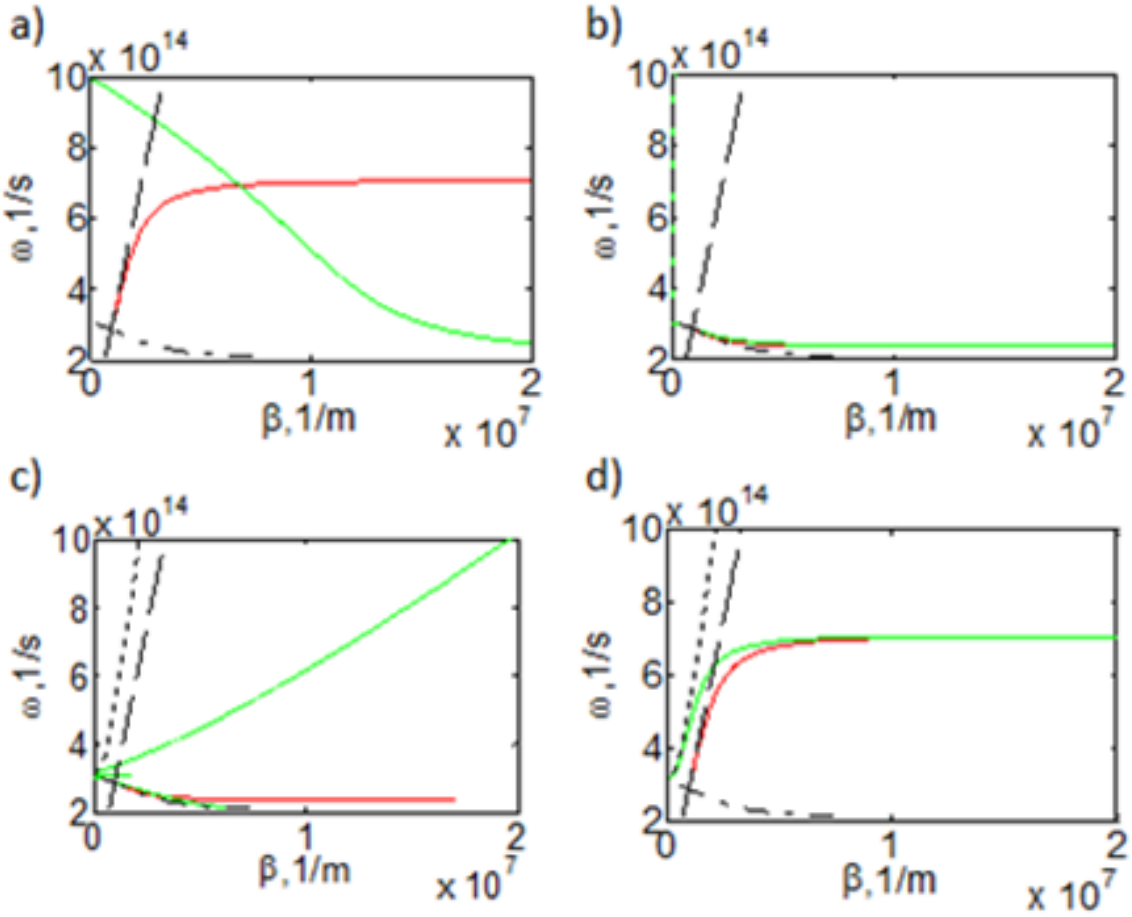

Figure 4.3: ε_1 is dispersive Eq. (4.3); μ_1 is dispersive Eq. (4.4) with 0 loss. a) p-polarised dispersion curves for dispersive ε_2; $\mu_2 = 1$ (green), $\varepsilon_2 = 1$; $\mu_2 = 1$ (red). b) s-polarised dispersion curves for dispersive ε_2; $\mu_2 = 1$ (green), $\varepsilon_2 = 1$; $\mu_2 = 1$ (red). c) s-polarised dispersion curves for $\varepsilon_2 = 1$; dispersive μ_2 (green),$\varepsilon_2 = 1$; $\mu_2 = 1$ (red). d) s-polarised dispersion curves for $\varepsilon_2 = 1$; dispersive μ_2 (green), ,$\varepsilon_2 = 1$; $\mu_2 = 1$ (red).

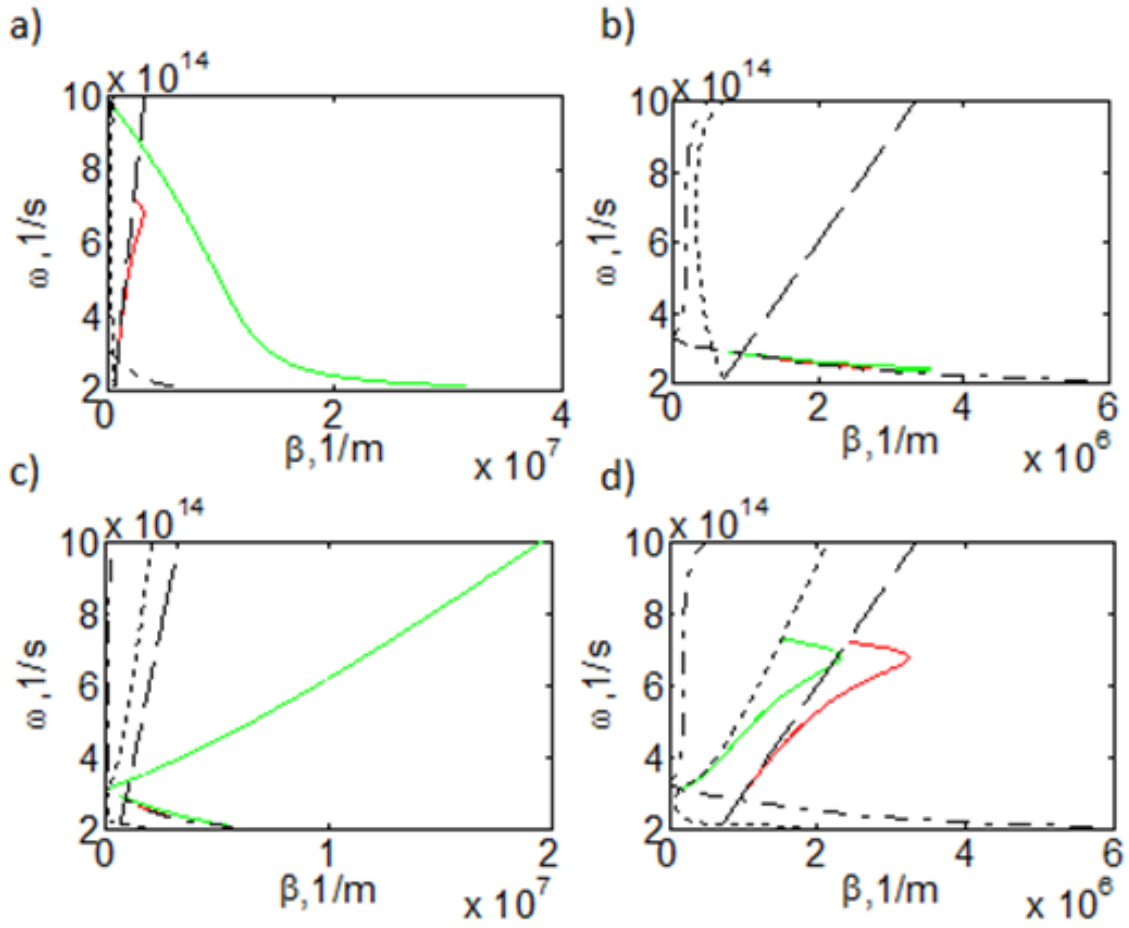

Figure 4.4: ε_1 is dispersive Eq. (4.3); μ_1 is dispersive Eq. (4.4) with $\gamma = 1 \times 10^{14}$, $\Gamma = 1 \times 10^{13}$. a) p-polarised dispersion curves for dispersive ε_2; $\mu_2 = 1$ (green), $\varepsilon_2 = 1$; $\mu_2 = 1$ (red). b) s-polarised dispersion curves for dispersive ε_2; $\mu_2 = 1$ (green), $\varepsilon_2 = 1$; $\mu_2 = 1$ (red). c) s-polarised dispersion curves for $\varepsilon_2 = 1$; dispersive μ_2 (green),$\varepsilon_2 = 1$; $\mu_2 = 1$ (red). d) s-polarised dispersion curves for $\varepsilon_2 = 1$; dispersive μ_2 (green), ,$\varepsilon_2 = 1$; $\mu_2 = 1$ (red).

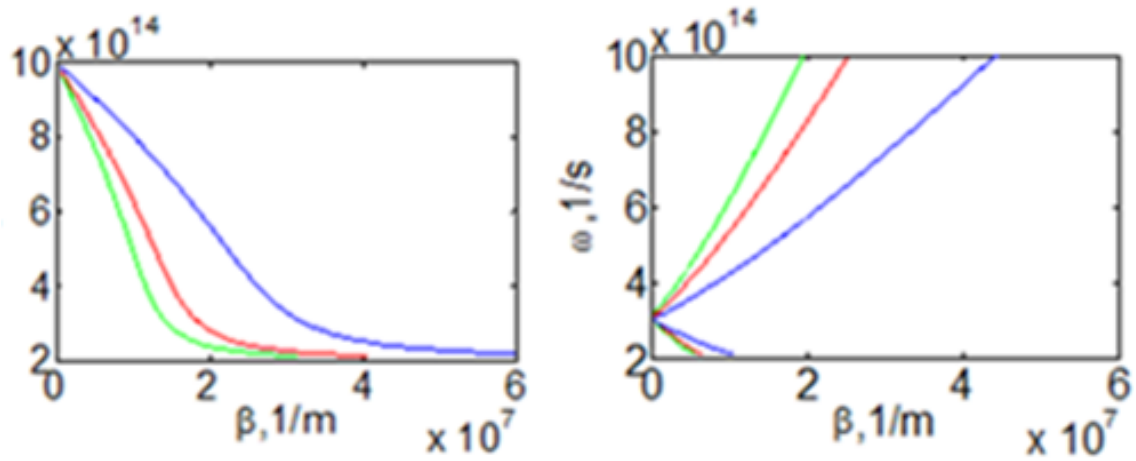

Figure 4.5: ε_1 is dispersive Eq. (4.3); μ_1 is dispersive Eq. c4) with $\gamma = 1 \times 10^{14}$, $\Gamma = 1 \times 10^{13}$. Left: p-polarised dispersion curves for dispersive ε_2, $\mu_2 = 1$, $\omega_p = 10.1$ (green), 10.06 (red), 10.02 (blue) Right: s-polarised dispersion curves for $\varepsilon_2 = 1$; dispersive μ_2, $\omega_0 = 2.1$ (green), 2.06 (red), 2.02 (blue).

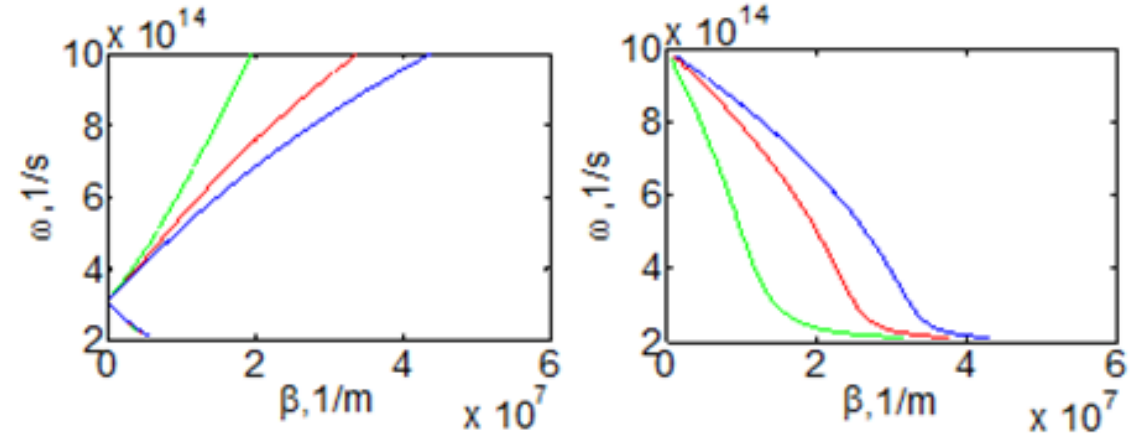

Figure 4.6: ε_1 is dispersive Eq. (4.3); μ_1 is dispersive Eq. (4.4) with $\gamma = 1 \times 10^{14}$, $\Gamma = 1 \times 10^{13}$. Left: s-polarised dispersion curves for dispersive μ_2, $\varepsilon_2 = 1$ (green), 3 (red),5 (blue). Right: p-polarised dispersion curves for dispersive ε_2; $\mu_2 = 1$ (green), 3(red), 5(blue).

CHAPTER 5

SP MODES IN IDEAL AND LOSSY METAMATERIAL SLAB

In this chapter, we consider SP propagation in a slab with 2 interfaces. Each single interface can sustain bound SP. When the separation between adjacent interfaces is comparable to or smaller than the decay length of the interface mode, interactions between SP at both interface give rise to coupled modes. Their properties depend on the slab thickness and the dielectric medium on both sides of the slab. The thin slab we investigate here is a metamaterial slab.

5.1 SP Modes In Thin Slab

There existence of two thermally excited SP modes, one symmetric(even mode) and one antisymmetric(odd mode), that propagate on thin slab. Looking back to Fig. (2.2), the symmetric environment on both sides of the metal slab, medium 2 = medium 3, has interesting properties, especially if the thickness, d ($d = 2a$ refer to Fig. (2.2)), of the metal slab becomes small, more exactly $k_y/d \ll 1$. The symmetry causes the SP frequency to be the same on both sides of the slab. Hence, in the case of a thin slab the electromagnetic fields of both surfaces interact and the frequency splits into odd mode (electric field asymmetric to the plane $y = 0$ with higher frequency) and even mode (electric field symmetric to the plane $y = 0$ with lower frequency).

In chapter 2, we derived SP dispersion relation of double interface for s-polarized and p-polarized cases. Recall Eq. (2.72) and Eq. (2.73),

$$\tanh(k_1 a) = -\frac{\mu_1 k_2}{\mu_2 k_1} \tag{5.1}$$

$$\coth(k_1 a) = -\frac{\mu_1 k_2}{\mu_2 k_1} \tag{5.2}$$

Eq. (5.1) is s-polarised odd mode while Eq. (5.2) is s-polarised even modes. Meanwhile

from Eq. (2.96) and Eq. (2.97), we have

$$\tanh(k_1 a) = -\frac{\varepsilon_1 k_2}{\varepsilon_2 k_1} \tag{5.3}$$

$$\coth(k_1 a) = -\frac{\varepsilon_1 k_2}{\varepsilon_2 k_1} \tag{5.4}$$

Eq. (5.3) is p-polarised odd mode while Eq. (5.4) is p-polarised even modes. The expression of the tangential wave vector for p-polarization is completely symmetrical to that of the s-polarization, due to the symmetry between the electric and magnetic responses in Maxwell equations. Also, from Eq. (2.90)

$$k_i^2 = \beta^2 - k_0^2 \varepsilon_i \mu_i \tag{5.5}$$

which relate tangential wavevector to normal wavevector, we can solve for SP wavevector dispersion for both polarization.

5.2 Dispersions Of Surface Polaritons In Ideal Thin slab

Considering medium 2 is air where $\mu_2 = 1$ and $\varepsilon_2 = 1$, and medium 1 be a metamaterial which is created with an array of wires interspersed with an array of split ring resonators. The dielectric function is

$$\varepsilon(\omega) = 1 - \frac{\omega_p^2}{\omega(\omega + i\gamma)} \tag{5.6}$$

and magnetic permeability is

$$\mu(\omega) = 1 - \frac{F\omega^2}{\omega^2 - \omega_0^2 + i\omega\Gamma} \tag{5.7}$$

Without consider damping, we will solve for tangential wavevector in this metamaterial slab. Parameters used are $F = 0.56$, $\omega_p = 10 \times 10^9$ and $\omega_0 = 4 \times 10^9$, consistent with (Smith et al., 2000). The frequency range we analyzed is 0 to $10 \times 10^9\, Hz$. The properties of each dispersion curves will be analyzed.

5.2.1 s-polarised SP

To find the odd mode dispersion of s-polarization, we solve for tangential wavevector, β, by substituting Eq. (5.5) into Eq. (5.1),

$$\begin{aligned}
\tanh(a\sqrt{\beta^2-k_0^2\varepsilon_1\mu_1}) &= -\frac{\mu_1\sqrt{\beta^2-k_0^2\varepsilon_2\mu_2}}{\mu_2\sqrt{\beta^2-k_0^2\varepsilon_1\mu_1}} \\
\exp\left(-2a\sqrt{\frac{1}{c^2}(c^2\beta^2-\omega^2\mu_1\varepsilon_1)}\right) & \\
\left[\left(\mu_2\sqrt{\frac{1}{c^2}(c^2\beta^2-\omega^2\mu_1\varepsilon_1)}\right)-\left(\mu_1\sqrt{\frac{1}{c^2}(c^2\beta^2-\omega^2\mu_2\varepsilon_2)}\right)\right] & \\
+\mu_2\sqrt{\frac{1}{c^2}(c^2\beta^2-\omega^2\mu_1\varepsilon_1)} &= \mu_1\sqrt{\frac{1}{c^2}(c^2\beta^2-\omega^2\mu_2\varepsilon_2)} \\
\exp\left(-2a\sqrt{\frac{1}{c^2}(c^2\beta^2-\omega^2\mu_1\varepsilon_1)}\right) &= \frac{1+\frac{\mu_1\sqrt{\frac{1}{c^2}\left(c^2\beta^2-\omega^2\mu_2\varepsilon_2\right)}}{\mu_2\sqrt{\frac{1}{c^2}\left(c^2\beta^2-\omega^2\mu_1\varepsilon_1\right)}}}{1-\frac{\mu_1\sqrt{\frac{1}{c^2}\left(c^2\beta^2-\omega^2\mu_2\varepsilon_2\right)}}{\mu_2\sqrt{\frac{1}{c^2}\left(c^2\beta^2-\omega^2\mu_1\varepsilon_1\right)}}}
\end{aligned} \tag{5.8}$$

Eq. (5.8) is solved numerically as in appendix A. Next, to find the even mode dispersion of s-polarization, we solve for tangential wavevector, β, by substitute Eq. (5.5) into Eq. (5.2), we get

$$\exp(2a\sqrt{\beta^2-(\frac{\omega}{c})^2\varepsilon_1\mu_1}) = \frac{1-\frac{\mu_2\sqrt{\beta^2-(\frac{\omega}{c})^2\varepsilon_1\mu_1}}{\mu_1\sqrt{\beta^2-(\frac{\omega}{c})^2\varepsilon_2\mu_2}}}{1+\frac{\mu_2\sqrt{\beta^2-(\frac{\omega}{c})^2\varepsilon_1\mu_1}}{\mu_1\sqrt{\beta^2-(\frac{\omega}{c})^2\varepsilon_2\mu_2}}} \tag{5.9}$$

Eq. (5.9) is solved numerically as in appendix B.

Using this method, we calculate the dispersion curves for thickness, d, 0.01m to 0.02m. Fig. (5.1) shows dispersions of ideal s-polarized even mode of thin slab. The wavevector solution is only found at frequency shown. The wavevector is dispersive for both frequency and thickness. We see that, by reducing thickness, the wavevector is increasing. Hence, we can always increase the SP confinement by using thinner slab. Then, β is increasing with increasing frequency until resonance happen at $4.71\times10^9\,s^{-1}$. For thicker thickness, the increasing frequency range is shorter. In fact, when we continue to increase the thickness, the increasing frequency range will be continued to reduce until it vanishes. It is where the SP at both interfaces do not interact anymore because it is too

"thick" for them to interact. If this is the case, we will return to Eq. (3.1), single interface tangential wavevector solution, to solve for β.

Meanwhile, we calculate the dispersion curves of odd mode for thickness, d, 0.01m to 0.014m. Fig. (5.2) shows dispersions of ideal s-polarized odd mode of thin slab. Again, we noticed that SP resonance happen at $4.71 \times 10^9\, s^{-1}$, same with even mode. This resonance frequency, ω_r can be calculated by letting $\mu_1 = -\mu_2$, from Eq. (5.7):

$$\begin{aligned} \mu_1 &= -\mu_2 \\ 1 - \frac{F\omega_r^2}{\omega_r^2 - \omega_0^2} &= -\mu_2 \\ \omega_r^2 &= \frac{\omega_0^2 + \mu_2\omega_0^2}{\mu_2 + 1 - F} \\ \omega_r &= \omega_0\sqrt{\frac{1+\mu_2}{1+\mu_2-F}} \end{aligned} \tag{5.10}$$

We are able to calculate resonance frequency for any materials by using Eq. (5.10). Since $\mu_2 = 1$ in our case,

$$\omega_r = 4 \times 10^9\sqrt{\frac{1+1}{1+1-0.56}} = 4.714 \times 10^9\, s^{-1}$$

From the graph, wavevector, β, solution is found at the frequency range shown. The other frequency range has no solution. β is dispersive for both frequency and thickness. For increasing thickness, β is reducing, similiar to even mode. However, there are two branch of solutions in odd mode. One with positive $d\omega/d\beta$, another with negative $d\omega/d\beta$. We enlarge Fig. (5.2), to show the positive $d\omega/d\beta$ branch clearer in Fig. (5.3). There is a turning point for positive $d\omega/d\beta$ change to negative $d\omega/d\beta$ and this turning point frequency is increasing with decreasing thickness. The positive branch of β (blue color surface in Fig. (5.2)) shows interesting feature when we consider damping in next subsection. Besides that, we also see that for increasing thickness, frequency range of solution is shorter. Same with even mode, when we continue to increase the thickness, the frequency range of solution will be continue to reduce until vanish. The SP at both interface do not interact anymore because it is too "thick" for them to interact. Hence, the β solution is return to the one interface solution (Eq. (3.1)) again.

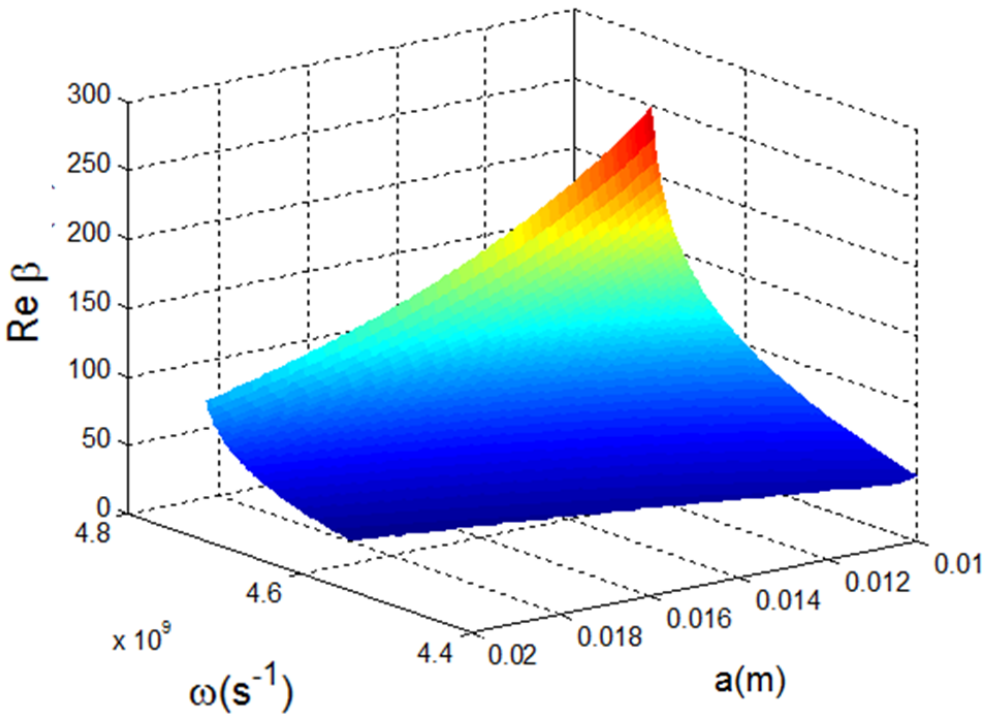

Figure 5.1: Dispersion of ideal s-polarized even mode

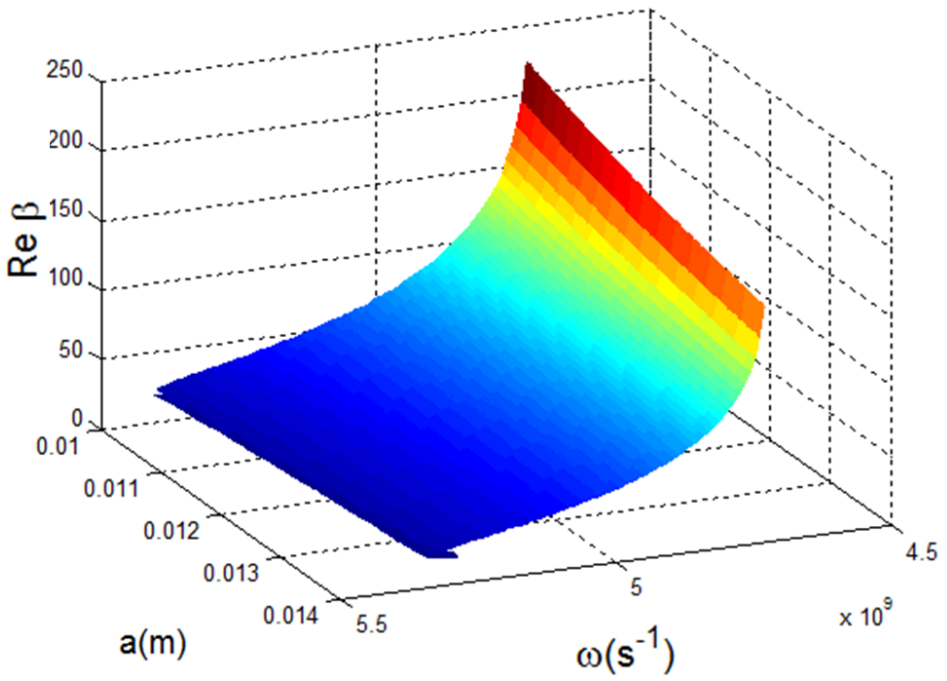

Figure 5.2: Dispersion of ideal s-polarized odd mode

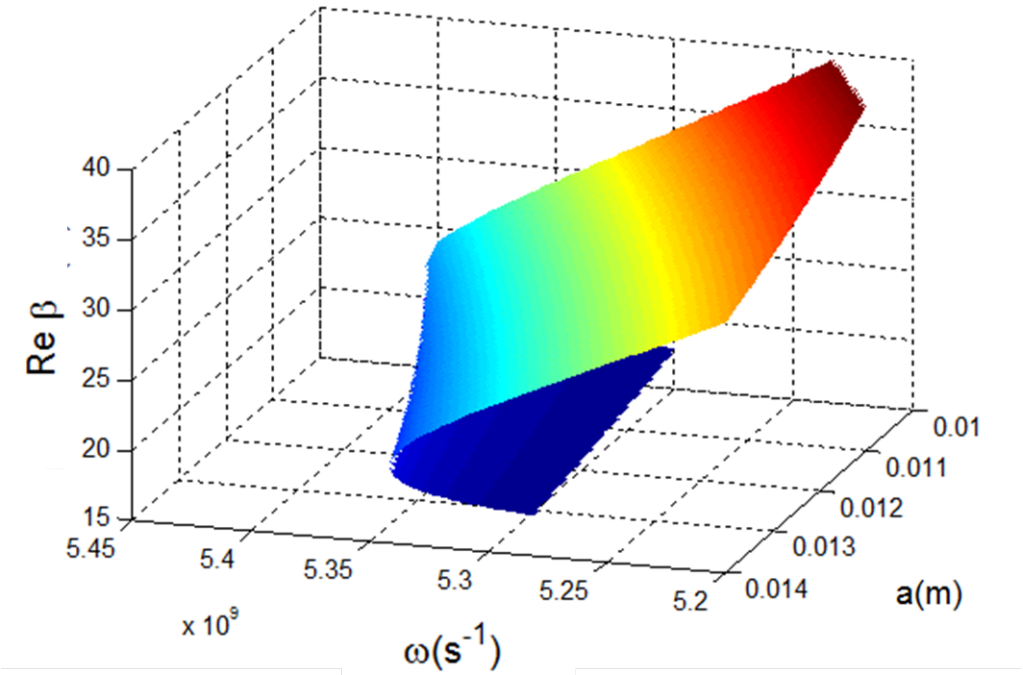

Figure 5.3: Dispersion of ideal s-polarized odd mode(enlarged)

5.2.2 p-polarised SP

Next, we move to p-polarization. To find the odd mode dispersion, we solve for tangential wavevector, β, by substitute Eq. (5.3) into Eq. (5.3),

$$\exp(-2a\sqrt{\beta^2-(\frac{\omega}{c})^2\varepsilon_1\mu_1}) = \frac{1+\frac{\varepsilon_1\sqrt{\beta^2-(\frac{\omega}{c})^2\varepsilon_2\mu_2}}{\varepsilon_2\sqrt{\beta^2-(\frac{\omega}{c})^2\varepsilon_1\mu_1}}}{1-\frac{\varepsilon_1\sqrt{\beta^2-(\frac{\omega}{c})^2\varepsilon_2\mu_2}}{\varepsilon_2\sqrt{\beta^2-(\frac{\omega}{c})^2\varepsilon_1\mu_1}}} \tag{5.11}$$

Eq. (5.11) is solved numerically as in appendix C. For even mode dispersion of p-polarization, we solve for tangential wavevector, β, by substitute Eq. (5.5) into Eq. (5.4), we get

$$\exp(-2a\sqrt{\beta^2-(\frac{\omega}{c})^2\varepsilon_1\mu_1}) = \frac{1+\frac{\varepsilon_2\sqrt{\beta^2-(\frac{\omega}{c})^2\varepsilon_1\mu_1}}{\varepsilon_1\sqrt{\beta^2-(\frac{\omega}{c})^2\varepsilon_2\mu_2}}}{1-\frac{\varepsilon_2\sqrt{\beta^2-(\frac{\omega}{c})^2\varepsilon_1\mu_1}}{\varepsilon_1\sqrt{\beta^2-(\frac{\omega}{c})^2\varepsilon_2\mu_2}}} \tag{5.12}$$

Eq. (5.12) is solved numerically as in appendix D.

Therefore, we calculate the dispersion curves for p-polarized even mode for thickness, d, 0.01m to 0.02m. Fig. (5.4) shows dispersions of ideal p-polarized even mode of thin slab. There are two branch of solution for p-polarized even mode. One is from 0 to 4 s^{-1}, another is above 4 s^{-1}. Hence, there are two resonance peaks. The first resonance peak is at ω_0. Another one is when $\varepsilon_1 = \varepsilon_2$. This resonance frequency, ω_R can be calculated by letting $\varepsilon_1 = -\varepsilon_2$, from Eq. (5.6):

$$\begin{aligned} \varepsilon_1 &= -\varepsilon_2 \\ 1-\frac{\omega_p^2}{\omega_R^2} &= -\varepsilon_2 \\ \omega_R &= \frac{\omega_p}{\sqrt{1+\varepsilon_2}} \end{aligned} \tag{5.13}$$

We are able to calculate p-polarized resonance frequency for any materials by using Eq. (5.13). Since $\varepsilon_2 = 1$ in our case,

$$\omega_R = \frac{10\times10^9}{\sqrt{1+1}} = 7.07\times10^9 \tag{5.14}$$

Hence another resonance peak at $7.07\times10^9\, s^{-1}$. β is increasing with reducing thickness,

same with s-polarization. But, the upper frequency branch β is increasing much more than the lower frequency branch. If large field confinement application is needed, upper frequency with smaller thickness is a favour.

Next, we look at odd mode solutions. We calculated p-polarized wavevector for odd mode as in Fig. (5.5). There are two resonance peak also. One at at $\omega_0 = 4 \times 10^9$ and another when $\varepsilon_1 = \varepsilon_2$ where ω is $7.07 \times 10^9\, s^{-1}$. Above this resonance frequency, there is no any solution for ideal metamaterial slab. Similar to s-polarized odd mode, in the upper frequency range, there are two branch of solutions in p-polarized odd mode. One with positive $d\omega/d\beta$, another with negative $d\omega/d\beta$. The positive branch of β shows interesting feature when we consider damping in next subsection. Also, wavevector is increasing with reducing thickness. Besides that, look at both even and odd, there is a frequency gap in the middle where no solution is found. That is between ω_0, $4 \times 10^9\, s^{-1}$ and the starting frequency of the upper branch. It is because the forbidden frequency range does not satisfy these conditions:

$$\beta \gg k_0^2 \varepsilon_i \mu_i \tag{5.15}$$

Looking at Eq. (5.5), for surface polariton propagation to be valid, normal wavevector k_i has to be real.

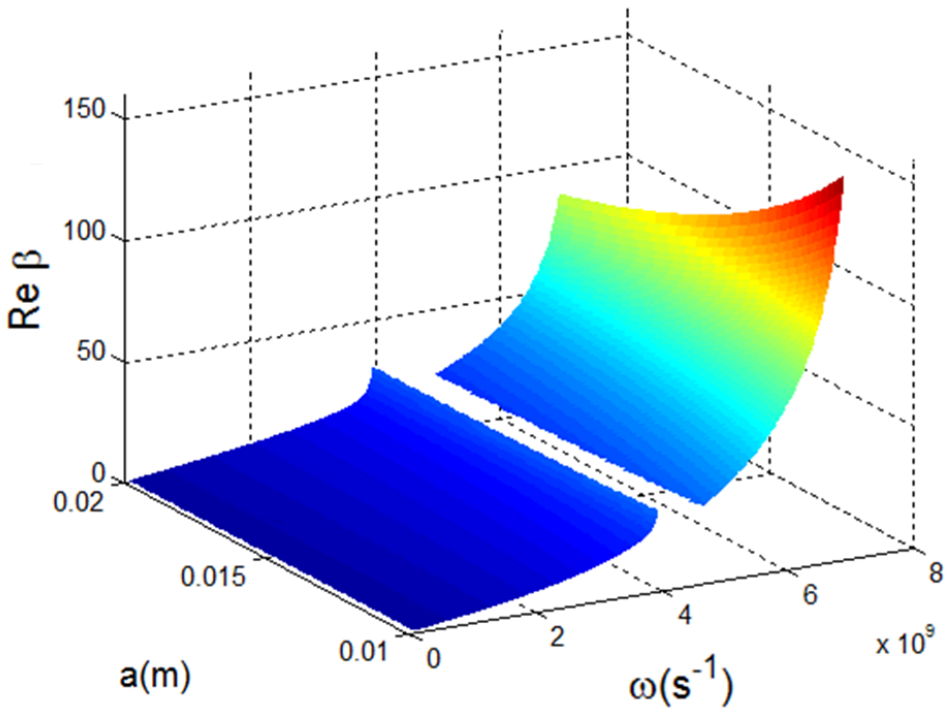

Figure 5.4: Dispersion of ideal p-polarized even mode

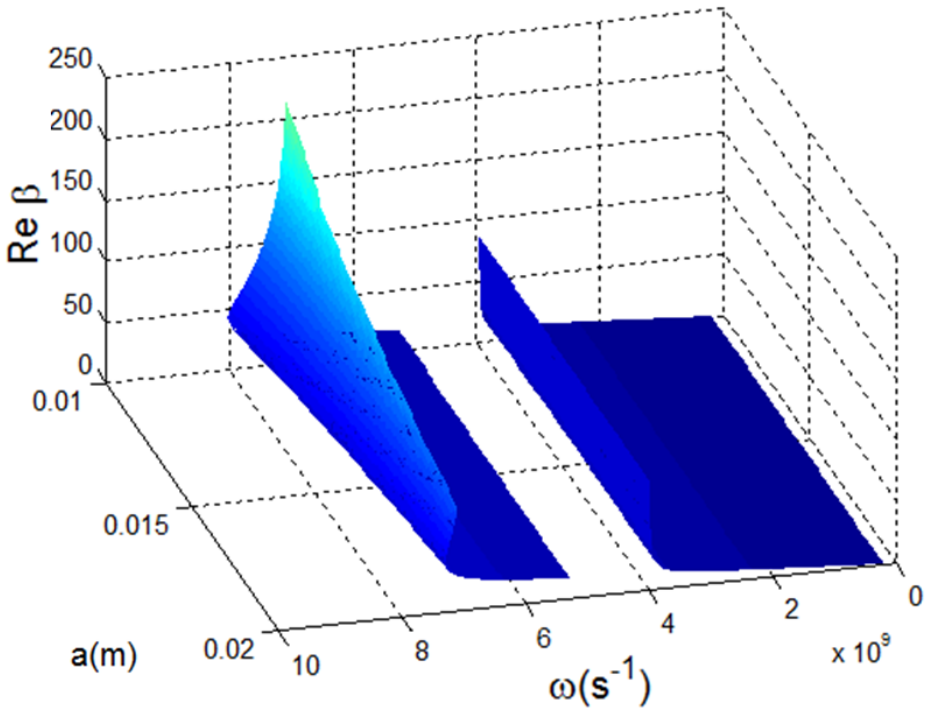

Figure 5.5: Dispersion of ideal p-polarized odd mode

5.3 Dispersions Of Surface Polaritons In Lossy Thin slab

Real material usually comes with damping. In this section, with consider damping in the matematerial slab, we will solve for tangential wavevector. The parameters used are $\gamma = 1 \times 10^9$ in Eq. (5.6), and $\Gamma = 4.2441 \times 10^8$ in Eq. (5.7). The frequency range we analyzed is 0 to $10 \times 10^9\, Hz$. The properties of each dispersion curves will be analyzed.

5.3.1 s-polarised SP

The even mode of s-polarized SP in this lossy thin slab is solved numerically. With considering damping, the solution is shown in Fig. (5.6). Since we have put in the imaginary part, we have dispersion solutions of real wavevector and imaginary wavevector. Fig. (5.6) shows real wavevector of even mode, while Fig. (5.7) shows imaginary wavevector. We see that, with damping, wavevector is approaching to a maximum value around 55 /m while it is go to infinity for the ideal case. Then, when we increase the thickness, the frequency range of solution will be reduce until vanish at thickness around 0.017m. SP at both interfaces do not interact anymore. For imaginary wavevector, it is increasing with increasing thickness and dispersive with frequency also.

Recall from the last section that the ideal solution has two branches of solutions. Fig. (5.8) shows real wavevector dispersions of s-polarized odd mode for negative $d\omega/d\beta$ branch. Fig. (5.9) shows imaginary wavevector dispersions of s-polarized odd mode for negative $d\omega/d\beta$ branch. In the negative branch, at the resonance frequency, real wavevector is approaching to a maximum value around 62 /m while it is go to infinity for the ideal case. There is no solution outside the frequency range shown in Fig. (5.8). Again, reducing thickness will lead to increasing wavevector. Same to imaginary wavevector, reducing thickness will lead to increasing wavevector to a large value.

Divert to the positive branch of odd mode, Fig. (5.10) shows that by reducing the slab thickness, the imaginary wavevector is reducing. In fact, imaginary wavevector is related to SP propagation length, L by

$$L = (2\, Im[\beta])^{-1} \tag{5.16}$$

Hence, from above equation, we can say that in s-polarized odd mode, propagation length

increase with decreasing thickness. This property can not be found in even mode and single interface SP. If we reduce the thickness further as in Fig. (5.11), the imaginary wavevector is reducing further. So when the propagation length increase further, there is no cutoff thickness for this property.

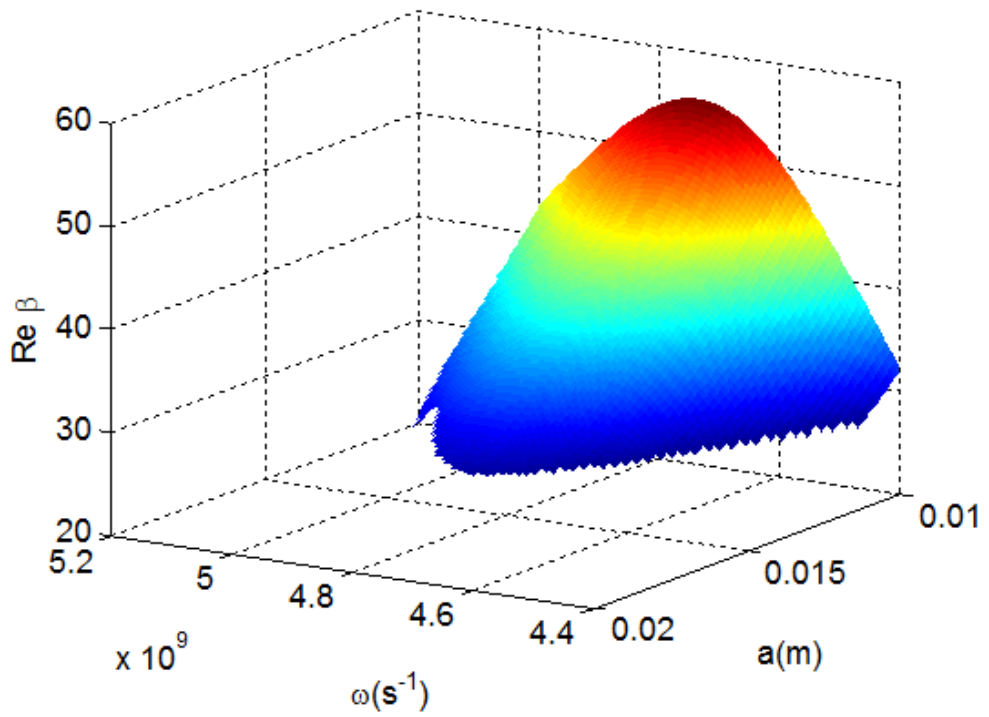

Figure 5.6: Dispersion of s-polarized even mode with damping (real wavevector)

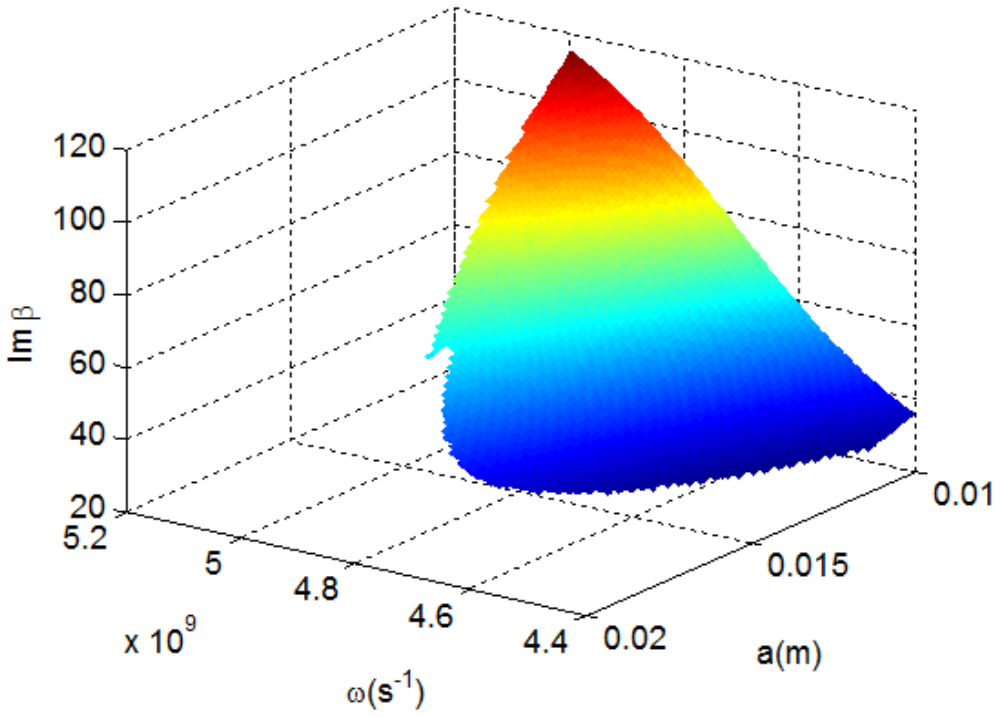

Figure 5.7: Dispersion of s-polarized even mode with damping (imaginary wavevector)

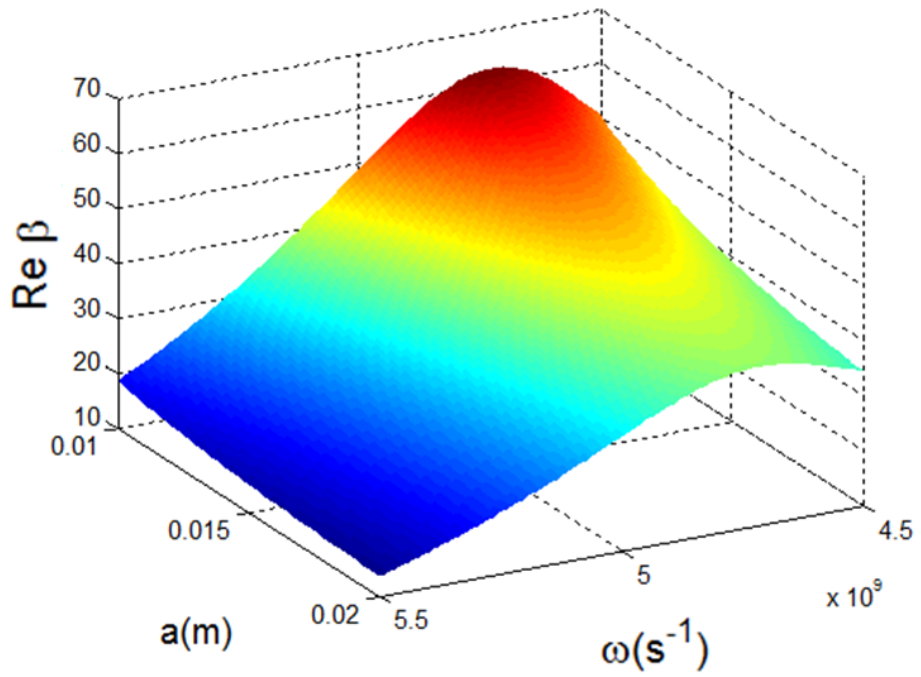

Figure 5.8: Dispersion of s-polarized odd mode (negative $d\omega/d\beta$) with damping (real wavevector)

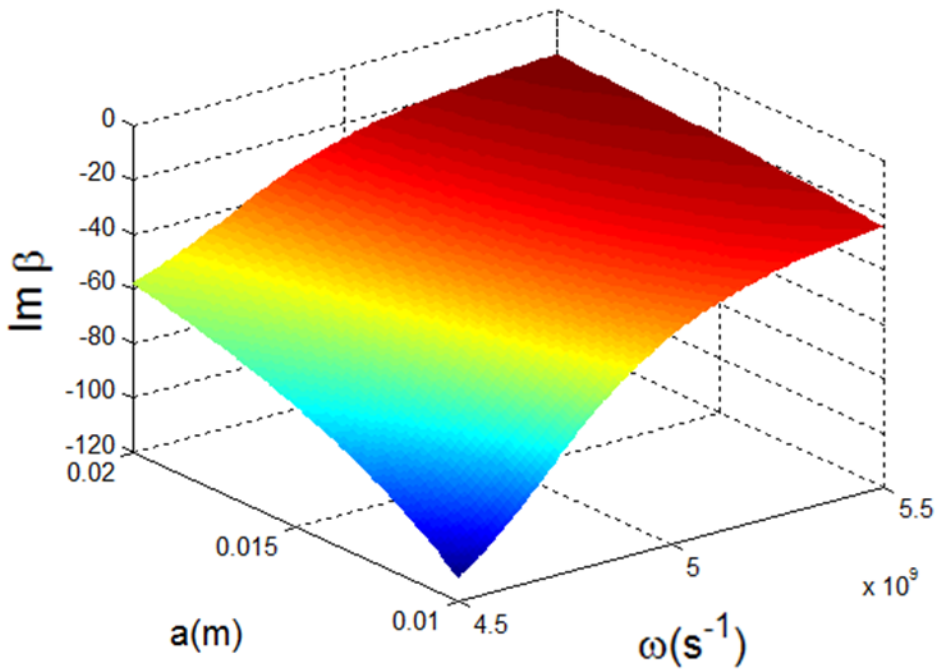

Figure 5.9: Dispersion of s-polarized odd mode (negative $d\omega/d\beta$) with damping (imaginary wavevector)

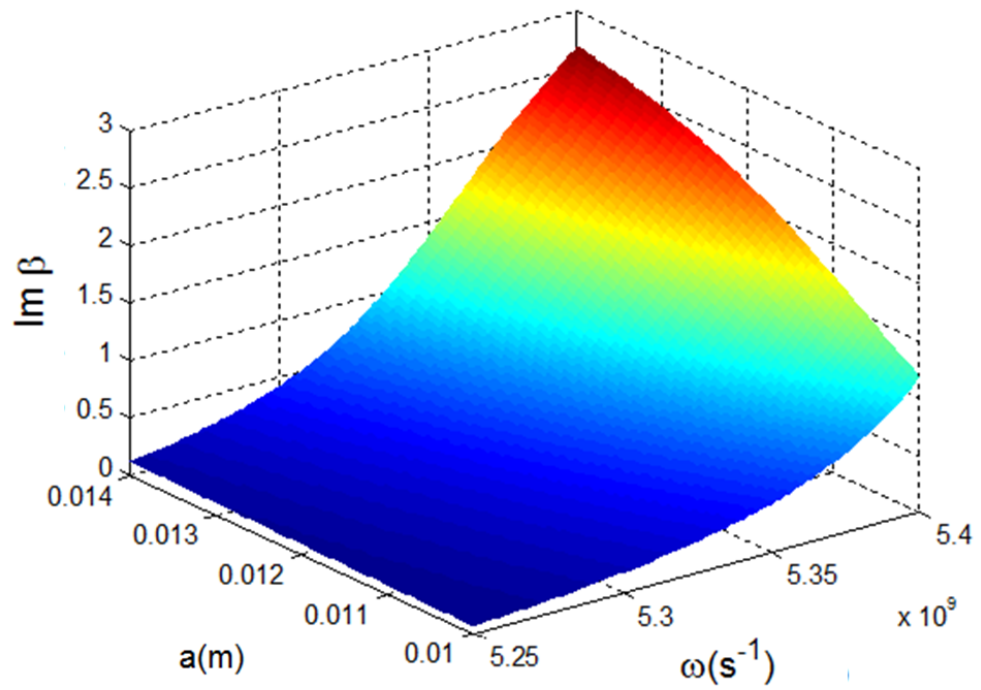

Figure 5.10: Dispersion of s-polarized odd mode (positive $d\omega/d\beta$), propagation length increase with decreasing thickness

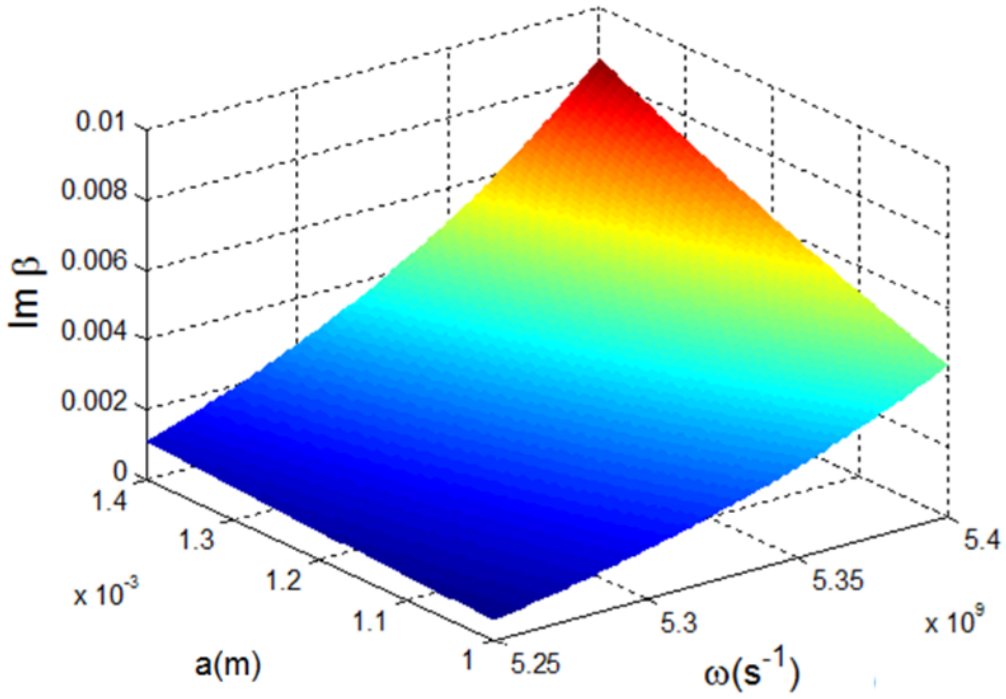

Figure 5.11: Dispersion of s-polarized odd mode (positive $d\omega/d\beta$), propagation length increase with decreasing thickness further. (no cutoff thickness)

5.3.2 p-polarised SP

Next, even mode of s-polarized SP in the lossy thin metamaterial slab is solved numerically. Again, since we have put in the imaginary part, we have dispersion solutions of real wavevector and imaginary wavevector. In Fig. (5.12), real wavevector dispersion of p-polarized even mode shows two resonance peaks, similar to ideal case. But, damping is included, so only a small resonance peak around $4 \times 10^9\ s^{-1}$. And another higher peak at resonance frequency $7.1 \times 10^9\ s^{-1}$, with around 100 /m. After the resonance frequency, the real wavevector drops to zero. No SP propagation mode is allowed. In Fig. (5.13), same with real wavevector, imaginary wavevector is increasing with reducing thickness. There are two peaks in the imaginary graph also.

Recall from the last section that the ideal solution has two branches of solutions. One with negative $d\omega/d\beta$, another one with positive $d\omega/d\beta$. Fig. (5.14) shows real wavevector dispersions, while Fig. (5.15) shows imaginary wavevector dispersions. For negative branch, same with even mode, reducing thickness will lead to increasing real wavevector and imaginary wavevector. Different from the even mode, there is a forbidden frequency gap (around the region of $4 \times 10^9\ s^{-1}$) where there is no propagation SP mode.

Diverting to the positive branch of p-polarized odd mode, Fig. (5.16) shows that by reducing the slab thickness, the imaginary wavevector is reducing. Similar to s-polarized solution, in p-polarized odd mode, propagation length increase with decreasing thickness. Again, this property can not be found in p-polarized even mode, negative $d\omega/d\beta$ branch of odd mode and single interface SP. If we reduce the thickness further as in Fig. (5.17) , the imaginary wavevector is reducing further. So propagation length increase further, there is no cutoff thickness for this property.

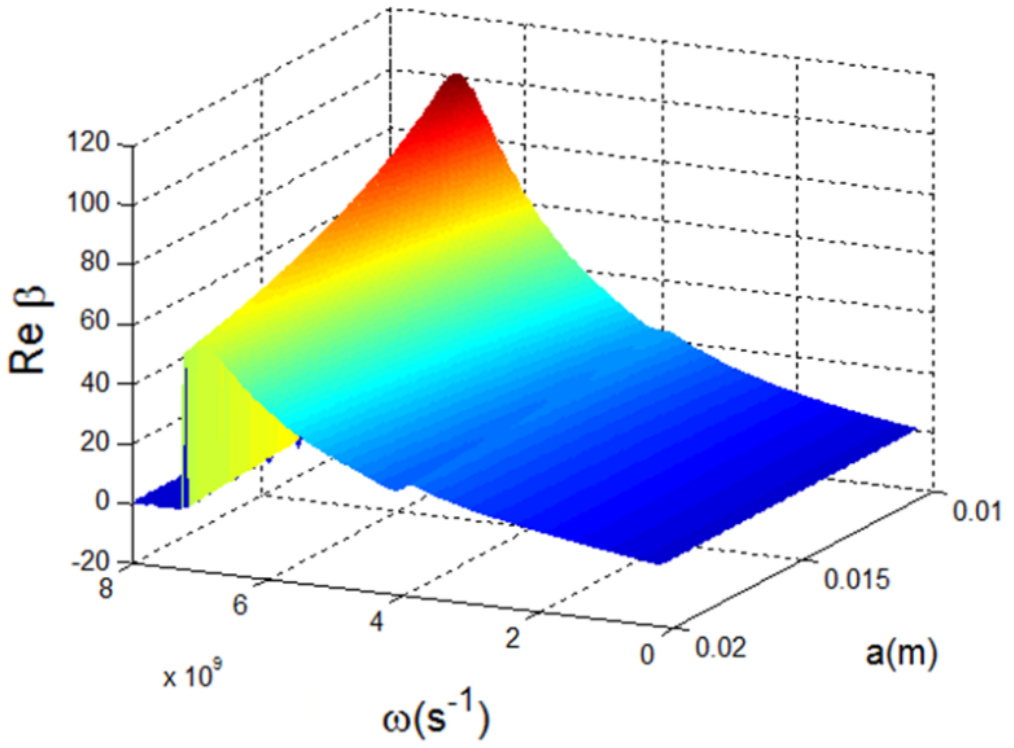

Figure 5.12: Dispersion of p-polarized even mode with damping (real wavevector)

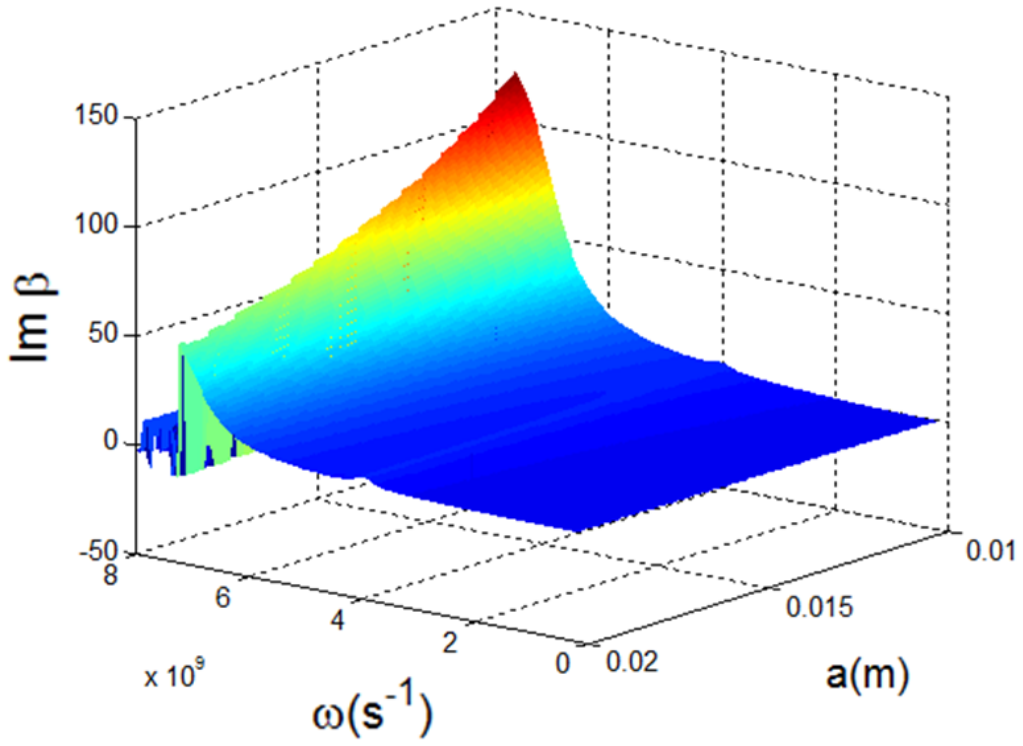

Figure 5.13: Dispersion of p-polarized even mode with damping (imaginary wavevector)

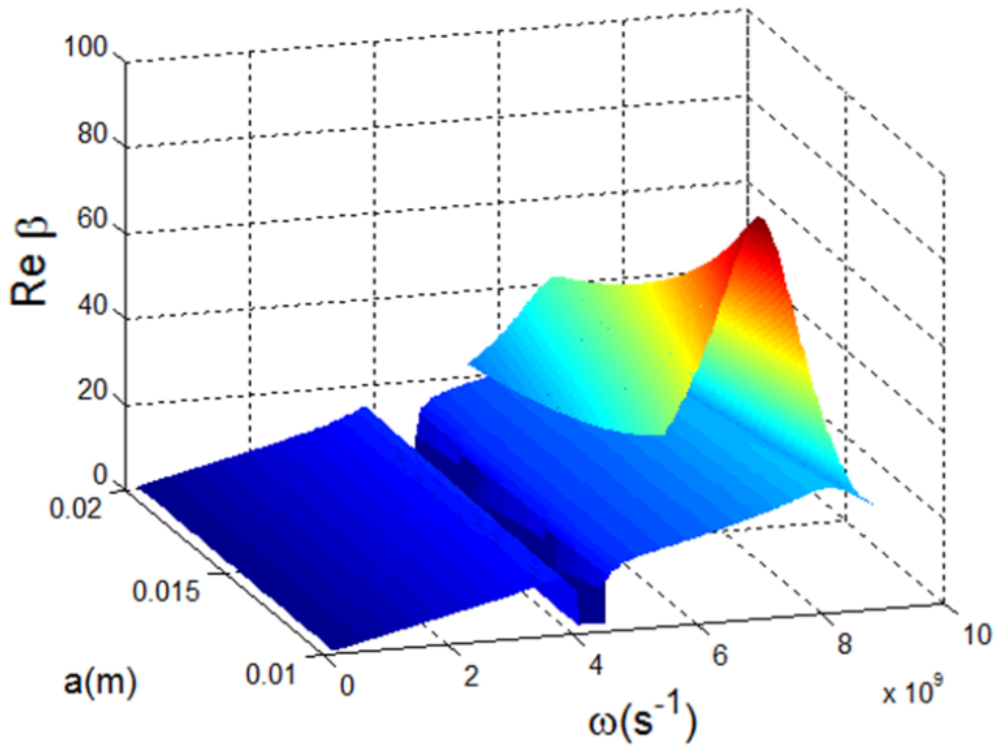

Figure 5.14: Dispersion of p-polarized odd mode with damping (real wavevector)

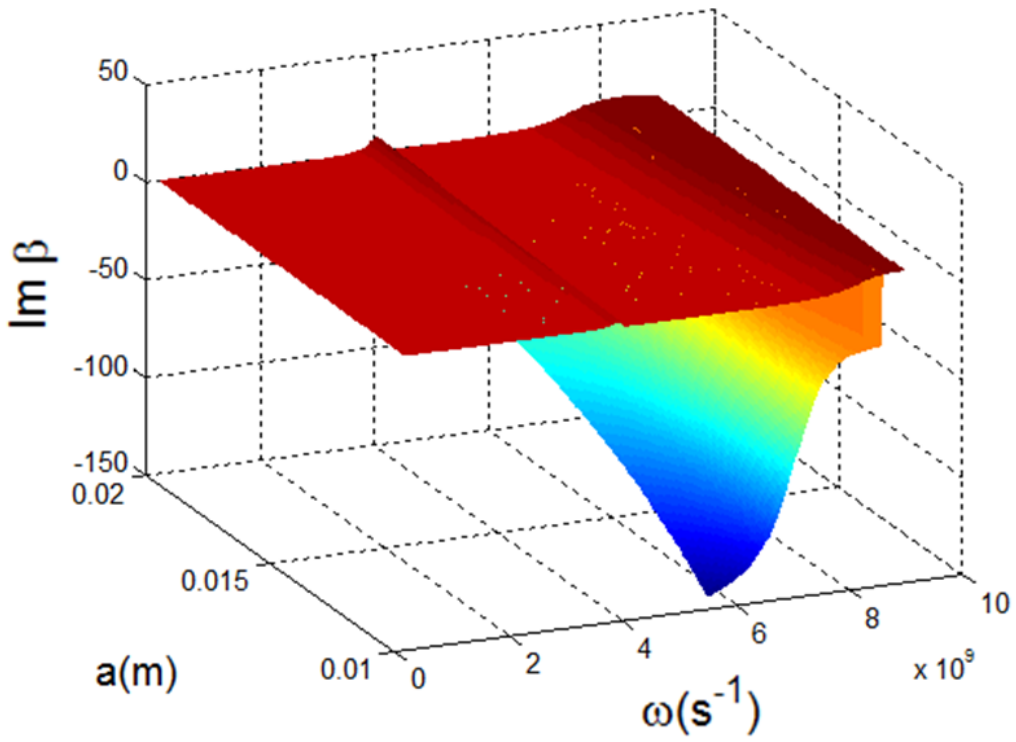

Figure 5.15: Dispersion of p-polarized odd mode with damping (imaginary wavevector)

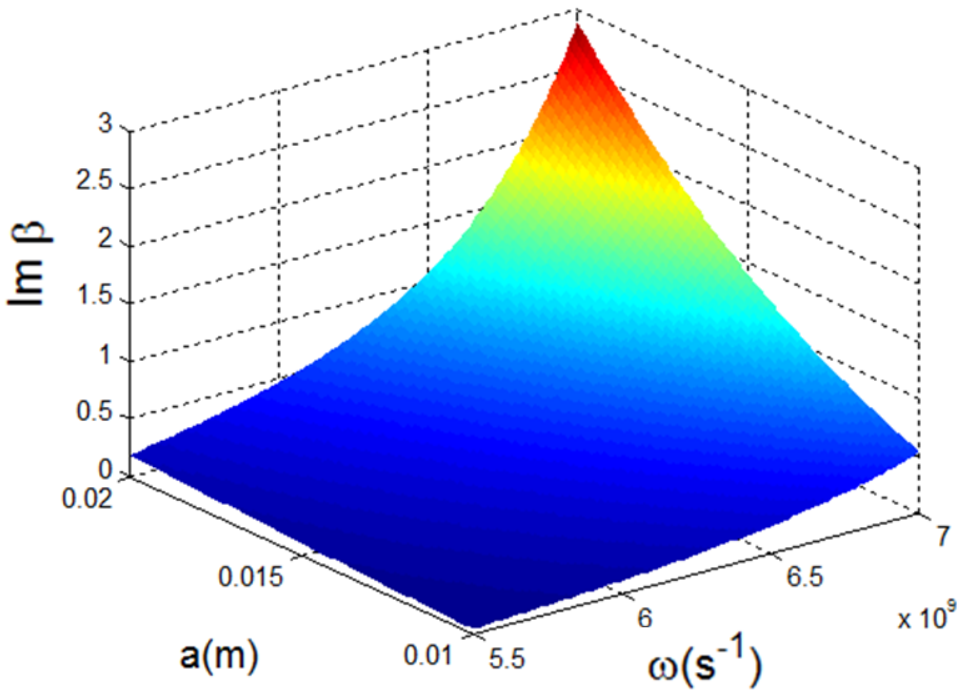

Figure 5.16: Dispersion of p-polarized odd mode (positive $d\omega/d\beta$), propagation length increase with decreasing thickness

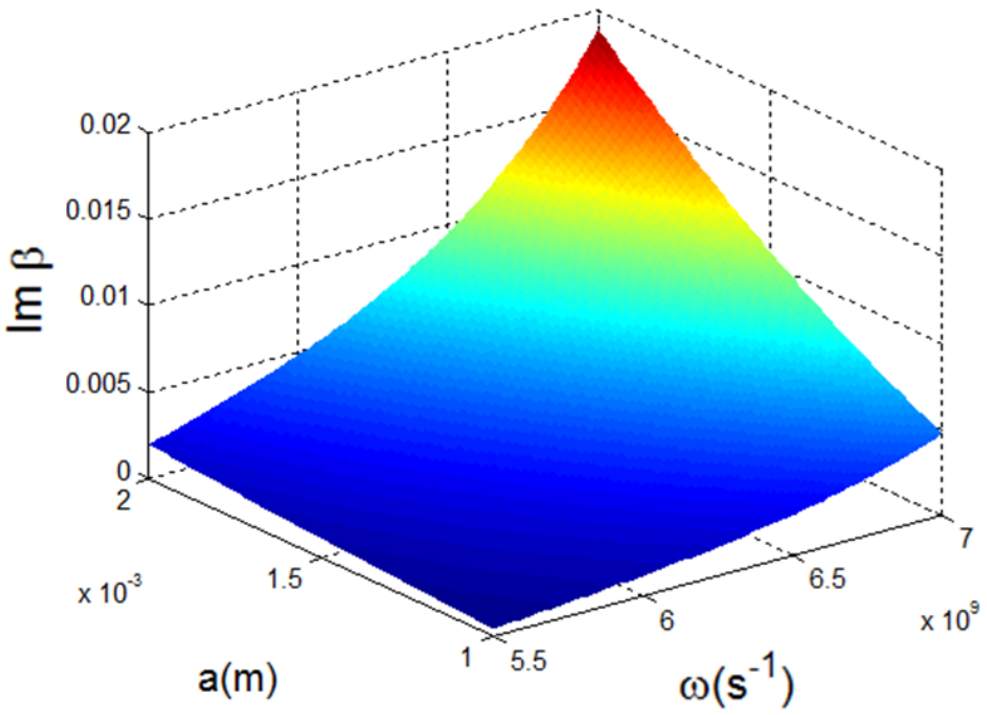

Figure 5.17: Dispersion of p-polarized odd mode (positive $d\omega/d\beta$), propagation length increase with decreasing thickness further. (no cutoff thickness)

5.4 Field Distribution

In this section, we draw the field distribution of surface polariton in thin metamaterial thin slab. From Chapter 2, for s-polarized SP, we have equations E_z (2.56, 2.59, 2.62), H_x (2.57, 2.60, 2.63), H_y (2.58, 2.61, 2.64) for medium 3, 2 and 1. For p-polarized SP, we have equations H_z (2.74, 2.77, 2.80), E_x (2.75, 2.78, 2.81), E_y (2.76, 2.79, 2.82) for medium 3, 2 and 1. Take Eq. (2.63) as example,

$$H_x = -iC\frac{1}{\omega\mu_0\mu_r}k_1\exp(i\beta x)\exp(k_1 y) + iD\frac{1}{\omega\mu_0\mu_1}k_1\exp(i\beta x)\exp(-k_1 y) \qquad (5.17)$$

we can draw this H_x field if we have the values of C, D, since we already have the solutions of β as in the dispersions curve at previous sections. While k_1, normal wavevector, is calculated by Eq. (5.5). Next we will get the ratio of A: B: C: D by solving Eqs. (2.65, 2.66, 2.67, 2.68) simultaneously.

Next we plot the ideal electric field in x-direction for p-polarized odd mode. Taking $\omega = 7.28 \times 10^9\, s^{-1}$, the parameters and solutions are:

$$\mu_1 = 0.19819$$

$$\varepsilon_1 = -0.88486$$

$$\mu_2 = 1$$

$$\varepsilon_2 = 1$$

$$\beta = 79.945$$

$$k_1 = 80.589$$

$$k_2 = 76.169$$

For this p-polarized odd mode, to get the ratio of A: B: C: D, we solve Eqs. (2.83, 2.84, 2.85, 2.86) simultaneously. We have

$$A : B : C : D = 1 : -1 : 0.10456 : -0.10456$$

Using all these values, we plot the electric field, E_x using Eqs. (2.75, 2.78, 2.81) as in Fig. (5.18). E_x field is oscillating rapidly along x-direction. Meanwhile, it is continuous at the interface $y = a$ and $y = -a$. The intensity is maximum at the interface and exponentially

decaying perpendicular to it. Also, we notice electric field in x-direction is asymmetric to the plane $y = 0$.

After that, we plot the ideal electric field in x-direction for p-polarized even mode. Taking $\omega = 6.88 \times 10^9\, s^{-1}$, the parameters and solutions are:

$$\mu_1 = 0.15390$$

$$\varepsilon_1 = -1.1134$$

$$\mu_2 = 1$$

$$\varepsilon_2 = 1$$

$$\beta = 106.92$$

$$k_1 = 107.34$$

$$k_2 = 104.43$$

to get the ratio of A: B: C: D, we solve Eqs. (2.83, 2.84, 2.85, 2.86) simultaneously also. We have

$$A : B : C : D = 1 : 1 : 0.040122 : 0.040122$$

Using all these values, we plot the electric field, E_x of even mode using Eqs. (2.75, 2.78, 2.81) as in Fig. (5.19). Again, E_x field is oscillating rapidly along x-direction. Meanwhile, it is continuous at the interface $y = a$ and $y = -a$. Intensity is maximum at the interface and exponentially decaying perpendicular to it. Then, we notice electric field in x-direction is symmetric to the plane $y = 0$. Note, the thickness of the slab is shown in Fig. (5.20).

Next, we introduce damping into them and plot the fields again. The imaginary wavevector will cause attenuation in the fields amplitude. Taking the same frequency we used above, with damping, the solutions of real wavevector, $Re(\beta)$, and imaginary wavevector, $Im(\beta)$, for p-polarized odd mode are 56.044 and 42.101. While p-polarized even mode are 71.500 and 42.608. We plot the fields again. Fig. (5.21) shows electric field, E_x of odd mode with damping. Fig. (5.22) shows electric field, E_x of even mode with damping. If the material is lossy, the field is dropping to 0 rapidly without

much oscillation. Hence, fabrication of low loss metamaterial is favour to SP propagation application in the future.

In fact, we can draw all the magnetic fields and electric fields for equations [s-polarized SP, E_z (2.56, 2.59, 2.62), H_x (2.57, 2.60, 2.63), H_y (2.58, 2.61, 2.64) ; p-polarized SP, H_z (2.74, 2.77, 2.80), E_x (2.75, 2.78, 2.81), E_y (2.76, 2.79, 2.82)]. Detail solution and graphs are not shown in here. However, we summarize the fields' symmetry property in below table.

Fields	symmetric	anti symmetric
odd mode, H_z	$\surd$	
odd mode, E_x		$\surd$
odd mode, E_y	$\surd$	
even mode, H_z		$\surd$
even mode, E_x	$\surd$	
even mode, E_y		$\surd$

Table 5.1: p-polarized fields symmetry property

Fields	symmetric	anti symmetric
odd mode, E_z	$\surd$	
odd mode, H_x		$\surd$
odd mode, H_y	$\surd$	
even mode, E_z		$\surd$
even mode, H_x	$\surd$	
even mode, H_y		$\surd$

Table 5.2: s-polarized fields symmetry property

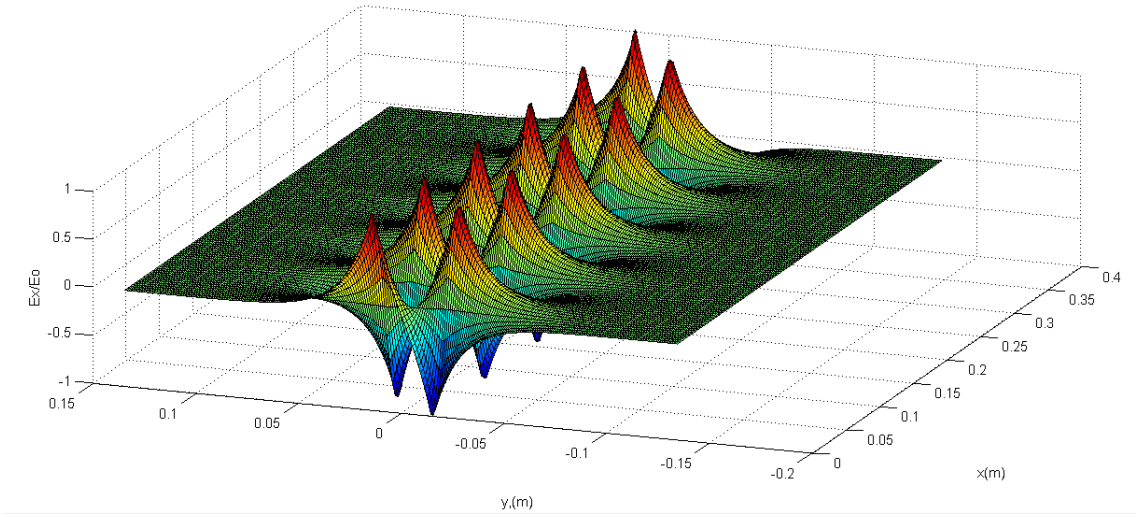

Figure 5.18: Electric field of odd mode (anti-symmetry)

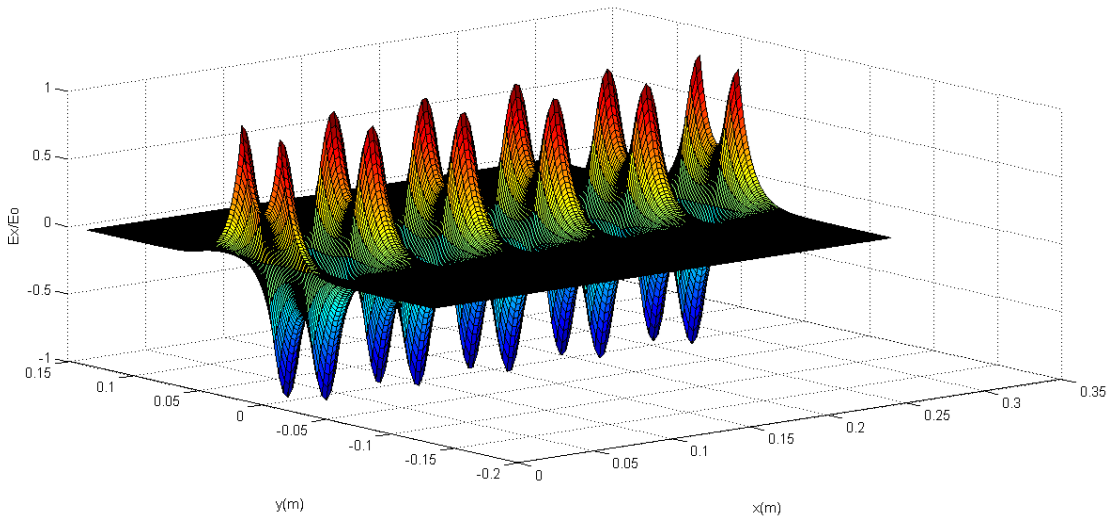

Figure 5.19: Electric field of even mode (symmetry)

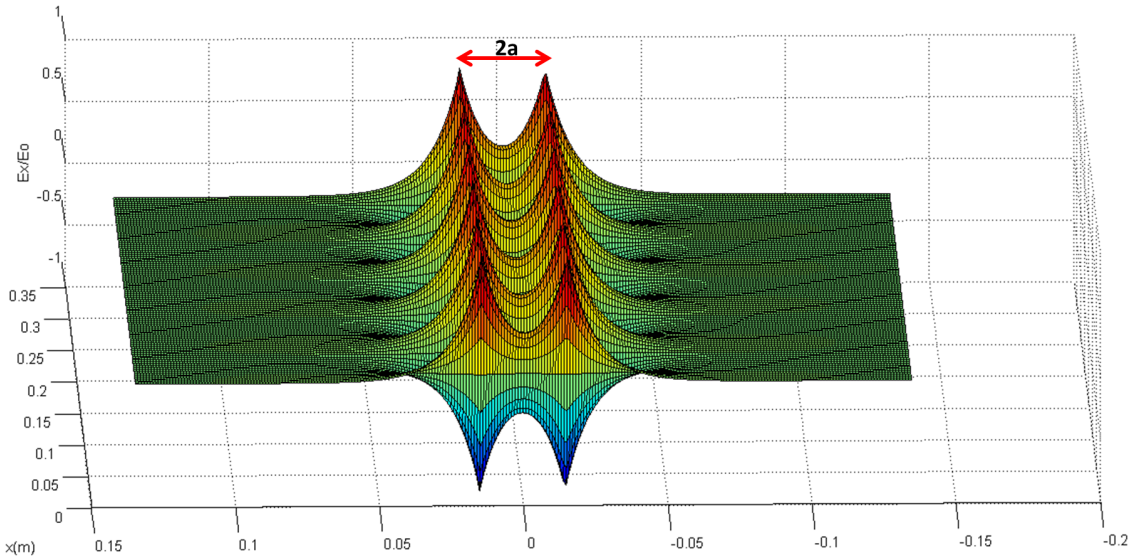

Figure 5.20: Electric field of even mode(front view)

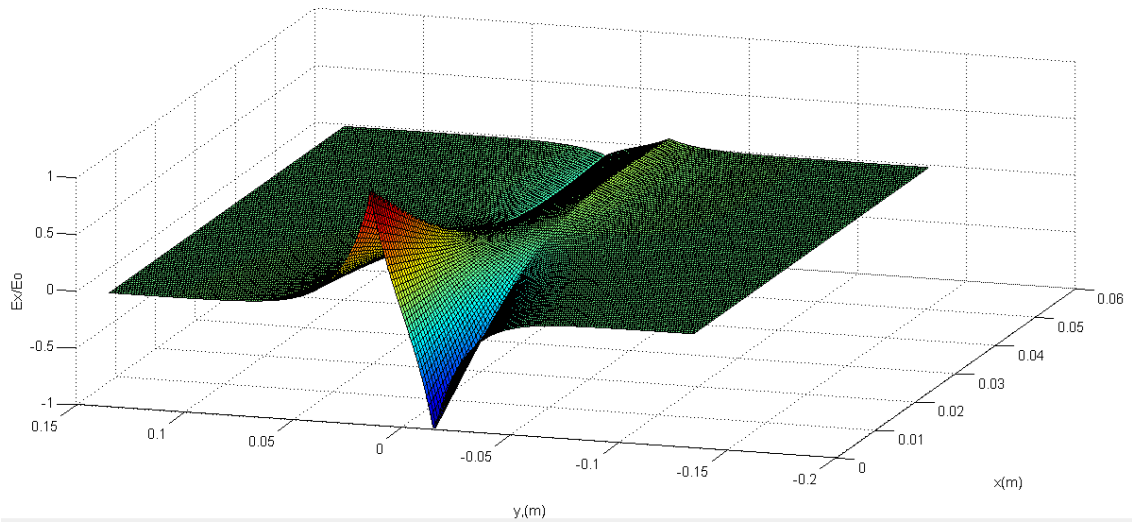

Figure 5.21: Electric field of odd mode with damping

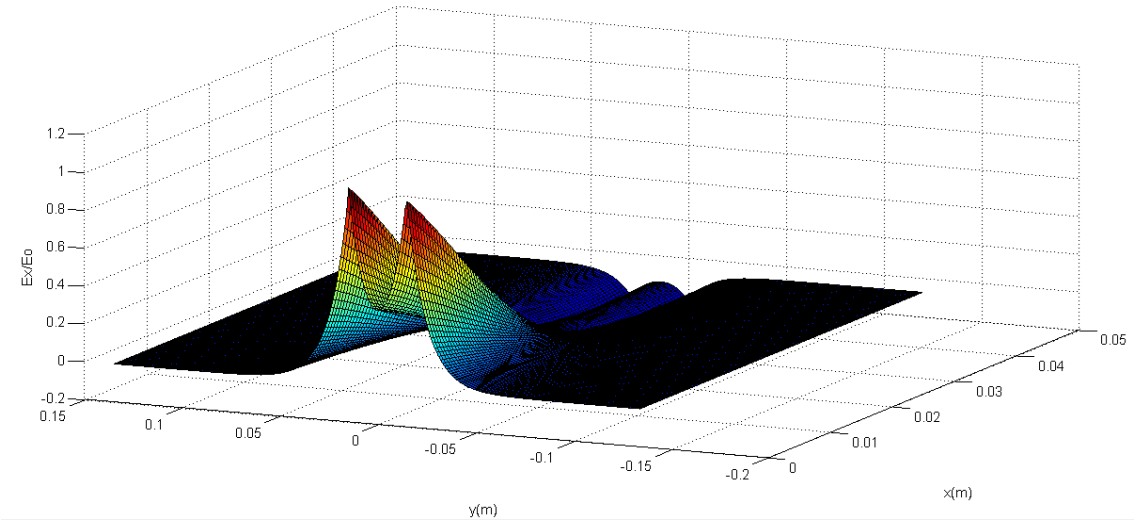

Figure 5.22: Electric field of even mode with damping

To conclude, the SP in thin metamaterial slab has been analyzed. Similarly, s-polarized wave can also excite the propagating surface modes, not just the p-polarized wave. The odd and even modes are noticed in metamaterial slab, happened for both s- and p-polarization. From the dispersion curves, tangential wavevector, β, is highest at the resonance frequency when $\mu_1 = -\mu_2$, $\varepsilon_1 = -\varepsilon_2$ and at ω_0. For even mode, the SP confinement can be enhanced by using thinner slab. For odd mode of lossy medium, imaginary wavevector(related to propagation length) is reducing with decreasing thickness. Hence propagation length is increasing when slab thickness is reduced. There is no cutoff thickness is observed. Meanwhile, the symmetry property of the fields for both modes is displayed in section 5.4. For s-polarized odd mode, H_x field is anti symmetry at $y = 0$, while even mode, H_x field is symmetry. For p-polarized odd mode, E_x field is anti symmetry at $y = 0$, while even mode, E_x field is symmetry.

CHAPTER 6

CONCLUSIONS

In conclusion, we have analyzed surface polariton with arbitrary dielectric and magnetic materials for both polarizations intensively. We showed that s-polarized wave can also excite the propagating surface modes, not just the p-polarized wave. The requirement for enhancement is that either the μ or the ε has opposite signs in the two media and either the μ or the ε has almost equal value in the two media. The expression of the tangential wave vector for s-polarization is completely symmetrical to that of the p-polarization, due to the symmetry between the electric and magnetic responses in the Maxwell equations.

The presence of dispersion with a resonance in μ gives rise to an additional peak in the spectrum of k_x for both polarizations. By introducing superconductor, the s-polarization wave vector is large for small frequency, enabling superresolution at terahertz frequency range. By considering matematerial, for a dispersive medium 1 with both permittivity and permeability are dispersive with frequency, surface polariton resonance in large frequency range can be achieved if permittivity or permeability of medium 2 is always close to medium 1.

Two SP modes are found in metamaterial slab, namely odd and even modes which occurs for both s- and p-polarization. We showed that SP confinement can be enhanced by using thinner slab for even mode. For the odd mode of lossy medium, imaginary wavevector (related to propagation length) is reducing with decreasing thickness. it happen for both s- and p- polarized wave. Hence propagation length is increasing when slab thickness is reduced, but no cutoff thickness is observed. These long ranging SP are very beneficial to waveguiding application.

The use of magnetic materials extends the field of plasmonics to magnonics. Instead of using metals in the region of negative permittivity ε, we could use magnetic materials or engineered metamaterial with negative μ. The main novelty is that surface magnon polariton, SMP opens up surface polaritons in the new regimes. The SMP can now be realized artificially with metamaterials through microstructural and nanostructural engi-

neering. The use of magnetic materials enables all physical features of plasmonics to be mapped into magnonics with one-to-one correspondence.

Finally, there are new technological possibilities with the significant impact of using magnetic materials in addition to metallic and dielectric materials. Some possible applications such as magnetic recording (data storage) and spintronics devices can merge with photonic circuits where SMPs serve as efficient information carriers and processors. In this research, experimentally realistic parameters have been used to model the dispersions of the materials, enhancing the prospect for applications.

Appendices

APPENDIX A

PROGRAM LISTING TO SOLVE THIN SLAB DISPERSION OF S-POLARISED ODD MODE

```
function result=kclowte1(omega,var_a,guess)

CONST.mu_2=1;
CONST.epsilon_2=1;
CONST.c=3e8;
F=0.56;
wp=10e9;
w0=4e9;

% effective dielectric constant
CONST.epsilon_1=1-wp^2./omega.^2;
% effective magnetic permeability
CONST.mu_1=1-(F*omega.^2)./(omega.^2-w0^2);
%solve for the value of beta
result=fsolve(@(beta) zerokernel(beta,omega,CONST,var_a),guess);

end

function result=zerokernel(beta,omega,CONST,var_a)
temp_sqrt=CONST.mu_1 .* sqrt_mu_2(beta,omega,CONST) ./ CONST.mu_2 ./ sqrt_mu_1(beta,omega,CONST);
temp_exp=exp(-2 .* var_a .* sqrt_mu_1(beta,omega,CONST));
result=((1+temp_sqrt) ./ (1-temp_sqrt)) - temp_exp;
end

function result=sqrt_mu_1(beta,omega,CONST)
    result=sqrt((CONST.c.^2 .* beta.^2 - omega.^2 .* CONST.mu_1 .* CONST.epsilon_1)./CONST.c.^2);
end

function result=sqrt_mu_2(beta,omega,CONST)
    result=sqrt((CONST.c.^2 .* beta.^2 - omega.^2 .* CONST.mu_2 .* CONST.epsilon_2)./CONST.c.^2);
end
```

APPENDIX B

PROGRAM LISTING TO SOLVE THIN SLAB DISPERSION OF S-POLARISED EVEN MODE

```
function result=kclowte2(omega,var_a,guess)

CONST.mu_2=1;
CONST.epsilon_2=1;
CONST.c=3e8;
F=0.56;
wp=10e9;
w0=4e9;

% effective dielectric constant
CONST.epsilon_1=1-wp^2./omega.^2;
% effective magnetic permeability
CONST.mu_1=1-(F*omega.^2)./(omega.^2-w0^2);
%solve the value of beta
result=fsolve(@(beta) zerokernel(beta,omega,CONST,var_a),guess);

end

function result=zerokernel(beta,omega,CONST,var_a)
temp_sqrt=CONST.mu_2 .* sqrt_mu_1(beta,omega,CONST) ./ CONST.mu_1 ./ sqrt_mu_2(beta,omega,CONST);
temp_exp=exp(2 .* var_a .* sqrt_mu_1(beta,omega,CONST));
result=((1-temp_sqrt) ./ (1+temp_sqrt)) - temp_exp;
end

function result=sqrt_mu_1(beta,omega,CONST)
    result=sqrt((CONST.c.^2 .* beta.^2 - omega.^2 .* CONST.mu_1 .* CONST.epsilon_1)./CONST.c.^2);
end

function result=sqrt_mu_2(beta,omega,CONST)
    result=sqrt((CONST.c.^2 .* beta.^2 - omega.^2 .* CONST.mu_2 .* CONST.epsilon_2)./CONST.c.^2);
end
```

APPENDIX C

PROGRAM LISTING TO SOLVE THIN SLAB DISPERSION OF P-POLARISED ODD MODE

```
function result=kclowtm1(omega,var_a,guess)

CONST.mu_2=1;
CONST.epsilon_2=1;
CONST.c=3e8;
F=0.56;
wp=10e9;
w0=4e9;

% effective dielectric constant
CONST.epsilon_1=1-wp^2./omega.^2;
% effective magnetic permeability
CONST.mu_1=1-(F*omega.^2)./(omega.^2-w0^2);
%the value of beta
result=fsolve(@(beta) zerokernel(beta,omega,CONST,var_a),guess);

end

function result=zerokernel(beta,omega,CONST,var_a)
temp_sqrt=CONST.epsilon_1 .* sqrt_mu_2(beta,omega,CONST) ./ CONST.epsilon_2 ./ sqrt_mu_1(beta,omega,CONST);
temp_exp=exp(-2 .* var_a .* sqrt_mu_1(beta,omega,CONST));
result=((1+temp_sqrt) ./ (1-temp_sqrt)) - temp_exp;
end

function result=sqrt_mu_1(beta,omega,CONST)
    result=sqrt((CONST.c.^2 .* beta.^2 - omega.^2 .* CONST.mu_1 .* CONST.epsilon_1)./CONST.c.^2);
end

function result=sqrt_mu_2(beta,omega,CONST)
    result=sqrt((CONST.c.^2 .* beta.^2 - omega.^2 .* CONST.mu_2 .* CONST.epsilon_2)./CONST.c.^2);
end
```

APPENDIX D

PROGRAM LISTING TO SOLVE THIN SLAB DISPERSION OF P-POLARISED EVEN MODE

```
function result=kclowtm2(omega,var_a,guess)

CONST.mu_2=1;
CONST.epsilon_2=1;
CONST.c=3e8;
F=0.56;
wp=10e9;
w0=4e9;

% effective dielectric constant
CONST.epsilon_1=1-wp^2./omega.^2;
% effective magnetic permeability
CONST.mu_1=1-(F*omega.^2)./(omega.^2-w0^2);
%the value of beta
result=fsolve(@(beta) zerokernel(beta,omega,CONST,var_a),guess);

end

function result=zerokernel(beta,omega,CONST,var_a)
temp_sqrt=CONST.epsilon_2 .* sqrt_mu_1(beta,omega,CONST) ./ CONST.epsilon_1 ./ sqrt_mu_2(beta,omega,CONST);
temp_exp=exp(2 .* var_a .* sqrt_mu_1(beta,omega,CONST));
result=((1-temp_sqrt) ./ (1+temp_sqrt)) - temp_exp;
end

function result=sqrt_mu_1(beta,omega,CONST)
    result=sqrt((CONST.c.^2 .* beta.^2 - omega.^2 .* CONST.mu_1 .* CONST.epsilon_1)./CONST.c.^2);
end

function result=sqrt_mu_2(beta,omega,CONST)
    result=sqrt((CONST.c.^2 .* beta.^2 - omega.^2 .* CONST.mu_2 .* CONST.epsilon_2)./CONST.c.^2);
end
```

APPENDIX E

PUBLISHED PAPER

Surface polaritons with arbitrary magnetic and dielectric materials: new regimes, effects of negative index, and superconductors

C. H. Raymond Ooi,[1,*] K. C. Low,[1] Ryota Higa,[2] and Tetsuo Ogawa[2]

[1]*Department of Physics, University of Malaya, 50603 Kuala Lumpur, Malaysia*
[2]*Department of Physics and Graduate School, Osaka University, Toyonaka, Osaka 560-0043, Japan*
**Corresponding author: rooi@um.edu.my*

Received June 11, 2012; revised July 30, 2012; accepted August 2, 2012;
posted August 7, 2012 (Doc. ID 170151); published September 7, 2012

A surface magnon-polariton can be excited by both *p*- and *s*-polarized light if at least one of the layers is a magnetic material. We present general expressions of the tangential wave vectors of *s*- and *p*-polarized light at an interface of two media. Analysis reveals additional new regimes of surface polariton resonances with magnetic materials for *s*- and *p*-polarized light. The tangential wave vectors are found to be equal in magnitude to the normal wave vectors at surface polariton resonances. The spatial distributions of the fields at resonant enhancement and the spectra of the tangential wave vectors are studied for different dielectric permittivities and magnetic permeabilities of the two media. If one of the media has dispersive dielectric function and permeability function, additional surface polariton resonance peaks appear for both *s*- and *p* polarizations. For a medium with a superconductor, the tangential component increases asymptotically at lower frequencies, providing subwavelength capability at the terahertz regime.

OCIS codes: 240.6690, 240.5420, 160.3918, 240.6680, 350.3618.

1. INTRODUCTION

Surface plasmon-polaritons (SPPs) have promising potential for realizing compact optical circuits in next-generation compact optoelectronic systems integrated with nanoplasmonic components [1], semiconductor lasers with plasmonic polarizers [2] and plasmonic collimation that produces light beams with small divergence [3], and sensitive photodetectors using plasmonic lenses [4]. Low-threshold, low-current operation of semiconductor lasers and optical devices is needed. Nanosystems, e.g., quantum dots, are promising for these purposes, while nanoplasmonics and/or metamaterials provide large optical nonlinearity through the field enhancement effect.

An SPP can be excited through sculptured thin film [5], a corrugated surface, triangular grooves, or wedges [6]. Recently, SPPs have been incorporated into metamaterials [7] that mimic the permeability of magnetic materials. Some remarkable effects of SPPs are field enhancement, the subwavelength effect [8], superresolution [9], efficient guiding [10], and tight focusing [11]. SPPs also affect light–matter interactions, such as photoelectron generation [12]. They enhance the photoelectric effect [13], multiphoton ionization [14], and acceleration of electrons [15]. The strong coupling [16] between SPPs and atoms enhances light emissions [17], nonlinear optical interactions [18], and pulse propagation [19], and alters the dynamics of interactions with femtosecond lasers [20].

SPPs also modify the Casimir energy [21] and the radiation force [22], causing dispersion anomalies in electron diffraction on metallic gratings [23]. Nanoparticles of various structures [24] use SPPs for chemical sensing [25]. Recent works have shown that SPPs can help photons squeeze through subwavelength holes [26] and transmit entangled photons [27]. Their subwavelength diffraction and extraordinary transmission through small apertures led to high resolution near-field microscopy [28]. Suitable designs of structures with SPPs are useful for optical trapping [29,30] and laser cooling [31]. Collective excitations of plasmons [32], stimulated emission [33], and plasmonic lasing [34] are also enhanced by SPPs.

Surface phonon-polaritons (SFPs) and surface exciton-polaritons (SEPs) (the counterparts of dielectric and semiconductor SPPs in metals) have been widely explored in the context of thin films and multilayers [35]. A number of works have shown that magnetic materials can excite surface magnon-polaritons (SMPs), i.e., strong coupling of photons to quantized magnetization waves due to collective spins [36]. Ruppin showed that surface polariton can exist for both *s*- and *p*-polarized light in left-handed metamaterials [37], but damping (imaginary parts) was neglected. Excitation of SMPs in gyromagnetic materials and anisotropic antiferromagnetic crystals have been discussed by Hartstein *et al.* [38] and Arakelian *et al.* [39], respectively. The presence of magnon-polaritons was demonstrated in a YIG slab using the attenuated total reflectance technique [40]. The dispersion relations for magnetic polaritons have been obtained for anisotropic systems, such as ordered ferromagnetic slabs [41] and uniaxial antiferromagnets [42,43]. It has been shown that *s*-polarized (TE) optical waves can propagate at the interface of media with negative refractive index and negative dielectric constant of low-dimensional nanowaveguides [44]. However, the underlying theory (with magnetic materials) was not given. Despite these works, the recent boom in the field of plasmonics has been predominantly based on the *p*-polarized light fields to excite surface plasmon resonance (SPR) at the interface of dielectric and metallic media, while the use of *s*-polarized light with magnetic materials is not so popular.

In this paper, we analyze the new regimes in the dispersion property and the modes (s and p polarizations) of surface waves propagating between two media with at least one with magnetic permeability that differs from unity. We present the underlying theoretical expressions for the wave vectors and field distributions across two media with arbitrary materials. The theory is generally valid in the entire electromagnetic spectrum, but we focus on the optical regime due to potential attractive applications in optical technologies. The theory provides insights for studying the spectrum of the surface polaritons formed by various combinations of metallic, dielectric, and magnetic materials where SMPs exist, in addition to SFPs, SEPs, and SPPs. Although dielectric and/or metallic materials can coexist, the magnetic material or metamaterial with effective permeability is the main component needed to show the new regimes/possibilities provided by SMPs.

Let us first analyze the surface polariton regimes as summarized in Fig. 1. In the case of using only dielectric materials with single interface $\frac{\mu_1}{\mu_2}=1$, the ratio Re $\frac{\varepsilon_1}{\varepsilon_2}$ has to be negative to excite a p-polarized surface polariton [Fig. 1(a)] with the well-known tangential wave vector $k_x^p=\frac{\omega}{c}\sqrt{\frac{\varepsilon_1\varepsilon_2}{\varepsilon_1+\varepsilon_2}}$. On the other hand, using only magnetic materials $\frac{\varepsilon_1}{\varepsilon_2}=1$, we have the opposite result, $k_x^s=\frac{\omega}{c}\sqrt{\frac{\mu_1\mu_2}{\mu_1+\mu_2}}$, for s polarization. Figure 1(b) shows the new regimes where surface waves also exist for an s-polarized field when the materials are both dielectric and magnetic. The red solid lines in the second (fourth) quadrant show that s-polarized light can excite surface waves with large wave vectors if the materials are slightly magnetic, such as paramagnetic and ferromagnetic insulators [38], provided that Re μ_1 and Re μ_2 are almost equal in magnitude but with the *same (opposite)* sign, while Re ε_1 and Re ε_2 have *opposite (same)* signs. Similarly, the green dashed lines in the second (fourth) quadrant show that a p-polarized surface polariton with an enhanced wave vector can also be excited if the materials are slightly dielectric, provided Re ε_1 and Re ε_2 are almost equal but with *opposite (same)* signs while Re μ_1 and Re μ_2 have the *same (opposite)* sign.

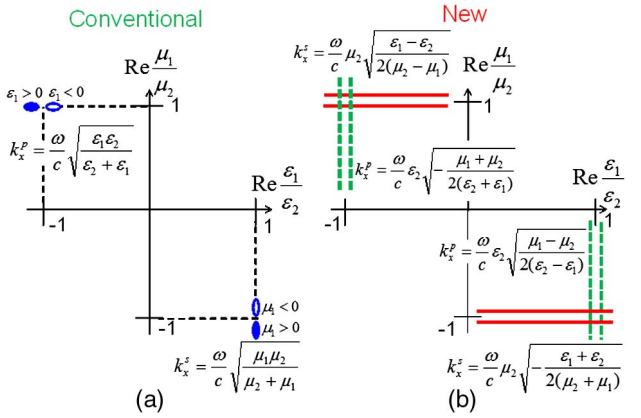

Fig. 1. (Color online) Quadrants showing regimes of enhanced tangential wave vectors k_x of surface polaritons propagating between medium 1 and medium 2 with permittivities ε_i and permeabilities μ_i for s-polarized light and p-polarized light. (a) Conventional scenario of plasmonic enhancement and its magnetic analog (indicated by open/filled dots). (b) New resonant regimes due to both electric and magnetic properties. The enhancement regions are indicated by two solid (red) lines and two dashed (green) lines slightly less and more than 1 and –1.

2. FIELDS AND WAVE VECTORS OF SURFACE POLARITONS

We consider a plane wave traversing the interface between medium 1 and 2 on the x–y plane. For s polarization, $\mathbf{E}_j^s(\mathbf{r},t)=E_j^s(0,0,1)e^{i(k_x^s x+k_{jy}^s y)}$ and, for p polarization, $\mathbf{E}_j^p(\mathbf{r},t)=E_j^p\left(-\frac{k_{jy}^p}{k_j},\frac{k_x^p}{k_j},0\right)e^{i(k_x^p x+k_{jy}^p y)}$, where $j=1,2$ is the index for the medium. A linear combination of these fields yields the resulting field $\mathbf{E}_j=\mathbf{E}_j^s e^{i\phi}+\mathbf{E}_j^p$ that is generally elliptically polarized:

$$\mathbf{E}_j=\left[-E_j^p\frac{k_{jy}^p}{k_j}e^{i\Phi_j^p},E_j^p\frac{k_x^p}{k_j}e^{i\Phi_j^p},E_j^s e^{i(\Phi_j^s+\phi)}\right], \tag{1}$$

where $\Phi_j^\lambda(x,y)=k_x^\lambda x+k_{jy}^\lambda y$. Since the two vector fields are orthogonal, there would be no interference between the two in the total intensity $|\mathbf{E}_j|^2$. An interesting effect of the surface polariton enhancement is that a circularly/elliptically polarized light becomes almost linearly y-polarized light, since $E_j^p\frac{k_x^p}{k_j}\gg E_j^p\frac{k_{jy}^p}{k_j}, E_j^s$.

By applying the continuity of the tangential components (i.e., on the x–z plane) for the E field and the H field, when there is no reflected field, we have $\frac{k_{1y}}{\mu_1}=\frac{k_{2y}}{\mu_2}$. Using $k_{iy}^2=\varepsilon_i\mu_i(\frac{\omega}{c})^2-k_x^2$ $(i=1,2)$ the tangential wave vector for s-polarized light is found:

$$k_x^s=\frac{\omega}{c}\sqrt{\left(\frac{\varepsilon_1\mu_2-\mu_1\varepsilon_2}{\mu_2-\mu_1}\right)\frac{\mu_1\mu_2}{\mu_1+\mu_2}}, \tag{2}$$

which reduces to $k_x^s=\frac{\omega}{c}\sqrt{\varepsilon_1\frac{\mu_1\mu_2}{\mu_1+\mu_2}}$ when $\varepsilon_1=\varepsilon_2$, in close analogy to the usual expression for p polarization.

Similarly, for p-polarized light, the continuity of the fields along the x direction gives $\frac{k_{1y}}{\varepsilon_1}=\frac{k_{2y}}{\varepsilon_2}$ and the tangential wave vector is

$$k_x^p=\frac{\omega}{c}\sqrt{\left(\frac{\mu_1\varepsilon_2-\varepsilon_1\mu_2}{\varepsilon_2-\varepsilon_1}\right)\frac{\varepsilon_1\varepsilon_2}{\varepsilon_1+\varepsilon_2}}, \tag{3}$$

which reduces to the famous formula $k_x^p=\frac{\omega}{c}\sqrt{\frac{\varepsilon_1\varepsilon_2}{\varepsilon_1+\varepsilon_2}}$ for nonmagnetic materials when $\mu_1=\mu_2=1$. Equation (3) generalizes the usual plasmonic enhancement for p polarization to magnetic materials, while Eq. (2) is obtained by interchanging μ and ε. Both wave vectors are zero when $\varepsilon_1\mu_2=\mu_1\varepsilon_2$. Equations (2) and (3) form the central results to be discussed in subsequent sections.

The normal wave vectors follow as

$$k_{jy}^s=\frac{\omega}{c}\mu_j\sqrt{\frac{\mu_2\varepsilon_2-\varepsilon_1\mu_1}{(\mu_2-\mu_1)(\mu_1+\mu_2)}}, \tag{4}$$

$$k_{jy}^p=\frac{\omega}{c}\varepsilon_j\sqrt{\frac{\mu_2\varepsilon_2-\varepsilon_1\mu_1}{(\varepsilon_2-\varepsilon_1)(\varepsilon_1+\varepsilon_2)}}, \tag{5}$$

where $j=1,2$. We show below that the tangential wave vector k_x and the normal wave vector k_{jy} have equal magnitude at surface polariton resonances.

3. REGIMES OF SURFACE POLARITON RESONANCES

We consider (below) the limiting possibilities when both $\mu = \mu^r + i\mu^i$ and $\varepsilon = \varepsilon^r + i\varepsilon^i$ are approximately (a) real and (b) imaginary, and show that the resulting tangential wave vector is real, describing a propagating surface polariton. Approximate relationships between k_x, the tangential wave vector, and k_{jy} the normal wave vector, can be found when k_x is enhanced by surface polariton resonance.

A. μ and ε Are Mostly Real

In the conventional case, the p-polarized surface polariton enhancement effect gives large k_x^p when ε_1 or ε_2 has a negative value, as in metals, such that $\varepsilon_1 + \varepsilon_2 \simeq 0$. It is known that there is no plasmonic enhancement for s-polarized light. However, Eq. (2) clearly shows that, for s polarization, it is also possible to have surface polariton enhancement, when $\varepsilon_1 = \varepsilon_2$ are real, but the material must be magnetic with μ_1 and μ_2 having opposite signs, as illustrated in Fig. 1. Let us analyze the new resonance regimes, particularly due to the bracketed terms of Eqs. (2) and (3).

Second Quadrant (in Fig. 1). For the s polarization, the wave vector k_x^s is large when $\delta_m = \mu_2 - \mu_1 \simeq 0^+(0^-)$, with $|\mathrm{Re}\,\delta_m| \simeq 0$, provided ε_2 and ε_1 have opposite signs, $\varepsilon_1 > |\varepsilon_2|$ ($\varepsilon_1 < |\varepsilon_2|$), giving

$$k_x^s \simeq \frac{\omega}{c}\mu_2\sqrt{\frac{\varepsilon_1 - \varepsilon_2}{2\delta_m}} \simeq ik_{1y}^s \simeq ik_{2y}^s. \tag{6}$$

Note that, in nonmagnetic materials or materials with the same magnetic properties, Eq. (6) is not valid since $\delta_m = 0$, so there is no surface mode for s polarization. Note that k_x^s would be negative, if μ_2 is negative.

Fourth Quadrant. When $\delta_m^+ = \mu_1 + \mu_2 \simeq 0^+(0^-)$ with $|\mathrm{Re}\,\delta_m^+| \simeq 0$ while ε_2 and ε_1 are both negative (positive), or vice-versa, we have a large enhancement of the propagating wave vector (for $\mu_2 > 0$)

$$k_x^s \simeq \frac{\omega}{c}\mu_2\sqrt{-\frac{\varepsilon_1 + \varepsilon_2}{2\delta_m^+}} \simeq ik_{2y}^s \simeq -ik_{1y}^s. \tag{7}$$

Fourth Quadrant. Similarly, the wave vector k_x^p can take a large value when ε_2 and ε_1 are almost equal (with the same sign), i.e., $\delta_e = \varepsilon_2 - \varepsilon_1 \simeq 0^+$, while $\mu_1 > |\mu_2|$ (or $\mu_1 \simeq -\mu_2 > 0$), giving

$$k_x^p \simeq \frac{\omega}{c}\varepsilon_2\sqrt{\frac{\mu_1 - \mu_2}{2\delta_e}} \simeq ik_{1y}^p \simeq ik_{2y}^p, \tag{8}$$

which is essentially Eq. (6) obtained by interchanging ε and μ. Propagating exists when $\mathrm{Re}(\mu_2 - \mu_1)$ has opposite sign from $\mathrm{Re}(\varepsilon_2 - \varepsilon_1)$. The wave vector has the largest value $k_x^p \simeq \frac{\omega}{c}\varepsilon_2\sqrt{\frac{|\mathrm{Re}\,\mu_1|}{\delta_e}}$ when $\mathrm{Re}\,\mu_1$ and $\mathrm{Re}\,\mu_2$ have opposite signs and are nearly equal in magnitude. Here, k_x^p is negative if ε_2 is negative.

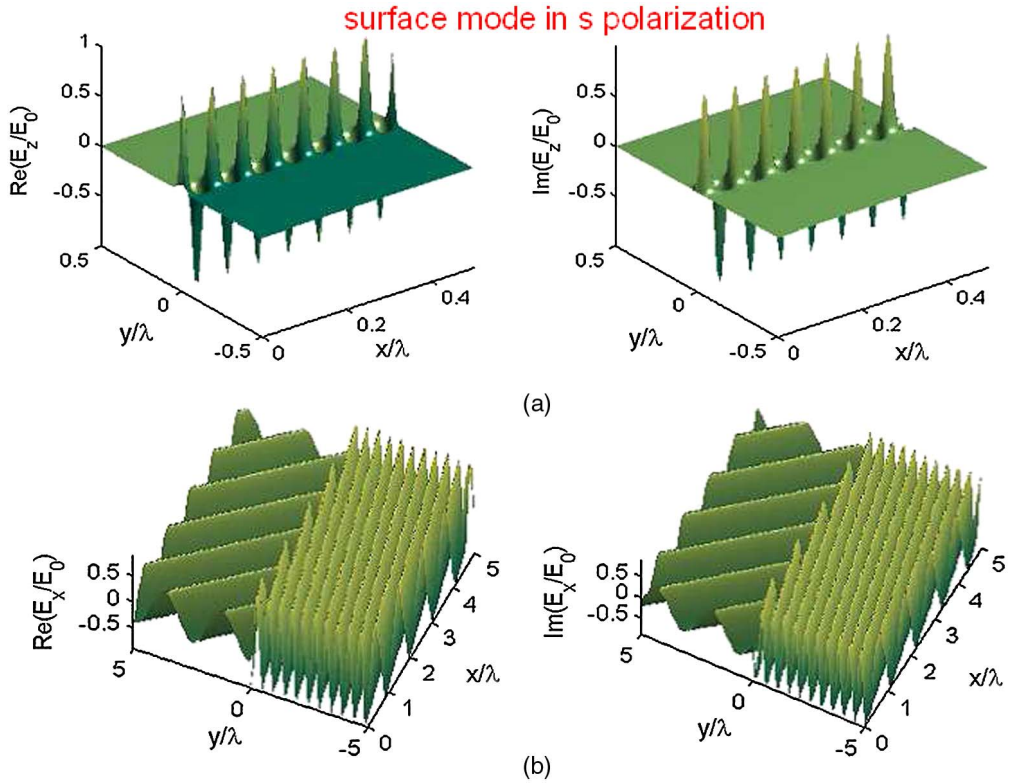

Fig. 2. (Color online) Tangential field distributions for s-polarized light (normalized by amplitude E_0). (a) E_z field with rapid oscillations (corresponding to an enhanced tangential wave vector) and (b) E_x field with normal oscillations. Here, $\mu_1 = 1$ and $\mu_2 = 1.008$, with $\varepsilon_1 = 5$ and $\varepsilon_2 = 1$, corresponding to the second quadrant in the diagram in Fig. 1(b). The normalization factor is $\lambda = 2\pi c/\omega$, where $\omega = 8 \times 10^{13}$ s^{-1}. Note that the E_z field is continuous along $y = 0$ but the E_x field need not be continuous (the scale is 10 times larger).

Second Quadrant. If ε_2 and ε_1 have opposite signs, i.e., $\delta_e^+ = \varepsilon_1 + \varepsilon_2 \simeq 0^+$, while μ_2 and μ_1 have the same sign (assuming $\varepsilon_2 > 0$) we have, similar to Eq. (7),

$$k_x^p \simeq \frac{\omega}{c}\varepsilon_2\sqrt{-\frac{\mu_1+\mu_2}{2\delta_e^+}} \simeq ik_{2y}^p \simeq -ik_{1y}^p. \tag{9}$$

B. μ and ε are Mostly Imaginary

Here, $\mu^i \gg \mu^r$ and $\varepsilon^i \gg \varepsilon^r$. So, the denominator of k_x^s may be approximated as $(\mu_2-\mu_1)(\mu_1+\mu_2) \simeq -(\mu_2^i-\mu_1^i)(\mu_2^i+\mu_1^i)$. Similarly, for k_x^p. Therefore, the tangential wave vectors have expressions similar to that of Eqs. *2) and (3), except there is a negative sign:

$$k_x^s \simeq \frac{\omega}{c}\sqrt{-\left(\frac{\varepsilon_1^i\mu_2^i-\mu_1^i\varepsilon_2^i}{\mu_2^i-\mu_1^i}\right)\frac{\mu_2^i\mu_1^i}{\mu_2^i+\mu_1^i}}. \tag{10}$$

The expression for k_x^p is obtained from Eq. (10) by interchanging μ and ε. Thus, the discussions above for real μ and ε apply, except that the numerator is $\varepsilon_1^i\mu_2^i - \mu_1^i\varepsilon_2^i$ instead of $\varepsilon_1\mu_2 - \mu_1\varepsilon_2$ for s polarization, and $\mu_1^i\varepsilon_2^i - \varepsilon_1^i\mu_2^i$ instead of $\mu_1\varepsilon_2 - \varepsilon_1\mu_2$ for p polarization.

To summarize, the tangential wave vector for s-polarized light is finite for magnetic materials, according to Eqs. (6) and (7). Magnetic materials also give surface polariton resonant enhancement for s polarization [Eq. (6)] just like metallic materials give plasmonic enhancement in p polarization. In addition, magnetic materials also give new regimes of the enhancement effect for p polarization, based on Eq. (8). These analyses show that metals are not the only means for achieving surface enhancement effects. Thus, plasmonics can be extended to magnonics, by using magnetic materials and also metamaterials whose magnetic response can be tailored structurally using nonmagnetic materials.

4. FIELD DISTRIBUTIONS

We show what the field distribution of the surface polariton looks like and how it can be achieved with one of the two possible polarizations. In Fig. 2, medium 1 is a nonmagnetic dielectric [$\mu_1 = 1$ with $\varepsilon_1 = 5$ (e.g., glass)] and medium 2 is paramagnetic [$\mu_2 = 1.008$ with $\varepsilon_2 = 1$ (e.g., FeO)], corresponding to the second quadrant in Fig. 1(b). The permeabilities with nearly equal magnitudes provide the propagating feature of the surface polariton for s-polarized light; i.e., the Re E_z oscillates rapidly across the x direction, corresponding to a large real tangential wave vector k_x^s, but decays along the y direction away from the interface due to imaginary k_{jy}^s.

For Fig. 3, medium 1 is a ferromagnet ($\varepsilon_1 = 1$ with $\mu_1 = 4$ (e.g., AlNiCo), while medium 2 is almost pure diamagnetic ($\varepsilon_2 = 1.009$ at 13 eV with $\mu_2 = -3$ (e.g., mercury [45]), corresponding to the fourth quadrant in Fig. 1(b). Here, the surface propagation feature is shown by the p-polarized field or E_x corresponding to a large k_x^p.

The tangential z component of the E field is always continuous. However, the x component of the E field is not continuous (it is the H_x that is continuous). The field distribution around the interface shows large surface enhancement of

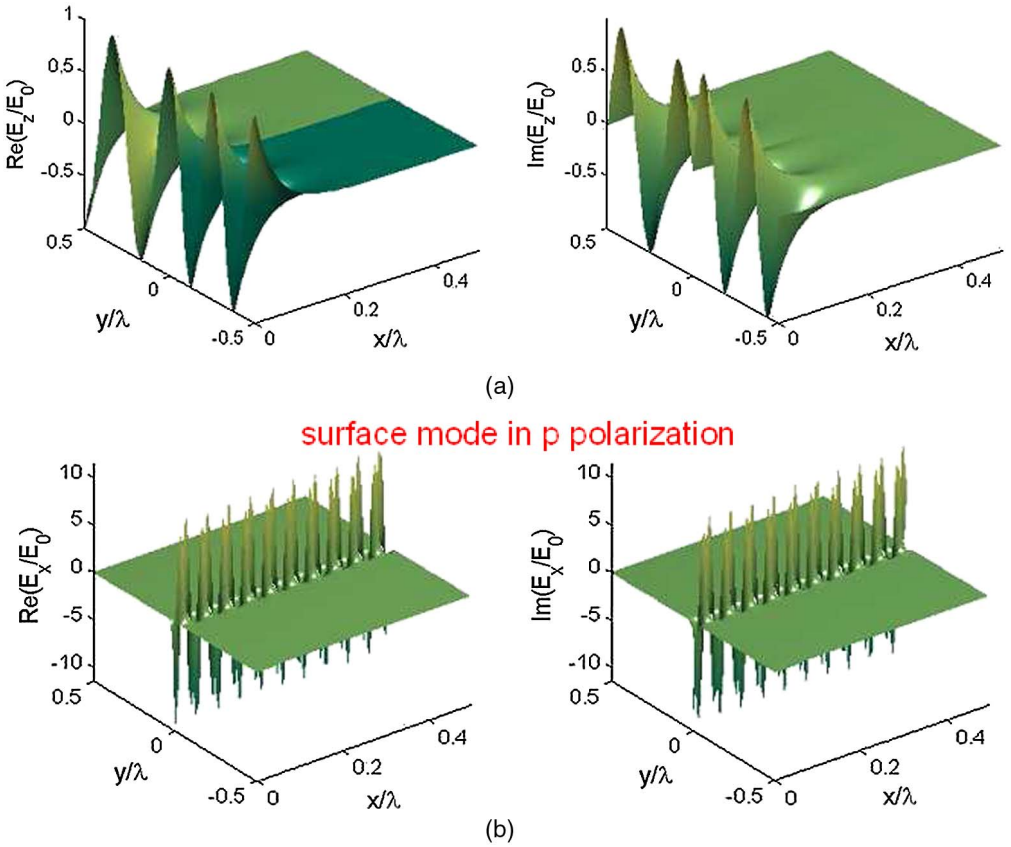

Fig. 3. (Color online) Tangential field distributions for p-polarized light. (a) E_z field with normal oscillations and (b) E_x field with rapid oscillations. Here, $\varepsilon_1 = 1$ and $\varepsilon_2 = 1.009$, with $\mu_1 = 4$ and $\mu_2 = -3$, corresponding to the fourth quadrant in the diagram in Fig. 1.

the tangential wave vector k_x^s for s polarization, as illustrated in Fig. 2. For small $|\delta_m|$, the oscillations for E_z across the x direction are more rapid (with period $2\pi/k_x^s$) than the oscillations for E_x, since k_x^s is enhanced. The tangential component of the E field, i.e., the E_z, is continuous. However, the tangential x component, E_x need not be continuous (see Fig. 2). It is the H_x that must be continuous for s-polarized light.

The case of p polarization also shows enhancement in the tangential wave vector k_x^p (Fig. 3). For small $|\delta_e|$, the oscillations for E_x across the x direction are more rapid (with period $2\pi/k_x^p$) than the oscillations of E_z, since, here, the k_x^p is enhanced, instead. Also, the E_z is continuous while E_x is not continuous, similar to the case of s polarization in Fig. 2.

5. DISPERSIONS OF SURFACE POLARITONS

To study the effects of dispersions in SMR and SFR, we model the dielectric permittivity ε and magnetic permeability μ using [35,46]

$$\alpha(\omega) = 1 + \frac{\tilde{\omega}_\alpha^2}{\omega_\alpha^2 - \omega^2 - i\gamma_\alpha\omega}, \tag{11}$$

with single resonances ω_α of line widths γ_α and oscillator strengths $\tilde{\omega}_\alpha$ ($\alpha = \varepsilon, \mu$). The $\varepsilon(\omega)$ in Eq. (11) describes the dispersion of typical dielectric material due to phonon-polaritons and $\mu(\omega)$ gives the magnetic response of typical metamaterials with single resonance.

Interesting double resonance spectra are found in the tangential wave vectors when one of the media is filled with dispersive dielectric and magnetic materials, modeled by Eq. (11). For dispersive dielectric $\varepsilon_2(\omega)$ and a constant positive permeability $\mu_2 = 5$, Fig. 4 shows only a single resonant peak for s polarization around $\omega_\varepsilon = 1.32 \times 10^{14}$ s^{-1} (the resonance of $\varepsilon_2(\omega)$), while, for p polarization, the peak is at a higher frequency $\sqrt{\omega_\varepsilon^2 + \frac{1}{2}\tilde{\omega}_\varepsilon^2} = 2.41 \times 10^{14}$ s^{-1}. The analytical expressions for the locations of the peaks are obtained from the root in the denominator of k_x^2 for both polarizations (ignoring the damping γ_α) and valid for all possibilities of $\varepsilon_1 = \pm 1$ and $\mu_1 = \pm 1$.

However, when μ_2 is also dispersive with resonance close to the resonance of ε_2, there is a negative refractive index region around the resonance. Figure 5 shows two peaks corresponding to two roots in the denominator of k_x^2. The s polarization shows the second peak at a higher frequency $\sqrt{\omega_\mu^2 + \frac{1}{2}\tilde{\omega}_\mu^2} = 2.52 \times 10^{14}$ s^{-1}, while p polarization shows a second peak around $\omega_\mu = 1.19 \times 10^{14}$ s^{-1} [the magnetic resonance of $\mu_2(\omega)$]. We may deduce that the coexistence of the dielectric dispersion in $\varepsilon_2(\omega)$ and the magnetic dispersion in

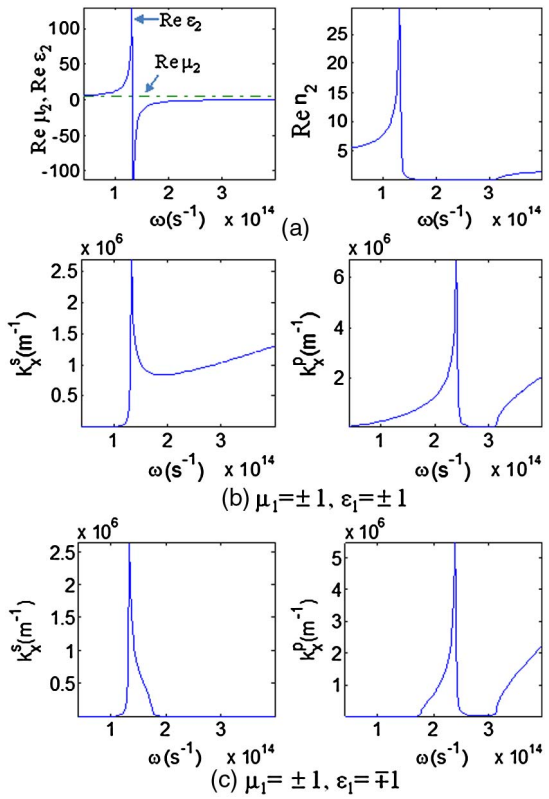

Fig. 4. (Color online) Positive refractive index case: (a) real parts of $\varepsilon_2(\omega)$ [in Eq. (11)], $\mu_2 = 5$ and refractive index $n_2(\omega) = \sqrt{\varepsilon_2(\omega)\mu_2}$. Wave vector dispersions for s-polarized and p-polarized light in two situations: ε_1 and μ_1 with (b) the same sign and (c) opposite signs. For $\varepsilon_2(\omega)$, we use parameters for ionic (BeO) crystal [47]: $\omega_\varepsilon = 2\pi 2.1036 \times 10^{13}$ s^{-1}, $\gamma_\varepsilon = 2\pi 3.6512 \times 10^{11}$ s^{-1}, and $\tilde{\omega}_\varepsilon = 2.8532 \times 10^{14}$ s^{-1}.

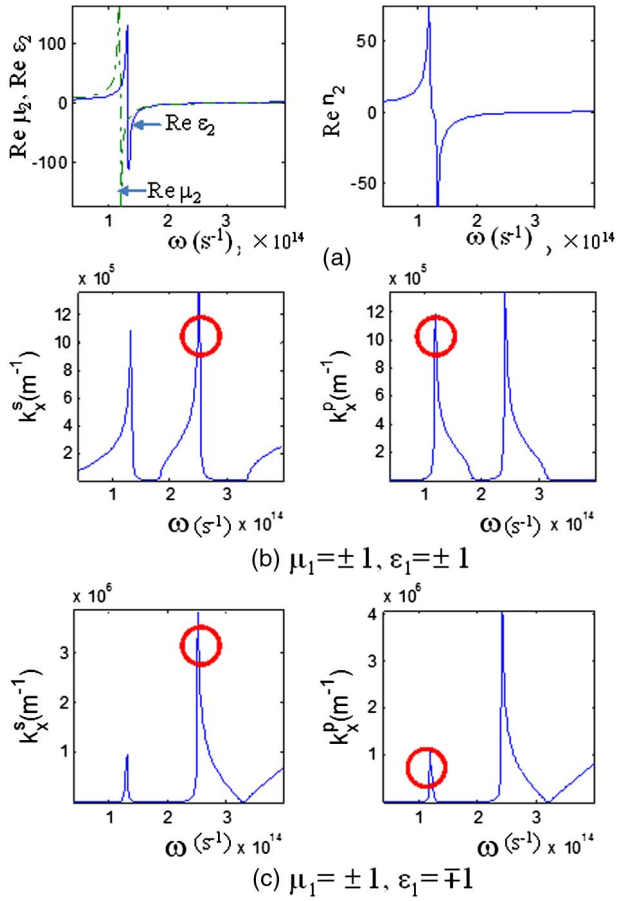

Fig. 5. (Color online) Negative refractive index case: (a) real parts of $\varepsilon_2(\omega)$, $\mu_2(\omega)$, and $n_2(\omega) = \sqrt{\varepsilon_2(\omega)\mu_2(\omega)}$. Wave vector dispersions for s-polarized and p-polarized light in two situations: ε_1 and μ_1 with (b) the same sign and (c) opposite signs. The parameters for $\varepsilon_2(\omega)$ are the same as Fig. 4. For $\mu_2(\omega)$, the magnetic resonance is characterized by $\omega_\mu = 0.9\omega_\varepsilon$, $\tilde{\omega}_\mu = 1.1\tilde{\omega}_\varepsilon$, and $\gamma_\mu = \gamma_\varepsilon$.

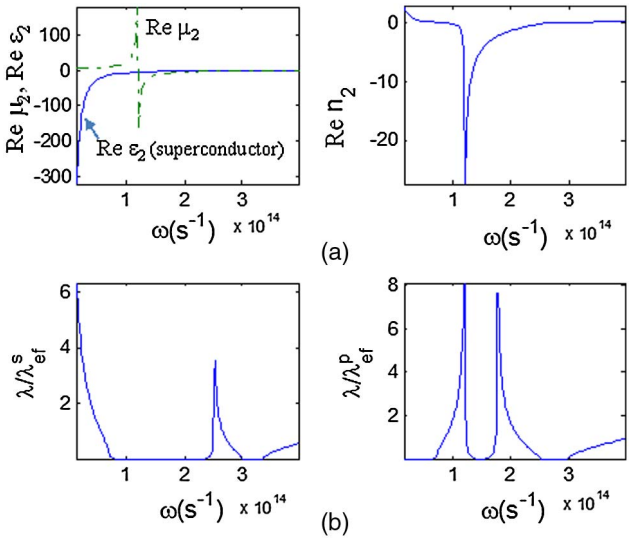

Fig. 6. (Color online) (a) Dispersive superconductor with $\varepsilon_2(\omega)$ and dispersive magnetic material with $\mu_2(\omega)$ (as in Fig. 5) and the resulting $n_2(\omega) = \sqrt{\varepsilon_2(\omega)\mu_2(\omega)}$ with negative refractive index region. (b) The enhancement $\lambda/\lambda_{\text{ef}}^{s,p}$ of surface polaritons for s-polarized and p-polarized light. Here, Eq. (12) is used for $\varepsilon_2(\omega)$, and $\omega = 2\pi c/\lambda$ and $k^{s,p} = 2\pi/\lambda_{\text{ef}}^{s,p}$. Other parameters are $\varepsilon_1 = -1$ and $\mu_1 = 1$.

$\mu_2(\omega)$ give rise to the second peaks in the spectra of k_x for s and p polarizations.

Finally, Fig. 6 shows a remarkable effect of using superconducting material. The s-polarization wave vector is large for small frequency, enabling superresolution at terahertz frequency range $\omega = 10^{12}$ s^{-1}, with the effective wave vector reduced almost 80 times: $\lambda/\lambda_{\text{ef}}^{s} \simeq 80$, where $k_x^q = \frac{2\pi}{\lambda_{\text{ef}}^q}$, $\frac{\omega}{c} = \frac{2\pi}{\lambda}$, $q = s$, and p. The magnetic material, as in Fig. 5, also creates the second peaks for the s- and p-polarization cases. The effect of SPR is modeled by the dielectric function of metals, which includes both conductors and superconductors [48]:

$$\varepsilon_s(\omega) = 1 - \omega_p^2\left[\frac{f_n}{\omega(\omega + i\gamma)} + \frac{f_s}{\omega^2}\right], \tag{12}$$

where $f_n = n_n/n = 0.2$ is the normal (n) fluid fraction, $f_n = n_n/n = 0.8$ the superfluid fraction, with $n = n_s + n_n$ as the total electron number density, $\omega_p = \sqrt{\frac{ne^2}{m\varepsilon_0}} = 2.5 \times 10^{14}$ s^{-1} is the plasma frequency, and $\gamma = 1.3 \times 10^{13}$ s^{-1}. Typically $\omega_p = c10^{4-5}$ m^{-1} and $c10^{6-7}$ m^{-1} for $BiSr_2Ca_2Cu_2O_{8+x}$ and metallic superconductors, respectively [49].

6. CONCLUSIONS

To conclude, we have analyzed the surface polariton enhancement of the tangential wave vector for s- and p-polarized light. If the materials are both dielectric and magnetic, μ_i, $\varepsilon_i \neq 1$, the s-polarized light can also excite the propagating surface modes, not just the p-polarized light. The requirement for enhancement is that either the μ or the ε has opposite signs in the two media. Two or more types of surface polariton (SMP, SFP, SEP, or SPP) can coexist. The expression of the tangential wave vector for s polarization is completely symmetrical to that of the p polarization, due to the symmetry between the electric and magnetic responses in the Maxwell equations. Given the expressions of the wave vector for p polarization, we obtain the results for s polarization by interchanging the magnetic permeability μ and electric permittivity ε. The presence of dispersion with a resonance in μ gives rise to an additional peak in the spectrum of k_x for both polarizations. The use of magnetic materials extends the field of plasmonics to magnonics. Instead of using metals in the region of negative permittivity ε, we could use magnetic materials or engineered metamaterial with negative μ [expression given by Eq. (11)]. The main novelty is that SMP opens up surface polaritons in the new regimes discussed above. SMP can now be realized artificially with metamaterials through microstructural and nanostructural engineering. The use of magnetic materials enables all physical features of plasmonics to be mapped into magnonics with one-to-one correspondence. Finally, there are new technological possibilities with the significant impact of using magnetic materials in addition to metallic and dielectric materials. For example, magnetic recording (data storage) and spintronics devices can merge with photonic circuits where SMPs serve as efficient information carriers and processors. Actual parameters have been used to model the dispersions of the materials, enhancing the prospect for applications.

ACKNOWLEDGMENTS

We appreciate the support by the Ministry of Higher Education (MOHE)/University of Malaya High Impact Research (HIR) Grant A-000004-50001, and the MOHE Exploratory Research Grant Scheme (ERGS) ER014-2011A. This work was supported also by the Japan Society for the Promotion of Science (JSPS) through its FIRST Program and by Optical Science of Dynamically Correlated Electrons (DYCE), KAKENHI 20104008.

REFERENCES

1. E. Ozbay, "Plasmonics: merging photonics and electronics at nanoscale dimensions," Science **311**, 189–193 (2006).
2. N. Yu, Q. J. Wang, C. Pflügl, L. Diehl, F. Capasso, T. Edamura, S. Furuta, M. Yamanishi, and H. Kan, "Semiconductor lasers with integrated plasmonic polarizers," Appl. Phys. Lett. **94**, 151101 (2009).
3. N. Yu, J. Fan, Q. J. Wang, C. Pflügl, L Diehl, T. Edamura, M. Yamanishi, H. Kan, and F. Capasso, "Small divergence semiconductor lasers by plasmonic collimation," Nat. Photon. **2**, 564–570 (2008).
4. J. A. Shackleford, R. Grote, M. Currie, J. E. Spanier, and B. Nabet, "Integrated plasmonic lens photodetector," Appl. Phys. Lett. **94**, 083501 (2009).
5. J. A. Polo, Jr., and A. Lakhtakia, "On the surface plasmon polariton wave at the planar interface of a metal and a chiral sculptured thin film," Proc. R. Soc. A **465**, 87–107 (2009).
6. L. Martin-Moreno, F. J. García-Vidal, H. J. Lezec, A. Degiron, and T. W. Ebbesen, "Theory of highly directional emission from a single subwavelength aperture surrounded by surface corrugations," Phys. Rev. Lett. **90**, 167401 (2003).
7. S. Zhang, D. A. Genov, Y. Wang, M. Liu, and X. Zhang, "Plasmon-induced transparency in metamaterials," Phys. Rev. Lett. **101**, 047401 (2008).
8. W. L. Barnes, A. Dereux, and T. W. Ebbesen, "Surface plasmon subwavelength optics," Nature **424**, 824–830 (2003).
9. I. I. Smolyaninov, Y. J. Hung, and C. C. Davis, "Superresolution optics using short-wavelength surface plasmon polaritons," J. Mod. Opt. **53**, 2337–2347 (2006).
10. E. Moreno, S. G. Rodrigo, S. I. Bozhenyi, L. Martin-Moreno, and F. J. Garcia-Vidal, "Guiding and focusing of electromagnetic fields with wedge plasmon polaritons," Phys. Rev. Lett. **100**, 023901 (2008).

11. I. P. Radko, S. I. Bozhenyi, A. B. Evlyukhin, and A. Boltasseva, "Surface plasmon polariton beam focusing with parabolic nanoparticle chains," Opt. Express **15**, 6576–6582 (2007).
12. G. Farkas and C. Toth, "Energy spectrum of phoelectrons produced by picosecond laser-induced surface multiphoton photoeffect," Phys. Rev. A **41**, 4123–4126 (1990).
13. M. Raynaud and J. Kupersztych, "Ponderomotive effects in the femtosecond plasmon-assisted photoelectric effect in bulk metals: evidence for coupling between surface and interface plasmons," Phys. Rev. B **76**, 241402 (2007).
14. S. Varro and F. Ehlotzky, "High-order multiphoton ionization at metal surfaces by laser fields of moderate power," Phys. Rev. A **57**, 663–666 (1998).
15. J. Zawadzka, D. A. Jaroszynski, J. J. Carey, and K. Wynne, "Evanescent-wave acceleration of ultrashort electron pulses," Appl. Phys. Lett. **79**, 2130–2132 (2001).
16. D. E. Chang, A. S. Sørensen, P. R. Hemmer, and M. D. Lukin, "Strong coupling of single emitters to surface plasmons," Phys. Rev. B **76**, 035420 (2007).
17. K. Okamoto, I. Niki, A. Shvartser, Y. Narukawa, T. Mukai, and A. Scherer, "Surface-plasmon-enhanced light emitters based on InGaN quantum wells," Nat. Mater. **3**, 601–605 (2004).
18. J. E. Sipe, V. C. Y. So, M. Fukui, and G. I. Stegeman, "Analysis of second-harmonic generation at metal surface," Phys. Rev. B **21**, 4389–4402 (1980).
19. R. Rokitski, K. A. Tetz, and Y. Fainman, "Propagation of femtosecond surface plasmon polariton pulses on the surface of a nanostructured metallic film: space-time complex amplitude characterization," Phys. Rev. Lett. **95**, 177401 (2005).
20. J. Lehmann, M. Merschdorf, W. Pfeiffer, A. Thon, S. Voll, and G. Gerber, "Surface plasmon dynamics in silver nanoparticles studied by femtosecond time-resolved photoemission," Phys. Rev. Lett. **85**, 2921–2924 (2000).
21. F. Intravaia and A. Lambrecht, "Surface plasmon modes and the casimir energy," Phys. Rev. Lett. **94** 110404 (2005).
22. G. R. Quidant, G. Badenes, and D. Petrov, "Surface plasmon radiation forces," Phys. Rev. Lett. **96**, 238101 (2006).
23. D. Heitmann, N. Kroo, C. Schulz, and Z. Szentirmay, "Dispersion anomalies of surface plasmons on corrugated metal-insulator interface," Phys. Rev. B **35**, 2660–2666 (1987).
24. R. Jin, Y. W. Cao, C. A. Mirkin, K. L. Kelly, G. C. Schatz, and J. G. Zheng, "Photoinduced conversion of silver nanospheres to nanoprisms," Science **294**, 1901–1903 (2001).
25. J. Lee, P. Hernandez, J. Lee, A. O. Govorov, and N. A. Kotovi, "Exciton-plasmon interactions in molecular spring assemblies of nanowires and wavelength-based protein detection," Nat. Mater. **6**, 291–295 (2007).
26. J. B-Abad, A. Degiron, F. Przybilla, C. Genet, F. J. Garcia-Vidal, L. Martin-Moreno, and T. W. Ebbesen, "How light emerges from an illuminated array of subwavelength holes," Nature Phys. **2**, 120–123 (2006).
27. E. Moreno, F. J. Garcia-Vidal, Daniel Erni, J. I. Cirac, and L. Martin-Moreno, "Theory of plasmon-assisted transmission of entangled photons," Phys. Rev. Lett. **92**, 236801 (2004).
28. A. Drezet, J. C. Woehl, and S. Huant, "Difraction by a small aperture in conical geometry: application to metal-coated tips used in near-field scanning optical microscopy," Phys. Rev. E **65**, 046611 (2002).
29. L. Novotny, R. X. Bian, and X. S. Xie, "Theory of nanometric optical tweezers," Phys. Rev. Lett. **79**, 645–648 (1997).
30. M. Rosenblit, Y. Japha, P. Horak, and R. Folman, "Simultaneous optical trapping and detection of atoms by microdisk resonators," Phys. Rev. A **73**, 063805 (2006).
31. J. B. Khurgin, "Surface plasmon-assisted laser cooling of solids," Phys. Rev. Lett. **98**, 177401 (2007).
32. R. E. Camley and D. L. Mills, "Collective excitatation of semi-infinite superlattice structure: surface plasmons, bulk plasmon and the electron-energy-loss spectrum," Phys. Rev. B **29**, 1695 (1984).
33. J. Seidel, S. Grafström, and L. Eng, "Stimulated emission of surface plasmons at the interface between a silver film and an optically pumped dye solution," Phys. Rev. Lett. **94**, 177401 (2005).
34. E. Cubukcu, E. A. Kort, K. B. Crozier, and F. Capasso, "Plasmonic laser antenna," Appl. Phys. Lett. **89**, 093120 (2006).
35. See V. M. Agranovich and D. L. Mills, ed., *Surface Polaritons : Electromagnetic Waves at Surfaces and Interfaces* (North-Holland 1982).
36. M. G. Cottam and D. R. Tilley, *Introduction to Surface and Superlattice Excitations* (Cambridge University, 1989).
37. R. Ruppin, "Surface polaritons of a left-handed medium," Phys. Lett. A **277**, 61–64 (2000).
38. A. Hartstein, E. Burstein, A. A. Maradudin, R. Brewer, and R. F. Wallis, "Surface polaritons on semi-infinite gyromagnetic media," J. Phys. C Solid State Phys. **6**, 1266–1276 (1973).
39. V. H. Arakelian, L. A. Bagdassarian, and S. G. Simonian, "Electrodynamics of bulk and surface normal magnonpolaritons in antiferromagnetic crystals," J. Magn. Magn. Mater. **167**, 149–160 (1997).
40. J. Matsuura, M. Fukui, and O. Tada, "ATR mode of surface magnon polaritons on YIG," Solid State Commun. **45**, 157–160 (1983).
41. M. Marchand and A. Caill, "Asymmetrical guided magnetic polaritons in a ferromagnetic slab," Solid State Commun. **34**, 827–831 (1980).
42. C. Shu and A. Caillé, "Surface magnetic polaritons on uniaxial antiferromagnets," Solid State Commun. **42**, 233–238 (1982).
43. C. Thibaudeau and A. Caillé, "The magnetic polaritons of a semi-infinite uniaxial antiferromagnet," Solid State Commun. **87**, 643–647 (1993).
44. J. Takahara and T. Kobayashi, "Low-dimensional optical waves and nano-optical circuits," Opt. Photon. News **15**(10), 54–59 (2004).
45. T. Inagaki, E. T. Arakawa, and M. W. Williams, "Optical properties of liquid mercury," Phys. Rev. B **23**, 5246–5262 (1981).
46. J. B. Pendry, A. J. Holden, D. J. Robbins, and W. J. Stewart, "Magnetism from conductors and enhanced nonlinear phenomena," IEEE Trans. Microwave Theory Tech. **47**, 2075–2084 (1999).
47. C. G. Ribbing, H. Högström, and A. Rung, "Studies of polaritonic gaps in photonic crystals," Appl. Opt. **45**, 1575–1582 (2006).
48. C. H. R. Ooi, T. C. A. Yeung, C. H. Kam, and T. K. Lim, "Photonic band gap in a superconductor-dielectric superlattice," Phys. Rev. B **61**, 5920–5923 (2000).
49. T. van Duzer and C. W. Turner, *Principles of Superconductive Devices and Circuits* (Elsevier North-Holland, 1981).

REFERENCES

Agranovich, V., & Mills, D. (1982). *Surface polaritons: electromagnetic waves at surfaces and interfaces*. North-Holland Pub. Co.

Arakelian, V. H., Bagdassarian, L. A., & Simonian, S. G. (1997). Electrodynamics of bulk and surface normal magnonpolaritons in antiferromagnetic crystals. *J. Magn. Magn. Mater.*, *167*, 149–160.

B-Abad, J., Degiron, A., Przybilla, F., Genet, C., FGarcia-Vidal, . J., Martin-Moreno, L., et al. (2006). How light emerges from an illuminated array of subwavelength holes. *Nature Phys.*, *2*, 120–123.

Barnes, W. L., Dereux, A., & Ebbesen, T. W. (2003). Surface plasmon subwavelength optics. *Nature*, *424*, 824–830.

Camley, R. E., & Mills, D. L. (1984). Collective excitatation of semiinfinite superlattice structure: surface plasmons, bulk plasmon and the electron-energy-loss spectrum. *Phys. Rev. B*, *29*, 1695.

Chang, D. E., Sørensen, A. S., Hemmer, P. R., & Lukin, M. D. (2007). Strong coupling of single emitters to surface plasmons. *Phys. Rev. B*, *76*, 035420.

Cottam, M., Tilley, D., & Physics (Great Britain), I. of. (2005). *Introduction to surface and superlattice excitations*. Institute of Physics.

Cubukcu, E., Kort, E. A., Crozier, K. B., & Capasso, F. (2006). Plasmonic laser antenna. *Appl. Phys. Lett.*, *89*, 093120.

Drezet, A., Woehl, J. C., & Huant, S. (2002). Difraction by a small aperture in conical geometry: application to metal-coated tips used in near-field scanning optical microscopy. *Phys. Rev. E*, *65*, 046611.

Farkas, G., & Toth, C. (1990). Energy spectrum of phoelectrons produced by picosecond laser-induced surface multiphoton photoeffect. *Phys. Rev. A*, *41*, 4123–4126.

Hartstein, A., Burstein, A. A., E.and Maradudin, Brewer, R., & Wallis, R. F. (1973). Surface polaritons on semi-infinite gyromagnetic media. *J. Phys. C Solid State Phys*, *6*, 1266-1276.

Heitmann, D., Kroo, N., Schulz, C., & Szentirmay, Z. (1987). Dispersion anomalies of surface plasmons on corrugated metal-insulator interface. *Phys. Rev. B*, *35*, 2660–2666.

Inagaki, T., Arakawa, E. T., & Williams, M. W. (1981). Optical properties of liquid mercury. *Phys. Rev. B*, *23*, 5246–5262.

Intravaia, F., & Lambrecht, A. (2005). Surface plasmon modes and the casimir energy. *Phys. Rev. Lett.*, *94*, 110404.

Jin, R., Cao, Y. W., Mirkin, C. A., Kelly, K. L., Schatz, G. C., & Zheng, J. G. (2001). Photoinduced conversion of silver nanospheres to nanoprisms. *Science*, *294*, 1901–1903.

Khurgin, J. B. (2007). Surface plasmon-assisted laser cooling of solids. *Phys. Rev. Lett.*, *98*, 177401.

Lee, J., Hernandez, P., Lee, J., Govorov, A. O., & Kotovi, N. A. (2007). Exciton-plasmon interactions in molecular spring assemblies of nanowires and wavelength-based protein detection. *Nat. Mater.*, *6*, 291–295.

Lehmann, J., Merschdorf, M., Pfeiffer, W., Thon, A., Voll, S., & Gerber, G. (2000). Surface plasmon dynamics in silver nanoparticles studied by femtosecond time-resolved photoemission. *Phys. Rev. Lett.*, *85*, 2921–2924.

Maier, S. (2007). *Plasmonics: Fundamentals and applications*. Institute of Physics.

Marchand, M., & Caill, A. (1980). Asymmetrical guided magnetic polaritons in a ferromagnetic slab. *Solid State Commun.*, *34*, 827–831.

Martin-Moreno, L., García-Vidal, F. J., Lezec, H. J., Degiron, A., & Ebbesen, T. W. (2003). Theory of highly directional emission from a single subwavelength aperture surrounded by surface corrugations. *Phys. Rev. Lett.*, *90*, 167401.

Matsuura, J., Fukui, M., & Tada, O. (1983). Atr mode of surface magnon polaritons on yig. *Solid State Commun.*, *45*, 157–160.

Moreno, E., Garcia-Vidal, F. J., Erni, D., Cirac, J. I., & Martin-Moreno, L. (2004). Theory of plasmon-assisted transmission of entangled photons. *Phys. Rev. Lett.*, *92*, 236801.

Moreno, E., Rodrigo, S. G., Bozhenyi, S. I., Martin-Moreno, L., & Garcia-Vidal, F. J. (2008). Guiding and focusing of electromagnetic fields with wedge plasmon polaritons. *Phys. Rev. Lett.*, *100*, 023901.

Novotny, L., Bian, R. X., & Xie, X. S. (1997). Theory of nanometric optical tweezers. *Phys. Rev. Lett.*, *79*, 645–648.

Okamoto, K., Niki, I., Shvartser, A., Narukawa, Y., Mukai, T., & Scherer, A. (2004). Surface-plasmon-enhanced light emitters based on ingan quantum wells. *Nat. Mater.*, *3*, 601–605.

Ooi, R. C. H., Yeung, A. T. C., Kam, C. H., & Lim, T. K. (2006). Photonic band gap in a superconductor-dielectric superlattice. *Phys. Rev. B*, *61*, 5920–5923.

Ozbay, E. (2006). Plasmonics: merging photonics and electronics at nanoscale dimensions. *Science*, *311*, 189-193.

Park, K., Lee, B. J., Fu, C., & Zhang, Z. M. (2005). Study of the surface and bulk polaritons with a negative index metamaterial. *J. Opt. Soc. Am. B*, *22*, 1016-1023.

Pendry, J. B., Holden, A. J., Robbins, D. J., & Stewart, W. J. (1999). magnetism from conductors and enhanced nonlinear phenomena. *IEEE Trans. Microwave Theory Tech.*, *47*, 2075–2084.

Pendry, J. B., Holden, A. J., Stewart, W. J., & Youngs, I. (1996). Extremely low frequency plasmons in metallic mesostructures. *Prl.*, *76*, 4773.

Pendry, J. B., & Smith, D. R. (2004). Reversing light with negative refraction. *Phys. Today*, *57*, 37–43.

Polo, J. A., Jr., & Lakhtakia, A. (2009). On the surface plasmon polariton wave at the planar interface of a metal and a chiral sculptured thin film. *Proc. R. Soc. A*, *465*, 87–107.

Quidant, G. R., Badenes, G., & Petrov, D. (2006). Surface plasmon radiation forces. *Phys. Rev. Lett.*, *96*, 238101.

Radko, I. P., Bozhenyi, S. I., Evlyukhin, A. B., & Boltasseva, A. (2007). Surface plasmon polariton beam focusing with parabolic nanoparticle chains. *Opt. Express*, *15*, 6576–6582.

Raether, H. (1988). *Surface plasmons on smooth and rough surfaces and on gratings* (No. v. 111). Springer.

Rao, X. S., & Ong, C. K. (2003). Amplification of evanescent waves in a lossy left-handed material slab. *Phys. Rev. B*, *68*, 113103.

Raynaud, M., & Kupersztych, J. (2007). Ponderomotive effects in the femtosecond plasmon-assisted photoelectric effect in bulk metals: evidence for coupling between surface and interface plasmons. *Phys. Rev. B*, *76*, 241402.

Ribbing, C. G., Högström, H., & Rung, A. (2006). Studies of polaritonic gaps in photonic crystals. *Appl. Opt.*, *45*, 1575–1582.

Ritchie, R. H. (1957, June). Plasma Losses by Fast Electrons in Thin Films. *Physical Review*, *106*,

874-881.

Rokitski, R., Tetz, K. A., & Fainman, Y. (2005). Propagation of femtosecond surface plasmon polariton pulses on the surface of a nanostructured metallic film: space-time complex amplitude characterization. *Phys. Rev. Lett.*, *95*, 177401.

Rosenblit, M., Japha, Y., Horak, P., & Folman, R. (2006). Simultaneous optical trapping and detection of atoms by microdisk resonators. *Phys. Rev. A*, *73*, 063805.

Ruppin, R. (2000). Surface polaritons of a left-handed medium. *Phys. Lett. A*, *277*, 61–64.

Seidel, J., Grafström, S., & Eng, L. (2005). Stimulated emission of surface plasmons at the interface between a silver film and an optically pumped dye solution. *Phys. Rev. Lett.*, *94*, 177401.

Shackleford, J. A., Grote, R., Currie, M., Spanier, J. E., & Nabet, B. (2009). Integrated plasmonic lens photodetector. *Appl. Phys. Lett.*, *94*, 083501.

Shadrivov, I. V., Sukhorukov, A. A., & Kivshar, Y. S. (2003). Guided modes in negative-refractive-index waveguides. *Phys. Rev. E*, *67*, 057602.

Shelby, R. A., Smith, D. R., & Schultz, S. (2001). Experimental verification of a negative index of refraction. *Science*, *292*, 77–79.

Shu, C., & Caille, A. (1980). Surface magnetic polaritons on uniaxial antiferromagnets. *Solid State Commun.*, *34*, 827–831.

Sipe, J. E., So, Y. V. C., Fukui, M., & Stegeman, G. I. (1980). Analysis of second-harmonic generation at metal surface. *Phys. Rev. B*, *21*, 4389–4402.

Smith, D. R., Padilla, W. J., Vier, D. C., Nemat-Nasser, S. C., & Schultz, S. (2000). Composite medium with simultaneously negative permeability and permittivity. *Phys. Rev. Lett.*, *84*, 4184–4187.

Smolyaninov, I. I., Hung, Y. J., & Davis, C. C. (2006). Superresolution optics using short-wavelength surface plasmon polaritons. *J. Mod. Opt.*, *53*, 2337-2347.

Takahara, J., & Kobayashi, T. (2004). Low-dimensional optical waves and nano-optical circuits. *Opt. Photon. News*, *15*, 54–59.

Thibaudeau, C., & Caille, A. (1993). The magnetic polaritons of a semi-infinite uniaxial antiferromagnet. *Solid State Commun.*, *87*, 643–647.

Van Duzer, T., & Turner, C. (1981). *Principles of superconductive devices and circuits*. Elsevier.

Varro, S., & Ehlotzky, F. (1998). High-order multiphoton ionization at metal surfaces by laser fields of moderate power. *Phys. Rev. A*, *57*, 663–666.

Veselago, V. G. (1968). The electrodynamics of substances with simultaneously negative values of epsilon and mu. *Sov. Phys. Usp*, *10*, 509–514.

Yu, N., Fan, J., Wang, Q. J., Pflugl, C., Diehl, L., Edamura, T. ., et al. (2008). Small divergence semiconductor lasers by plasmonic collimation. *Nat. Photon.*, *2*, 564–570.

Yu, N., Wang, Q. J., Pflugl, C., Diehl, L., Capasso, F. ., & Kan, H. (2009). Semiconductor lasers with integrated plasmonic polarizers. *Appl. Phys. Lett.*, *94*, 151101.

Zawadzka, J., Jaroszynski, D. A., Carey, J. J., & Wynne, K. (2001). Evanescent-wave acceleration of ultrashort electron pulses. *Appl. Phys. Lett.*, *79*, 2130–2132.

Zhang, S., Genov, D. A., Wang, Y., Liu, M., & Zhang, X. (2008). Plasmon induced transparency in metamaterials. *Phys. Rev. Lett.*, *101*, 047401.